NONLINEAR WAVE INTERACTIONS IN SUPERSONIC WIND GENERATED WAVES

by

Spyridon G. Lekoudis

Dissertation submitted to the Graduate Faculty of the Virginia Polytechinc Institute and State University in partial fulfillment of the requirements for the degree of

DOCTOR OF PHILOSOPY

in

Engineering Mechanics

APPROVES:

Ali H. Nayfeh
A. H. Nayfeh, Chairman

W. S. Saric
W. S. Saric

Terry A. Weisshaar
T. A. Weisshaar

Dean T. Mook
D. T. Mook

John E. Kaiser, Jr.
J. E. Kaiser

April 1977

Blacksburg, Virginia

ACKNOWLEDGMENTS

The author wishes to express his graditude to his advisor, Professor A. H. Nayfeh for his guidance and contributions throughout the course of this study. He wishes to thank Professor W. S. Saric for many discussion about the problem and about hydrodynamic stability in general and for furnishing the computer, code SUPORT. Thanks are also due to Mrs. Janet Bryant for an excellent typing job.

The work contained in this report was sponsored by the Fluid Dynamics Program of the Office of Naval Research under Grant No. 00014-72-A-0136-0002 and the financial support is greatly acknowledged.

TABLE OF CONTENTS

Table of Contents Con't

LIST OF FIGURES

List of Figures Con't

List of Figures Con't

List of Figures Con't

NOMENCLATURE

a	wave amplitude (unless otherwise specified)
b	constant from Sutherland's law (unless otherwise specified)
C_f	friction factor
C_p	heat capacity
c	complex wave speed
e	constant
f	functions in the liquid phase (subscripted)
G	inverse Froude number squared (not subscripted)
g	vertical acceleration (not subscripted)
h	film thickness
i	$\sqrt{-1}$
k	dimensional wave number
IG	inhomogenities in the gas phase
IL	inhomogenities in the liquid phase
M	Mach number
m	harmonic number
P,p	pressure
Pr	Prandtl number
R	liquid Reynolds number
R_G	gas Reynolds number
r	recovery factor (unless otherwise specified)
T	temperature
t	time
U,u	x-component of velocity

Nomenclature Con't

u_ℓ	mean film-surface velocity
V,v	y-component of velocity
W	inverse Weber number
x	horizontal space coordinate
Y,y	vertical space coordinate
z	variables in the gas phase
α	dimensionless wave number
β	functions in the liquid phase
γ	ratio of heat capacities (1.4 for air)(unless otherwise specified)
δ	functions in the gas phase
ε	magnitude of wave amplitude
ζ	functions in the gas phase
η	wave-displacement function
κ	thermal conductivity
λ	eigenvalues in the gas free-stream solution
Λ	pressure-perturbation parameter
μ	viscosity
π	3.1415...
ρ	density
σ	normal stress
τ	shear stress
Φ	dissipation function (unless otherwise specified)
ϕ	function defined in Fourier expansion of Ψ
χ	shear-perturbation parameter

Nomenclature Con't

ψ	stream function
ω	frequency

Subscripts

x,y,t	partial derivative with respect to x,y,t
0	mean-flow quantities
1	first-order quantities
2	second-order quantities
∞	gas free-stream quantities
m	harmonic index

Superscripts

$( )'$	total derivative, also disturbance component
$\sim$	dimensional variable
$(\bar{})$	complex conjugate
*	adjoint

I. INTRODUCTION

The advent of new, sophisticated missions for reentry vehicles has generated a renewed interest in transpiration cooling as a protective system to insure the maintenance of reentry vehicle geometry and structural integrity from the effects of aerodynamic heating. The technique consists of injecting a liquid coolant in the stagnation region and allowing the liquid to be swept back over the body, providing a protective liquid layer. Thus, of particular importance in transpiration cooling is the estimation of the liquid removal by either entrainment or evaporation. To estimate the amount of liquid entrained by the gas, one needs to determine the stability characteristics of the liquid/gas interface. To estimate the amount of liquid removed by evaporation, one needs to know the roughness characteristics of the interface; that is, the interface wave characteristics such as the wave length and amplitude. These estimates are also important because the multi-phase flow near the interface might increase the degree of turbulent transport (in the case of turbulent gas boundary layers) and cause transition in the liquid film. This phenomenon is called volumetric boiling. Moreover for maximum protection, the dominant liquid loss mechanism must be evaporation.

If, as experiments indicate, the film is stable and relatively uniform in thickness, then the film will uniformly cool the body by evaporation. However, if the film is unstable, uncovered areas will appear on the body between wave crests, and liquid droplets will be entrained by the gas; consequently, the effectiveness of the coolant film will be reduced.

When the surface of the film is disturbed, a number of stabilizing and destabilizing mechanisms come into play. In the absence of an external gas flow, the instability is caused by body forces acting outward from the liquid (Rayleigh-Taylor mechanism).

The motion of the gas parallel to the liquid layer produces two important effects on the liquid. The first is the exertion of a mean shear stress at the liquid/gas interface, which in turn establishes a mean velocity profile in the liquid. The second is the exertion of pressure and shear stress perturbations on the liquid due to the appearance of waves on the interface. Whereas the former effect can be stabilizing or destabilizing depending on a number of conditions, the latter effect leads to pressure perturbation (Kelvin-Helmholtz) and shear perturbation (Craik-Benjamin) instability mechanisms. The former effect due to the mean vorticity in the liquid may lead to instabilities of the boundary-layer type (Tollmien-Schlicting mechanism).

Miles (1960) analyzed the stability of a thin liquid film in a shearing motion in the absence of pressure and shear perturbations. He found the critical liquid Reynolds number for the Tollmien-Schlicting mechanism to be 203 based on the surface speed and film thickness. Moreover, he found that the liquid stability problem has two solutions and the instability is associated with the "slow" wave solution. In this investigation we are interested in flows with Reynolds numbers less than 203; consequently, we did not find any type of Tollmien-Schlicting instability.

Chang and Russell (1965) extended the classical Kelvin-Helmholtz problem of two, parallel, incompressible, irrotational streams by including compressibility in one stream and viscosity in the other. Their results show that a fluid adjacent to a supersonic stream (pressure perturbation in phase with the wave slope) is much more unstable than a fluid adjacent to a subsonic stream (pressure perturbation in anti-phase with the wave amplitude). Nachtsheim (1970) and Cresci & Starkenburg (1971) extended the analysis of Chang & Russell by including the effect of a linear liquid velocity profile. They obtained numerical solutions. Unlike Miles' case, Nachtsheim found that the instability is associated with the "fast" wave which derives its energy from the gas motion. Nayfeh & Saric (1971b) studied the effect of a body force having an arbitrary direction on the stability of thin films. They found that the nonlinear velocity profile of the film can significantly affect the stability.

Benjamin (1959) extended the analysis of Miles (1957) by including first-order viscous terms and determined the pressure and shear stresses exerted by an incompressible stream on a rigid wavy wall. This work was adapted by a number of investigators to determine the pressure and shear perturbations exerted by the rotational gas flow on the wavy surface of a liquid and to determine their effects on the linear stability of waves. For example, Miles (1962) analyzed deep water waves, and Cohen & Hanratty (1965) and Craik (1966) analyzed the linear stability of a liquid film adjacent to an incompressible viscous stream for large and small liquid Reynolds numbers, respectively. Craik

found that for thin films the shear perturbations dominate the pressure perturbations while for thick films this is not necessarily the case; consequently, the thin films are more unstable.

For compressible supersonic flows, the mean-flow velocity decreases from its supersonic free-stream value at the edge of the boundary layer to a small velocity (nearly equal to that of the mean liquid surface) as shown in figure 1. Then, the phase of the pressure perturbation exerted on the gas by the liquid interface lies between the inviscid subsonic and supersonic values. The shear and pressure perturbations exerted by a compressible viscous stream in the absence of temperature gradients were analyzed by Lighthill (1953) for the case in which the mean flow is linear within the disturbance sublayer. Inger (1971) extended the supersonic analysis of Lighthill by including the effects of heat transfer and mass injection at the wall. However, Lekoudis et al (1976) showed that the aforementioned assumption is not valid for turbulent flows, because the disturbance boundary-layer thickness is not small when compared with the mean boundary-layer thickness; details of this work are included in Chapter 3.

Since the experimental results show that the liquid surface velocity and the wavespeeds are very small compared with the gas free-stream velocity, one can assume the liquid surface to be stationary in calculating the pressure and shear perturbations. Moreover, since the gas Reynolds numbers based on the observed wave lengths are large, the mean flow can be assumed to be parallel. Inger's model was used by Grabow & White (1973) to analyze the stability of a liquid film for small liquid Reynolds numbers within the long-wave approximation.

They found that the pressure perturbation in antiphase with the wave amplitude is the dominant destabilizing effect, while the dominant stabilizing effect is the shear perturbation in phase with the wave slope. Bordner et al (1975) removed the restriction of small Reynolds numbers. They showed that including the effects of the mean-flow profile strongly changes the stability characteristics of the liquid film. They also showed that including the effects of viscosity in calculating the shear and pressure perturbations changes the film stability characteristics, but to a lesser degree. In this work, we determined the linear stability characteristics of the liquid films by taking into account the gas mean profile and the gas viscosity without any restriction on the size of the disturbance boundary layer.

According to the linear analysis, the observed waves should correspond to the ones with maximum amplification rates. Although the linear analysis is in good agreement with the subsonic gas flow case, it is in poor agreement with the supersonic gas flow case. Moreover, the above linear theories predict that a liquid film adjacent to a supersonic stream is much more unstable than a liquid film adjacent to a subsonic stream, in disagreement with the experimental observations of Cohen & Hanratty (1965), Craik (1966), Gater & L'Ecuyer (1969), Saric & Marshall (1971), Gold, et al (1971), Marshall (1971), Gold (1973), and Saric et al (1976). Cohen & Hanratty and Craik gave data on the wave stability and wave properties for a stratified flow in a duct. In the experiments of Gater & L'Ecuyer, the gas flow was turbulent and nearly incompressible, and the liquid layer was found

to be unstable as evidenced by the liquid drops entrained by the gas. Gater & L'Ecuyer correlated the mass entrained with the entrainment group $(q)^{1/2}/T$ where q is the dynamic pressure of the gas and T is the surface tension of the liquid. In the experiments discussed next, the liquid was injected near the tip of a slender cone or wedge-shaped body placed in a supersonic wind tunnel. Gold and co-workers (1971, 1973) and Saric, et al (1976) maintained the same range of entrainment group as Gater & L'Ecuyer but at supersonic speeds. They did not observe any entrainment. In fact, they found that the ratio of the r.m.s. wave amplitude to the mean thickness of the liquid layer decreases as the surface pressure increases. This implies that increasing the entrainment group is stabilizing, in contrast with the subsonic experiments. In the experiments of Saric & Marshall (1971) and Marshall (1971), the gas flow was laminar and supersonic, and stable waves without entrainment were observed. Marshall (1971) measured the instantaneous depth of the liquid film using an "end-effect" capacitance gauge. Using this data, Nayfeh & Saric (1973) calculated the ratio of the r.m.s. wave amplitude to the mean depth and found that this ratio decreases as the shear increases. In contrast with the aforementioned experimental observations, Cresci & Strakenburg (1971) observed high entrainment rates. However, the entrainment might have occurred in the subsonic region around the blunt nose of the cone.

These experimental observations can be explained qualitatively by using the nonlinear theory of Nayfeh & Saric (1971a). They analyzed the nonlinear stability of a quiescent viscous liquid film parallel to an inviscid compressible gas for small liquid Reynolds numbers within

the long-wave approximation. In the subsonic case, they found that unstable linear disturbances continue to be unstable in the nonlinear case; thus conditions exist for liquid entrainment by the gas, in qualitative agreement with the experiments of Gater & L'Ecuyer. In the supersonic case, they found that stable linear disturbances dampen faster while unstable linear disturbances do not grow indefinitely but become steady periodic waves. Thus, conditions for entrainment do not exist in this case, in qualitative agreement with the experiments of Gold and Saric and their co-workers. In a later study, Nayfeh & Saric (1973) removed the initial quiescent liquid assumption of their previous study by taking the liquid velocity profile into account. The latter results also predict the existence of finite-amplitude periodic waves in the supersonic case, in qualitative agreement with the experimental observations.

However, neither study is capable of predicting quantitatively the observed wavelengths and their corresponding wave speeds and amplitudes. For the case of an infinite Reynolds number, Nayfeh & Mook (1973) found that all wavy disturbances were unstable; this result is contrary to what was found for low Reynolds numbers and suggests that an analysis valid for arbitrary Reynolds numbers is needed.

Bordner and Nayfeh (1974) refined the previous nonlinear models by relaxing the restriction on the magnitude of the liquid Reynolds number and by including the effects of the gas viscosity and velocity profile in calculating the pressure and shear perturbations exerted by the gas on the liquid/gas interface.

In spite of all the improvements, the quantitative agreement with the available experimental date is still poor. The present study removes all the assumptions made in the previous studies (linear and nonlinear). Chapter 3 deals with the gas problem and examines the accuracy of the previous models. Chapter 4 presents the linear stability analysis without any approximations. The result of Bordner & Nayfeh (1974) that the waves are weakly dispersive is confirmed. Finally, in Chapter 5, nonlinear resonant interactions are analyzed.

2. FORMULATION OF THE PROBLEM

The purpose of the present study is to obtain further understanding of phenomena affecting the stability of liquid films adjacent to subsonic or supersonic boundary layers. This is done by a refinement of previous models for analyzing the problem and by comparing the predictions of the models with experimental data. In this chapter, the governing equations are developed. The development of these equations follows closely that of Bordner (1973) but the long-wave approximation has been abandoned in both the gas and the liquid phases.

2.1 Equations for the Liquid Phase

Equations for the disturbed motion of the liquid are developed which take into account the mean motion of the film, the viscosity of the liquid, a perpendicular body force, and the pressure and shear perturbations on the interface due to the gas flow.

2.1.1 Dimensional Equations

We are concerned with two-dimensional disturbances of the liquid film, which are depicted in figure 1. The liquid is assumed to have a uniform density $\tilde{\rho}$ and viscosity $\tilde{\mu}$. The governing equations for the liquid motion in dimensional variables are

$$\tilde{u}_{\tilde{x}} + \tilde{v}_{\tilde{y}} = 0 \tag{2.1.1}$$

$$\tilde{u}_{\tilde{t}} + \tilde{u}\tilde{u}_{\tilde{x}} + \tilde{v}\tilde{u}_{\tilde{y}} + \frac{1}{\tilde{\rho}}\tilde{p}_{\tilde{x}} = \frac{\tilde{\mu}}{\tilde{\rho}}\left(\tilde{u}_{\tilde{x}\tilde{x}} + \tilde{u}_{\tilde{y}\tilde{y}}\right) \tag{2.1.2}$$

$$\tilde{v}_{\tilde{t}} + \tilde{u}\tilde{v}_{\tilde{x}} + \tilde{v}\tilde{v}_{\tilde{y}} + \frac{1}{\tilde{\rho}}\tilde{p}_{\tilde{y}} = \tilde{g} + \frac{\tilde{\mu}}{\tilde{\rho}}\left(\tilde{v}_{\tilde{x}\tilde{x}} + \tilde{v}_{\tilde{y}\tilde{y}}\right) \tag{2.1.3}$$

where u and v are the velocity components in the x and y directions. The boundary conditions at the solid/liquid interface are

$$\tilde{u} = 0,\ \tilde{v} = 0 \text{ at } \tilde{y} = 0 \tag{2.1.4}$$

The thickness of the disturbed film is $\tilde{h}(\tilde{x},\tilde{t})$. The kinematic boundary condition at the liquid/gas interface is

$$\tilde{h}_{\tilde{t}} + \tilde{u}\tilde{h}_{\tilde{x}} = \tilde{v}, \quad \text{at} \quad \tilde{y} = \tilde{h} \tag{2.1.5}$$

The normal and tangential stresses acting on the interface due to the gas are $\tilde{\sigma}$ and $\tilde{\tau}$. A balance of normal and tangential forces at the liquid/gas interface yields

$$-\tilde{\sigma} = \tilde{p} - \frac{2\tilde{\mu}}{1+\tilde{h}_{\tilde{x}}^2}\left[\tilde{v}_{\tilde{y}} - (\tilde{u}_{\tilde{y}} + \tilde{v}_{\tilde{x}})\tilde{h}_{\tilde{x}} + \tilde{u}_{\tilde{x}}\tilde{h}_{\tilde{x}}^2\right] + \frac{\tilde{T}\tilde{h}_{\tilde{x}\tilde{x}}}{(1+\tilde{h}_{\tilde{x}}^2)^{3/2}} \quad \text{at } \tilde{y} = \tilde{h} \tag{2.1.6}$$

$$\tilde{\tau} = \tilde{\mu}(\tilde{u}_{\tilde{y}} + \tilde{v}_{\tilde{x}})\frac{1-\tilde{h}_{\tilde{x}}^2}{1+\tilde{h}_{\tilde{x}}^2} + 2\tilde{\mu}(\tilde{v}_{\tilde{y}} - \tilde{u}_{\tilde{x}})\frac{\tilde{h}_{\tilde{x}}}{1+\tilde{h}_{\tilde{x}}^2} \quad \text{at } \tilde{y} = \tilde{h} \tag{2.1.7}$$

where $\tilde{T}$ is the surface tension coefficient.

2.1.2 Mean Flow

There is a mean flow of the liquid, as shown in Figure 1, due to the mean shear $\tilde{\tau}_0$ exerted by the gas. Also, the gas exerts a mean pressure $\tilde{p}_{0g}$. The undisturbed conditions in the liquid are given by the following steady laminar solution of the previous equations:

$$\tilde{u}_0 = \tilde{u}_{\ell}\tilde{y}/\tilde{h}_0\ ,\ \tilde{v}_0 = 0 \tag{2.1.8}$$

$$\tilde{P}_0 = \tilde{P}_{0g} - \tilde{\rho}\tilde{g}(\tilde{h}_0 - \tilde{y}) \tag{2.1.9}$$

where $\tilde{h}_0$ is the mean depth of the liquid film and the gas/liquid interface velocity $\tilde{u}_\ell$ is given by

$$\tilde{u}_\ell = \tilde{h}_0\tilde{\tau}_0/\tilde{\mu} \tag{2.1.10}$$

If the liquid Reynolds number is large, the flow of the liquid will be turbulent and the analysis would involve perturbations in the Reynolds stresses. An analysis of this type is beyond the scope of the present investigation.

2.1.3 Dimensionless Disturbance Equations

We introduce dimensionless variables as follows: The $\tilde{x}$ is made dimensional with the wave number $\tilde{k}$ of an assumed sinusoidal disturbance, while $\tilde{y}$ and $\tilde{h}$ are made nondimensional using the mean depth $\tilde{h}_0$. In addition, the flow velocities and pressure are each resolved into steady and disturbance components. Thus, we write

$$t = \tilde{k}\tilde{u}_\ell\tilde{t}, \qquad x = \tilde{k}\tilde{x}, \qquad y = \tilde{y}/\tilde{h}_0,$$
$$h = \tilde{h}/\tilde{h}_0, \qquad u_0 + u' = \tilde{u}/\tilde{u}_\ell \tag{2.1.11}$$
$$v' = \tilde{v}/\alpha\tilde{u}_\ell, \qquad p_0 + p' = \tilde{p}/\tilde{\rho}\tilde{u}_\ell^2$$

where

$$\alpha = \tilde{k}\tilde{h}_0, \qquad u_0 = \tilde{u}_0/\tilde{u}_\ell, \qquad p_0 = \tilde{p}_0/\tilde{\rho}\tilde{u}_\ell^2 \tag{2.1.12}$$

The transformation of the mean-flow relations of the previous section gives

$$u_0 = y, \qquad p_0 = \tilde{p}_{0g}/\tilde{\rho}\tilde{u}_\ell^2 + G(y-1) \tag{2.1.13}$$

where

$$G = \tilde{g}\tilde{h}_0/\tilde{\rho}\tilde{u}_\ell^2 \tag{2.1.14}$$

is the inverse of the Froude number.

We also introduce a dimensionless stream function $\psi'(x,y,t)$ as defined by the following

$$u' = \psi'_y , \quad v' = - \psi'_x \tag{2.1.15}$$

The stream function identically satisfies the dimensionless continuity equation. After transforming the momentum equations (2.1.2) and (2.1.3) by means of the relations (2.1.11) to (2.1.15), we obtain

$$\psi'_{yt} + (y + \psi'_y)\psi'_{xy} - (1 + \psi'_{yy})\psi'_x + p'_x = \frac{1}{\alpha R} (\psi'_{yyy} + \alpha^2\psi'_{xxy}) \tag{2.1.16}$$

$$\psi'_{xt} + (y + \psi'_y)\psi'_{xx} - \psi'_x\psi'_{xy} - \frac{1}{\alpha^2} p'_y = \frac{1}{\alpha R} (\psi'_{xyy} + \alpha^2\psi'_{xxx}) \tag{2.1.17}$$

where

$$R = \tilde{h}_0\tilde{u}_\ell\tilde{\rho}/\tilde{\mu} \tag{2.1.18}$$

is the liquid Reynolds number. The transformation of the boundary conditions (2.1.4) at y = 0 gives

$$\psi' = 0, \qquad \psi'_y = 0 \quad \text{at } y = 0 \tag{2.1.19}$$

The transformed kinematic boundary condition is

$$h_t + (h + \psi'_y)h_x + \psi'_x = 0 \quad \text{at} \quad y = h \tag{2.1.20}$$

The balance of normal and tangential stresses yields

$$\frac{\Lambda'}{\alpha R} = G(h-1) + \frac{\alpha^2 W h_{xx}}{(1+\alpha^2 h_x^2)} + \frac{2\alpha}{R} \psi'_{xy} \frac{1-\alpha^2 h_x^2}{1+\alpha^2 h_x^2} + \frac{2\alpha}{R} (\psi'_{yy} - \alpha^2\psi'_{xx}) \frac{h_x}{1+\alpha^2 h_x^2} \quad \text{at } y = h \tag{2.1.21}$$

$$\chi' = (\psi'_{yy} - \alpha^2\psi'_{xx}) \frac{1-\alpha^2 h_x^2}{1+\alpha^2 h_x^2} - 4\alpha^2\psi'_{xy} \frac{h_x}{1+\alpha^2 h_x^2} \text{ at } y = h \qquad (2.1.22)$$

where

$$\Lambda' = \frac{\alpha R}{\tilde{\rho}\tilde{u}_\ell^2} \left[- \tilde{\sigma}(h) - \tilde{p}_{0g} - \frac{2\tilde{\tau}_0 \tilde{h}_x}{1+\tilde{h}_x^2} \right] \qquad (2.1.23)$$

$$\chi' = \frac{R}{\tilde{\rho}\tilde{u}_\ell^2} \left[\tilde{\tau}(h) - \tilde{\tau}_0 \frac{1-\tilde{h}_x^2}{1+\tilde{h}_x^2} \right] \qquad (2.1.24)$$

$$W = \frac{\tilde{T}}{\tilde{\rho}\tilde{h}_0\tilde{u}_\ell^2} \qquad (2.1.25)$$

W is the inverse Weber number and the shear and pressure perturbation parameters Λ' and χ' are obtained from the analysis of the gas phase.

2.1.4 An Expansion for Small Amplitude

We shall assume a small, but finite-amplitude, disturbance of the liquid surface. Defining the parameter ε as the ratio of the wave amplitude to the mean depth, we let

$$\psi' = \varepsilon\psi_1 + \varepsilon^2\psi_2 + O(\varepsilon^3) \qquad (2.1.26)$$

$$h = 1 + \varepsilon\eta_1 + \varepsilon^2\eta_2 + O(\varepsilon^3) \qquad (2.1.27)$$

$$p' = \frac{1}{\alpha R} (\varepsilon p_1 + \varepsilon^2 p_2) + O(\varepsilon^3) \qquad (2.1.28)$$

$$\Lambda' = \varepsilon\Lambda_1 + \varepsilon^2\Lambda_2 + O(\varepsilon^3) \qquad (2.1.29)$$

$$\chi' = \varepsilon\chi_1 + \varepsilon^2\chi_2 + O(\varepsilon^3) \qquad (2.1.30)$$

where $\varepsilon << 1$. The boundary conditions at $y = h$ are transferred to $y = 1$ by expanding in a Taylor series. Since we are going to examine the temporal variation of the waves, we introduce the slow scale

$$T_1 = \varepsilon t \qquad (2.1.31)$$

Substituting (2.1.26) to (2.1.31) into (2.1.16) to (2.1.22) and balancing powers of ε, we obtain

$O(\varepsilon)$

$$\psi_{1yyyy} - \alpha R(\psi_{1yyt} + y\psi_{1xyy}) + 2\alpha^2\psi_{1xxyy} - \alpha^3 R(\psi_{1xxt} + y\psi_{1xxx}) + \alpha^4\psi_{1xxxx} = 0 \tag{2.1.32}$$

$$\psi_1 = \psi_{1y} = 0 \quad \text{at } y = 0 \tag{2.1.33}$$

$$p_1 + 2\alpha^2\psi_{1xy} + \alpha RG\eta_1 + \alpha^3 RW\eta_{1xx} = \Lambda_1 \text{ at } y = 1 \tag{2.1.34}$$

$$\psi_{1yy} - \alpha^2\psi_{1xx} = \chi_1 \text{ at } y = 1 \tag{2.1.35}$$

$$\eta_{1t} + \eta_{1x} + \psi_{1x} = 0 \quad \text{at } y = 1 \tag{2.1.36}$$

$O(\varepsilon^2)$

$$\psi_{2yyyy} - \alpha R(\psi_{2yyt} + y\psi_{2xyy}) + 2\alpha^2\psi_{2xxyy} - \alpha^3 R(\psi_{2xxt} + y\psi_{2xxx}) + \alpha^4\psi_{2xxxx} = \alpha R(\psi_{1yyT_1} + \psi_{1y}\psi_{1xyy} - \psi_{1x}\psi_{1yyy}) + \alpha^3 R(\psi_{1xxT_1} + \psi_{1y}\psi_{1xxx} - \psi_{1x}\psi_{1xxy}) \tag{2.1.37}$$

$$\psi_2 = \psi_{2y} = 0 \quad \text{at } y = 0 \tag{2.1.38}$$

$$p_2 + 2\alpha^2\psi_{2xy} + \alpha RG\eta_2 + \alpha^3 RW\eta_{2xx} = \Lambda_2 - 2\alpha^2(\psi_{1yy} - \alpha^2\psi_{1xx})\eta_{1x} - (p_{1y} + 2\alpha^2\psi_{1xyy})\eta_1 \quad \text{at } y = 1 \tag{2.1.39}$$

$$\psi_{2yy} - \alpha^2\psi_{2xx} = \chi_2 + 4\alpha^2\psi_{1xy}\eta_{1x} - \eta_1(\psi_{1yyy} - \alpha^2\psi_{1xxy}) \quad \text{at } y = 1 \tag{2.1.40}$$

$$\eta_{2t} + \eta_{2x} + \psi_{2x} = - \eta_{1T_1} - (\eta_1 + \psi_{1y})\eta_{1x} - \eta_1\psi_{1xy}$$

$$\text{at } y = 1 \qquad (2.1.41)$$

2.2 Equations for the Gas Phase

In this section, we develop the equations that govern the disturbances in the gas due to the appearance of waves on the liquid surface. These equations are required to evaluate the pressure and shear perturbations at the interface.

2.2.1 Dimensionless Equations

The following analysis will take into account the mean gas velocity profile, viscosity, compressibility, and thermal conductivity. The major assumption that we shall make is that the gas velocity is sufficiently higher than that of the liquid so that the latter can be neglected. The assumption of neglecting the liquid and wave velocities results in the gas problem being one of steady motion. Other assumptions are (1) ideal gas, (2) constant heat capacity, and (3) constant Prandtl number.

With the exception of the liquid depth $\tilde{h}$, all lengths in the gas problem are made nondimensionless by using the wave number $\tilde{k}$ of an assumed sinusoidal surface disturbance. A dimensionless normal coordinate Y is defined so that it vanishes at the undisturbed liquid surface. All flow quantities are made dimensionless by using the free-stream conditions, denoted by the subscript ∞. Thus, we let

$$x = \tilde{k}\tilde{x} \ , \qquad Y = \tilde{k}(\tilde{y}-\tilde{h}_0) \ , \qquad h = \tilde{h}/\tilde{h}_0$$
$$u = \tilde{u}/\tilde{u}_\infty \ , \qquad v = \tilde{v}/\tilde{u}_\infty \ , \qquad \rho = \tilde{\rho}/\tilde{\rho}_\infty \qquad (2.2.1)$$
$$p = \tilde{p}/\tilde{\rho}_\infty \tilde{u}_\infty^2 \ , \qquad T = \tilde{T}/\tilde{T}_\infty \ , \qquad \mu = \tilde{\mu}/\tilde{\mu}_\infty$$

The governing equations are

Continuity

$$(\rho u)_X + (\rho u)_Y = 0 \qquad (2.2.2)$$

x-Momentum

$$\rho u u_X + \rho v u_Y + p_X = \frac{1}{R_G}\left\{[\mu(\frac{4}{3}u_X - \frac{2}{3}v_Y)]_X + [\mu(u_Y + v_X)]_Y\right\} \qquad (2.2.3)$$

Y-Momentum

$$\rho u v_X + \rho v v_Y + p_Y = \frac{1}{R_G}\left\{[\mu(u_Y + v_X)]_X + [\mu(\frac{4}{3}v_Y - \frac{2}{3}u_X)]_Y\right\} \qquad (2.2.4)$$

Energy

$$\rho(uT_X + vT_Y) = (\gamma-1)M_\infty^2[up_X + vp_Y + \frac{1}{R_G}\Phi] + \frac{1}{PrR_G}[(\mu T_X)_X + (\mu T_Y)_Y] \qquad (2.2.5)$$

State

$$\gamma M_\infty^2 p = \rho T \qquad (2.2.6)$$

where

$$\Phi = \mu[2(u_X^2 + v_y^2) + (u_Y + v_X)^2 - \frac{2}{3}(u_X + v_Y)^2] \qquad (2.2.7)$$

$$R_G = \frac{\tilde{\rho}_\infty \tilde{u}_\infty}{\tilde{k}\tilde{\mu}_\infty} \ , \quad P_r = \frac{\tilde{c}_p\tilde{\mu}}{\tilde{k}} \ , \quad M_\infty^2 = \frac{\tilde{u}_\infty^2}{(\gamma-1)\tilde{c}_p T_\infty} \qquad (2.2.8)$$

are the dissipation function, the gas Reynolds number, the Prandtl number, and the free-stream Mach number, respectively.

The dependence of viscosity on the temperature is estimated by Sutherland's equation

$$\mu = \left(\frac{T}{T_i}\right)^{3/2}\left(\frac{T_i+B}{T+B}\right) \qquad (2.2.9)$$

where $T_i = \tilde{T}_i/\tilde{T}_\infty$ and $B = \tilde{B}/\tilde{T}_\infty$. It should be noted that it would be more appropriate to include the effects of the longitudinal viscosity coefficient, but this consideration becomes worthless when turbulent boundary layers are calculated.

Consistent with the previous assumption regarding the magnitude of the liquid velocities, the boundary conditions at the gas/liquid interface are

$$u = v = 0 \quad \text{at } Y = \alpha(h - 1) \qquad (2.2.10)$$

The outer boundary conditions (i.e. at $Y \to \infty$) are

$$\begin{aligned} \tilde{u} &= \tilde{u}_\infty \\ \tilde{p} &= \text{constant} \\ \tilde{T} &= \tilde{T}_\infty \end{aligned} \qquad (2.2.11)$$

which imply the vanishing of the perturbation quantities away from the interface.

2.2.2 Mean Gas Flow

The flowfields examined here have large Reynolds numbers. As a consequence, the gas problem can be simplified by neglecting the x variation of the mean-flow properties (boundary-layer flow). Details of the particular calulations will be given in Chapter 3.

2.2.3 Disturbance Equations

As in the analysis of the liquid motion, we let $h = 1 + \varepsilon\eta(x,t)$ where $\varepsilon << 1$ and $\eta = O(1)$. The position of the interface is therefore

at $Y = \varepsilon\alpha n$; this means that the disturbance components of the flow properties are $O(\varepsilon)$. Resolving all flow quantities into steady and disturbance components, we write

$$\begin{aligned}
u &= U_0(Y) + \varepsilon\alpha u_1 + \varepsilon^2\alpha u_2 + O(\varepsilon^3) \\
v &= \qquad\quad \varepsilon\alpha v_1 + \varepsilon^2\alpha v_2 + O(\varepsilon^3) \\
\rho &= \rho_0(Y) + \varepsilon\alpha\rho_1 + \varepsilon^2\alpha\rho_2 + O(\varepsilon^3) \\
T &= T_0(Y) + \varepsilon\alpha T_1 + \varepsilon^2\alpha T_2 + O(\varepsilon^3) \\
p &= p_0 + \varepsilon\alpha p_1 + \varepsilon^2\alpha p_2 + O(\varepsilon^3) \\
\mu &= \mu_0(Y) + \varepsilon\alpha\mu_1 + \varepsilon^2\alpha\mu_2 + O(\varepsilon^3)
\end{aligned} \tag{2.2.12}$$

Substituting (2.2.12) into (2.2.2) to (2.2.7) and balancing powers of ε, we obtain

$O(\varepsilon)$

$$(\rho_0 u_1 + \rho_1 u_0)_X + (\rho_0 v_1)_Y = 0 \tag{2.2.13}$$

$$\rho_0 U_0 u_{1X} + \rho_0 U_0' v_1 + p_{1X} - \frac{1}{R_G}\left[\mu_0\left(u_{1YY} + \frac{4}{3}u_{1XX} + \frac{1}{3}v_{XY}\right) + \mu_1 U_0'' + \mu_0'(u_{1X} + v_{1X}) + \mu_{1X} U_0'\right] = 0 \tag{2.2.14}$$

$$\rho_0 U_0 v_{1X} + p_{1Y} - \frac{1}{R_G}\left[\mu_0\left(v_{1XX} + \frac{4}{3}v_{1YY} + \frac{1}{3}u_{1XY} + \mu_{1X} U_0' + \mu_0'\left(\frac{4}{3}V_{1Y} - \frac{2}{3}u_{1X}\right)\right)\right] = 0 \tag{2.2.15}$$

$$\rho_0 U_0 T_{1X} + \rho_0 T_0' v_1 - (\gamma - 1)M_\infty^2\left[U_0 p_{1X} + \frac{1}{R_G}\left[\mu_1 U_0'^2 + 2\mu_0 U_0'(u_{1Y} + v_{1X}) - \frac{1}{R_G Pr}\left(\mu_0 T_{1XX} + \mu_0' T_{1Y} + T_0'\mu_{1Y} + \mu_0 T_{1YY} + \mu_1 T_0''\right)\right] = 0 \tag{2.2.16}$$

$$\gamma M_\infty^2 p_1 - \rho_1 T_0 - \rho_0 T_1 = 0 \tag{2.2.17}$$

$O(\varepsilon^2)$

$$(\rho_0 u_2 + \rho_2 U_0)_X + (\rho_0 v_2)_Y = (\rho_1 u_1)_X - (\rho_1 v_1)_Y \tag{2.2.18}$$

$$\rho_0 U_0 u_{2X} + \rho_0 U_0' v_2 + p_{2X} - \frac{1}{R_G}[\mu_0(u_{2YY} + \frac{4}{3} u_{2XX} + \frac{1}{3} v_{2XY}) + \mu_0'(u_{2Y} + v_{2X}) + \mu_{2Y} U_0' \tag{2.2.19}$$

$$= -(\rho_1 U_0 + \rho_0 u_1)u_{1X} - (\rho_1 U_0' + \rho_0 u_{1Y})v_1 + \frac{1}{R_G}[\mu_1(u_{1YY} + \frac{4}{3} u_{1XX} + \frac{1}{3} v_{1XY}) + \mu_{1X}(\frac{4}{3} u_{1X} - \frac{2}{3} v_{1Y}) + \mu_{1Y}(u_{1Y} + v_{1X})] \tag{2.2.20}$$

$$\rho_0 U_0 v_{2X} + p_{2Y} - \frac{1}{R_G}[\mu_0(v_{2XX} + \frac{4}{3} v_{2YY} + \frac{1}{3} u_{2XY}) + \mu_{2X} U_0' + \mu_0'(\frac{4}{3} v_{2Y} - \frac{2}{3} u_{2X})] = -(\rho_0 u_1 + \rho_1 U_0)v_{1X} - \rho_0 v_1 v_{1Y} + \frac{1}{R_G}[\mu_1(v_{1XX} + \frac{4}{3} v_{1YY} + \frac{1}{3} u_{1XY}] + \mu_{1Y}(\frac{4}{3} v_{1Y} - \frac{2}{3} u_{1X}) + \mu_{1X}(u_{1Y} + v_{1X})] \tag{2.2.21}$$

$$\rho_0 U_0 T_{2X} + \rho_0 T_0' v_2 - (\gamma - 1)M_\infty^2[U_0 p_{2X} + \frac{1}{R_G}[\mu_2 U_0'^2 + 2\mu_0 U_0'(u_{2Y} + v_{2X})] - \frac{1}{R_G Pr}(\mu_0 T_{2XX} + \mu_0' T_{2Y} + T_0' \mu_{2Y} + \mu_0 T_{2YY} + \mu_2 T_0'') = -(\rho_0 u_1 + \rho_1 U_0)T_{1X} - (\rho_0 T_{1Y} + \rho_1 T_0')v_1 + (\gamma - 1)M_\infty^2[u_1 p_{1X} + v_1 p_{1Y} + \frac{1}{R_G} \times [2\mu_1 U_0'(u_{1Y} + v_{1X}) + \frac{4}{3}(u_{1X}^2 + v_{1Y}^2) - \frac{4}{3} u_{1X} v_{1Y} + (u_{1Y} + v_{1X})^2] + \frac{1}{R_G Pr}(\mu_{1X} T_{1X} + \mu_1 T_{1XX} + \mu_{1Y} T_{1Y} + \mu_1 T_{1YY}) \tag{2.2.22}$$

$$\gamma M_\infty^2 p_2 - \rho_2 T_0 - \rho_0 T_2 = p_1 T_1 \tag{2.2.23}$$

Sutherland's viscosity law gives

$O(\varepsilon)$

$$\mu_1 = \mu_0(\frac{3}{2T_0} - \frac{1}{T_0 + B})T_1 = b_1 T_1 \tag{2.2.24}$$

$O(\varepsilon^2)$

$$\mu_2 = \mu_0\left(\frac{3}{2T_0} - \frac{1}{T_0+B}\right)T_2 + \mu_0\left[\frac{1}{8T_0^2} + \frac{1}{(T_0+B)^2} - \frac{3}{2T_0(T_0+B)}\right]T_1^2$$

$$= b_1 T_2 + b_2 T_1^2$$

We transfer the boundary conditions to the mean interface $Y = 0$ by using a Taylor series expansion. Assuming adiabatic flow, we obtain the following transferred conditions:

$O(\varepsilon)$

$$u_1(0) + \eta_1 U_0'(0) = 0$$

$$v_1(0) = 0 \qquad (2.2.25)$$

$$T_1(0) + \eta_1 T_0'(0) = 0$$

$O(\varepsilon^2)$

$$u_2(0) + \eta_2 U_0'(0) = -\alpha\eta_1 u_{1Y}(0) - \frac{1}{2} U_0''(0)\alpha\eta_1^2$$

$$v_2(0) = -\alpha\eta_1 v_{1Y}(0) \qquad (2.2.26)$$

$$T_2(0) + \eta_2 T_0'(0) = -\alpha\eta_1 T_{1Y}(0) - \frac{1}{2} T_0''(0)\alpha\eta_1^2$$

Substituting the expressions for the normal and tangential gas stresses at the interface into the definitions of Λ and χ, (2.1.23) and (2.1.24), we obtain

$O(\varepsilon)$

$$\frac{C_f\Lambda_1}{\alpha^2} - p_1 - \frac{2\mu_0}{R_G}(u_{1X} - 2v_{1Y}) = 0 \quad \text{at } Y = 0 \qquad (2.2.27)$$

$$\frac{C_f\chi_1}{\alpha} - \frac{1}{R_G}[\mu_0(u_{1Y} + v_{1X}) + U_0'\mu_1] = 0 \quad \text{at } Y = 0 \qquad (2.2.28)$$

$\underline{O(\varepsilon^2)}$

$$\frac{C_f \Lambda_2}{\alpha^2} - p_2 - \frac{2\mu_0}{R_G}(u_{2X} - 2v_{2Y}) = \alpha\eta_1 \frac{\partial}{\partial Y}\left[p_1 + \frac{2\mu_0}{R_G}(\mu_{1X} - 2v_{1Y})\right]$$

$$+ \alpha \frac{2\mu_1}{R_G}(u_{1X} - 2v_{1Y}) + \frac{2\alpha\mu_0}{R_G}\eta_{1X}(u_{1Y} + v_{1X}) \text{ at } Y = 0 \qquad (2.2.29)$$

$$\frac{C_f \chi_2}{\alpha} - \frac{1}{R_G}[\mu_0(u_{2Y} + v_{2X}) + U_0'\mu_2] = \alpha\eta_1 \frac{1}{R_G}\frac{\partial}{\partial Y}[\mu_0(u_{1Y} + v_{1X}) + U_0'\mu_1]$$

$$+ \alpha \frac{\mu_1}{R_G}(u_{1Y} + v_{1X}) - \frac{2\alpha}{R_G}\mu_0\eta_{1X}(v_{1Y} - u_{1X}) \text{ at } Y = 0 \qquad (2.2.30)$$

3. LINEAR GAS PROBLEM

Since the phase velocities of the waves examined in this study are much smaller than any typical velocity inside the gas boundary layer, the interface will appear as a stationary wavy wall to the gas. That is, the transient motion in the gas can be neglected. The waves on the interface introduce pressure and shear perturbations that affect their stability characteristics.

Examining the problem of a shock impinging on a boundary layer, Lighthill (1953) simplified the Navier-Stokes equations by confining the effects of viscosity on the disturbance to a small (compared with the boundary-layer thickness) region near the wall. Moreover, he assumed the mean-flow profiles to be linear within the sublayer region. Outside this region the flow is rotational, but inviscid. A number of investigators follwed his approach. In studying the separation problem, Stewartson (1969) included the effects of nonlinearity, Inger (1971) analyzed compressible boundary-layer flow past a wavy wall, while Mason and Inger (1974) studied the transonic-shock/boundary-layer interaction problem. Bordner, Nayfeh and Saric (1975) used the method of composite expansions (Nayfeh, 1973; Section 4.2) to analyze compressible, boundary-layer flows past wavy walls. When the wave amplitude is large enough to cause separation, the boundary-layer equations need to be solved numerically, as done by Fannelop and Flugge-Lotz (1963) and Polak et al (1975). Benjamin (1959) studied incompressible boundary-layer flows over compliant boundaries and pointed out that, in the case of turbulent flows, the velocity might not be linear in the sublayer (the basic

assumption in Lighthill's analysis) due to the large gradients involved. Next, we assess the validity of this assumption.

3.1 Problem Formulation

We use a semi-analytical technique to determine compressible viscous flows past wavy walls without restricting the mean flow to be linear in the disturbance sublayer. Comparisons are made with the experiments of Williams and Inger (1970).

We consider a two-dimensional steady compressible flow over a wavy wall having the equation (see Fig. 2)

$$y^* = \varepsilon^* \cos k^* x^* \tag{3.1.1}$$

or, equivalently, $\eta_1 = \eta_0 \exp(ix)$. We assume a parallel mean flow and a linear disturbance. The parallel mean flow assumption limits the applicability of the present results to subsonic and moderately supersonic flows as shown by Lees and Reshotko (1962) and Brown (1964). Equation (3.1.1) demands that any linear disturbance must vary sinusoidally with the axial distance.

The governing equations for the disturbance are equations (2.2.11), (2.2.13) to (2.2.17), (2.2.25). Moreover, equation (3.1.1) demands that

$$\begin{aligned} u_1(x,y) &= \eta_0 u(y) e^{ix} + cc, \\ v_1(x,y) &= \eta_0 v(y) e^{ix} + cc \\ T_1(x,y) &= \eta_0 T(y) e^{ix} + cc \\ p_1(x,y) &= \eta_0 p(y) e^{ix} + cc \\ \rho_1(x,y) &= \eta_0 \rho(y) e^{ix} + cc \end{aligned} \tag{3.1.2}$$

where $\eta_0 = \varepsilon^* k^*$ and cc stands for the complex conjugate of the preceding terms. Substituting equations (3.1.2) into (2.2.13) to (2.2.17), we can express the disturbance equations in the form:

$$\frac{dz_i}{dY} = \sum_{j=1}^{6} a_{ij} z_j \qquad i = 1,\ldots 6 \tag{3.1.3}$$

where

$$z_1 = u(Y)\ , \qquad z_2 = du/dY\ , \qquad z_3 = v(Y),$$
$$z_4 = p(Y)\ , \qquad z_5 = T(Y)\ , \qquad z_6 = dT/dY \tag{3.1.4}$$

and the a_{ij}'s are given in Appendix A, if m is set equal to unity.

At the wall the no-slip and no-penetration conditions (2.2.23) yield the boundary conditions

$$u_1 = -\frac{dU_0}{dY} \quad \text{at } Y = 0 \tag{3.1.5}$$

and

$$v_1 = 0 \quad \text{at } Y = 0 \tag{3.1.6}$$

For the temperature perturbation, we assume either an isothermal wall

$$T_1 = -\frac{dT_0}{dY} \quad \text{at } Y = 0 \tag{3.1.7}$$

or a constant heat-transfer rate

$$\frac{dT_1}{dY} = -\frac{d^2T_0}{dY^2} \quad \text{at } Y = 0 \tag{3.1.8}$$

In arriving at these boundary conditions, the actual boundary conditions were transferred to the mean position of the wall. This is justified when $\varepsilon << 1$; that is, when the amplitude ε^* of the disturbance is small compared with the disturbance wavelength λ^*. Since the flow is viscous, all disturbances must tend to zero as $y \to \infty$.

To determine the rate at which the disturbances decay as $y \to \infty$, we note that the mean-flow quantities become constants as $y \to \infty$ and

equations (3.1.3) reduce to the following system of equations with constant coefficients:

$$\frac{dz}{dY} = Az \tag{3.1.9}$$

where z is a 6 x 1 matrix and A is a 6 x 6 matrix that is defined in Appendix B. Equations (3.1.9) admit solutions of the form

$$z_i = \sum_{j=1}^{6} c_{ij}\exp(\lambda_j Y) \text{ for } i = 1,2,\ldots,6 \tag{3.1.10}$$

where the c_{ij} are constants and the λ_j are the eigenvalues of the system

$$|A - \lambda I| = 0 \tag{3.1.11}$$

Since A is a 6 x 6 matrix, equation (3.1.11) has six roots. Three of these roots have positive real parts and the other three have negative real parts as shown in Appendix B. In order for the disturbance to vanish away from the wall, the solutions that grow exponentially with y must be discarded. This leaves three linear independent solutions that decay exponentially with y. Hence, as $y \to \infty$, the boundary conditions are taken in the form

$$Dz = 0 \quad \text{at } Y = Y_0 \tag{3.1.12}$$

where Y_0 is any value larger than the boundary-layer thickness and D is a 6 x 3 constant coefficient matrix that is defined in Appendix B.

3.2 Mean-Flow Solution

The first step in the computational procedure is the generation of the elements of the matrix A of equation (3.1.3). These coefficients depend on the mean flow. For laminar flows, the mean-flow

profiles are generated by using the Illingworth-Stewartson transformation (1964), which leads to a second-order integro-differential equation of the form:

$$\frac{d}{dY}\left(c_1 \frac{dU_0}{dY}\right) + \left(c_2 \int_0^Y \frac{U_0}{T_0}\, dY\right) \frac{dU_0}{dY} = 0 \qquad (3.2.1)$$

where c_1 and c_2 depend on the variable viscosity. This equation is then solved by using finite differences. It is worthwhile to note the excellent stability of the Thomas algorithm and the insensitivity of the solution of this equation to the step size of integration. A representative of these calculations is shown in Figure 3.

For turbulent flows, the mean-flow profiles are calculated by using a combination of different approaches as developed and presented by Inger (1971). We are making the assumption of quasi-laminar behavior in the disturbance field; that is, the disturbance and the turbulent flow are uncorrelated. Then an equation of the form

$$\frac{dU_0}{dY} = f(c_f, R_G, \text{effective viscosity coefficient, shear stress, turbulent sublayer thickness}) \qquad (3.2.2)$$

is integrated. An interation scheme is used to update the turbulent sublayer thickness so that the condition $U_0(0) = 0$ is satisfied within any prescribed accuracy. The velocity and temperature are related by the Crocco relationship. A representative of these calculations is shown in Figure 4.

3.3 Computational Procedure

Once the mean profile is calculated, A, dU_0/dY, dT_0/dY, and d^2T_0/dY^2 can be determined. Thus, the problem is reduced to the solu-

tion of the system of six first-order differential equations (3.1.3) subject to the boundary conditions (3.1.5), (3.1.6), (3.1.12), and either (3.1.7) or (3.1.8).

A straightforward integration of equations (3.1.3) utilizing superposition of solutions fails because of parasitic errors among the six solutions, due to the finite word-length of computers. We consider the following example from Scott and Watts (1975). Let $\zeta_1(x)$ be the solution of

$$\begin{aligned} &\zeta_1''(x) = \zeta_1(x) \ , \\ &\zeta_1(0) = 1 \ , \ \zeta'(0) = 0 \end{aligned} \tag{3.3.1}$$

and $\zeta_2(x)$ be the solution of

$$\begin{aligned} &\zeta_2''(x) = \zeta_2(x) \\ &\zeta_2(0) = 0, \ \zeta_2'(0) = 1 \end{aligned} \tag{3.3.2}$$

Then $\zeta_1(x) = \cosh x$ and $\zeta_2(x) = \sinh x$. Mathematically, these two functions are linearly independent for all x. However, suppose we are using a computer which carries six digits. Then for x greater than about eight, the two functions $\zeta_1(x)$ and $\zeta_2(x)$ are identical. If the computer carries fourteen digits, the functions are distinguishable until about x = 17. In this study, we used a method developed by Scott and Watts (1975) which is based on the principle of superposition and a normalization procedure. The approach is due to Godonov (1961).

To explain the method, we consider linear boundary-value problems of the form

$$\begin{aligned} &\zeta'(x) = F(x)\zeta(x) + g(x) \\ &A\zeta(a) = \alpha \\ &B\zeta(b) = \beta \end{aligned} \tag{3.3.3}$$

where ζ and g are vector functions with n components, F is an n x n matrix, A is an (n - k) x n matrix of rank n - k, B is a k x n matrix of rank k, α is a vector with n - k components, and β is a vector with k components. We shall assume that the given boundary-value problem has a unique solution.

Any solution of (3.3.3) can be written as a linear combination of solutions of the homogeneous equation and a particular solution of the inhomogeneous equation; that is,

$$\begin{aligned}\zeta(x) &= c_1u_1(x) + c_2u_2(x) + \ldots + c_ku_k(x) + v(x) \\ &= U(x)c + v(x)\end{aligned} \tag{3.3.4}$$

where U(x) denotes an n x k matrix whose columns $u_1(x), \ldots, u_k(x)$ are linearly independent solutions of the homogeneous system

$$U'(x) = F(x)U(x) \tag{3.3.5}$$

and v(x) is the solution of

$$v'(x) = F(x)v(x) + g(x) \tag{3.3.6}$$

In particular, (3.3.4) will satisfy (3.3.3) if the initial conditions for the $u_i(x)$ and v(x) are chosen so that

$$\begin{aligned}AU(a) &= 0 \\ Av(a) &= \alpha\end{aligned} \tag{3.3.7}$$

respectively. In order to specify the constants $c_1, \ldots, c_k$ in (3.3.4), we evaluate (3.3.4) at x = b, substitute the result into (3.3.3), and obtain

$$B\zeta(b) = BU(b)c + Bv(b) = \beta \tag{3.3.8}$$

This represents a system of k linear equations for the k unknowns $c = (c_1, \ldots, c_k)^T$, which we refer to as the superposition or linear

combination coefficients. The solution of the original boundary-value problem (3.3.3) is now completely specified. Note that all of the equations to be integrated, namely (3.3.5) and (3.3.6) along with (3.3.7), can now be treated as initial-value problems. This allows us to use sophisticated integrators for the initial-value problems. We have arbitrarily defined the initial point to be a; so the integration proceeds from a to b. In practice, the choice of initial point is made by the user of the code. This can be important in achieving an efficient solution.

Although the superposition method is conceptually simple and works in many instances, it has two major drawbacks. In order for the method to yield accurate results, it is imperative that $v(x)$ and the columns of $U(x)$ be linearly independent for all x. The initial conditions, as given by (3.3.7), theoretically insure that $v(x)$ and the columns of $U(x)$ are linearly independent. However, due to the finite word-length used by computers, the solutions may lose their numerical independence. The resulting matrix problem in (3.3.8) may be so poorly conditioned that c cannot be determined accurately.

The second problem, although also related to the finite word-length of the computer, is a loss of significance and can occur even if the linear combination vector c has been computed accurately. This will normally occur if the base solutions are large compared with the desired solution; that is, accuracy is lost in the recombination of (3.3.4).

Since the real parts of the eigenvalues of A are well-separated, one cannot continue to calculate accurately six linearily independent

solution vectors of Equations (3.1.3). If two of the λ_j differ by a factor of 10, one solution grows by the factor $\exp(10n\Delta\zeta)$ relative to the other, as one integrates n steps toward the wall. Thus a round-off error of 10^{-12} may quickly dominate the solution. These characteristics are similar to those encountered in the solution of the Orr-Sommerfeld equation, and thus one can use one of the techniques that have been successfully used for its solution.

To reduce the computational time while keeping reasonable accuracy, we use a fifth-order Runge-Kutta routine to perform two integrations, the step size used in one of them is twice the step size used in the other. Comparing the results of these integrations, we determine a "global error" based on the difference between the results of these integrations. If this error is less than a prescribed value, the integration is continued and orthonormalization is not needed. However, if the global error is above the prescribed value, the solution vectors are orthonormalized and then the integration is continued. The orthonormalization is carried out using a modified Gram-Schmidt method.

The number of orthonormalizations needed depends on the eigenvalues of A, the Reynolds number being the main factor. For laminar mean-flows, about 8 orthonormalizations are needed, requiring about 5 minutes on an IBM 370/158 computer. For turbulent mean flows, we examined cases where up to 150 orthonormalizations were needed, requiring about 40 minutes. Application of the free-stream boundary conditions at different y-stations was used as a check. The mean-flow quantities quantities appear as parameters in (3.1.3). However, they need to be specified very accurately. Seventh-order polynomial interpolation has

failed to produce satisfactory results. Hence, the mean-flow equations are reintegrated as a nonlinear initial-value problem simultaneously with the solution of the perturbation equations.

3.4 Results of the Wavy-wall Problem and Discussion

Lighthill (1953) examined the interaction of shock waves with a boundary layer. Inger (1971), analyzing compressible flow over wavy walls, extended the analysis of Lighthill by including the effects of heat transfer. Their analyses are based on the assumption that the mean-flow profiles are linear within the disturbance sublayer. Figures 3 and 4 show that this assumption is invalid unless the disturbance sublayer is extremely thin in comparison with the mean boundary layer, especially for turbulent mean flows. Figure 5 shows that, for large wavelengths, the laminar sublayer in a turbulent boundary layer can be thinner than the disturbance sublayer.

In Figures 6 and 7, we investigate the validity of the assumption that the turbulent mean-flow profiles are linear within the disturbance sublayer. To this end, we show the variations of the amplitudes of the pressure and shear perturbations with the ratio of the thicknesses of the disturbance sublayer and the mean boundary layer as calculated from Lighthill's analysis and the present analysis. It is clear from Figure 6 that Lighthill's theory is valid only for very small values of δ_s/δ. When $(\delta_s/\delta) \approx 35 \times 10^{-4}$, there is an order-of-magnitude difference between the amplitudes of the shear perturbations calculated from the Lighthill and the present analysis. As δ_s/δ increases, the magnitude of the difference increases rapidly. Figure 7

shows the variations of the positions of the maximum pressure and shear perturbations with δ_s/δ. This figure shows that there are also large differences between the values calculated from Lighthill's theory and our results for values of δ_s/δ as small as 20×10^{-4}. Whereas Lighthill's theory predicts that $\Phi_p - \Phi_s = 120°$, regardless of the value of δ_s/δ, our results show that $\Phi_p - \Phi_s$ is a strong function of δ_s/δ as shown in Figure 7. Thus, the assumption that the mean-flow profiles are linear in the disturbance sublayer is valid only for very small values of δ_s/δ.

Williams and Inger (1970) presented experimental data for the pressure perturbations exerted by a compressible flow on a wavy wall. Figures 8 and 9 compare the experimental amplitudes and phases of the pressure perturbations with those calculated from both Lighthill's theory and our theory. These figures show clearly that our analysis is an improvement over Lighthill's theory, especially for the phase angle. We note that as the Mach number increases, the maximum pressure predicted by the present theory approaches its supersonic position faster than the maximum pressure predicted by Lighthill's theory.

Figures 10 and 11 show that in the case of laminar flows, the assumption of linear profiles within the disturbance sublayer is valid for quite large values of δ_s/δ compared with the case of turbulent flows, as one would expect.

4. LINEAR STABILITY ANALYSIS

In this chapter, we analyze the linear stability of a liquid film adjacent to a compressible gas stream. The solution is valid for all wavenumbers and Reynolds numbers. The principal assumption is that the wave amplitude is infinitisimal.

It will be assumed that the experimentally observed waves correspond to those with a maximum linear amplification rate. The results of this analysis are compared with both subsonic and supersonic experiments.

Improvements over the work of Bordner et al (1975) include a numerical solution of the Orr-Sommerfeld equation (without any simplifying assumptions) and an improved solution of the gas equations. Also calculations are made for turbulent boundary layers.

4.1 Linear Equations for the Liquid

The assumption of an infinitisimal disturbance, which implies $\varepsilon \to 0$, allows us to drop all nonlinear terms in the problem. However, in this chapter, we will not place any restrictions on the magnitude of α or R.

To eliminate p_1 from (2.1.34), we use the x-momentum equation

$$p_{1x} = \psi_{1yyy} + \alpha^2\psi_{1xxy} - \alpha R(\psi_{1yt} + y\psi_{1xy} - \psi_{1x}) \qquad (4.1.1)$$

The liquid interface is assumed to have the following two-dimensional travelling-wave form

$$n_1 = n_0 e^{i(x-ct)} \qquad (4.1.2)$$

The parameter c is the complex wave speed. The real part of c is the phase speed of the wave and the imaginary part is the amplification rate of the disturbance. The solution of (2.1.32) is assumed to have the form

$$\psi_1 = \phi(y)\eta_1(x,t) \tag{4.1.3}$$

Substituting (4.1.1) - (4.1.3) into equations (2.1.32) - (2.1.36) and eliminating the variable p, we obtain the following governing equations for the liquid problem:

$$\phi^{iv} - 2\alpha^2\phi'' + \alpha^4\phi = i\alpha R(y-c)(\phi_{yy} - \alpha^2\phi) \tag{4.1.4}$$

$$\phi(0) = 0 \ , \ \phi'(0) = 0 \tag{4.1.5}$$

$$C = 1 + \phi(1) \tag{4.1.6}$$

$$\phi''' - 3\alpha^2\phi' = i\Lambda + i\alpha R[\alpha^2 W - G - (c-y)\phi' - \phi] \text{ at } y = 1 \tag{4.1.7}$$

$$\phi'' + \alpha^2\phi = \chi \text{ at } y = 1 \tag{4.1.8}$$

where we have assumed

$$\Lambda_1 = \Lambda\eta_1 \ , \quad \chi_1 = \chi\,\eta_1 \tag{4.1.9}$$

Equation (4.1.4) is the Orr-Sommerfeld equation for a linear primary velocity profile which, together with the boundary conditions (4.1.5) (4.1.8), forms an eigenvalue problem for c. The constants Λ and χ are complex; the real and imaginary parts are the components of Λ and χ which are in phase with the amplitude and the slope of the wave, respectively. These constants are determined from the analysis of the gas phase in Section 4.2.

4.2 Linear Equations for the Gas

The gas problem is solved in Chapter 3. From the solution we calculate the pressure and shear-perturbation coefficients. Equations (2.2.27) and (2.2.28) give

$$\Lambda = \frac{\alpha^2}{c_f} \quad z_4(0) + \frac{2\mu_0}{R_G}\left[iz_1(0) - 2\,\frac{dz_3(0)}{dY}\right] \tag{4.2.1}$$

$$\chi - \frac{\alpha}{c_f R_G} \quad \mu_0[z_2(0) + iz_3(0)] + U_0' b_1 z_5(0) \tag{4.2.2}$$

4.3 Experiments

Early experiments with a nearly incompressible, turbulent gas flow by Gater and L'Ecuyer (1971) showed a stable liquid layer. However, they only considered laminar boundary layers. As part of an independent parallel effort, Gold (1973) conducted experiments with turbulent boundary layers.

In this work, we compare the analysis with the experimental result of Saric et al (1976). The experiments were conducted in New York University's hypersonic wind tunnel at a free-stream Mach number of 6. This tunnel is an intermittent, blowdown-to-vacuum type. It is electrically heated. The test section is axisymmetric, 60 cm long and 30 cm in diameter.

The model is a spherically blunted cone having a nosetip diameter Of 2.54 cm. The nosetip is removable and is made of porous stainless steel manufactured by McDonnell-Douglas using a special process. The liquid was expelled through the tip by means of a high-pressure system connected to the base of the model.

The interface response was photographed with high-speed 16 mm and 35 mm cameras. The cameras observed the model through a side window on the tunnel in the presence of top, bottom, and side lighting provided by high-intensity tungsten lamps. The depth of the liquid and the waves superposed on the liquid-gas interface measured by two "end-effect" capacitance gauges similar to those developed by Nachtsheim and Seegmiller (1968) and Marshall and Tiederman (1972).

Waves were observed to form on the surface of a stable liquid film. This was true for all liquid Reynolds numbers, fluids, and for both laminar and turbulent boundary layers, if the gas boundary layer is supersonic. However, experiments with subsonic boundary layers show considerable entrainment. Careful pressure measurements in the nose region of the model show that the entrainment is not due to flow separation, and it must be due to instabilities of the liquid surface.

The results of Gold (1973) are qualitatively in agreement with those of Saric et al (1976), but the experiments differ in their details. Gold used both wedge and cone-shaped models, but his collant was pure water. Therefore, the only way he could change the liquid Reynolds number was by changing the flow rate. Also he used a photo-densitometer to determine the wave characteristics, while Saric et al used an end-effect capacitance and motion pictures. Therefore, he did not present frequency or wavenumber data. He observed a reduction of the wave amplitude with increasing gas shear, which was also observed by Saric et al. The main difference between these two sets of experiments

is that Gold did not concentrate on the interface characteristics; instead he concentrated on the behavior of the heat-transfer rates and on the angle-of-attack effects.

4.4 Results of the Linear Model and Discussion

To determine solution of the liquid problem, we converted (4.1.4) into a system of four first-order equations and subsequently solved them as a two-point boundary-value problem. Thus, we avoided using approximate evaluations of integrals of the Airy Functions (which constitute a solution to the Orr-Sommerfeld equation for a linear velocity profile) as it was done by Bordner et al (1975). A complex Newton-Raphson iteration scheme that converges rapidly was used to obtain the correct eigenvalue c. Another improvement is the input data for the mean-flow calculations. These were taken from the output of BLIMPL. BLIMP is a computer code developed by Kendall and Bartlett (1972) and Anderson and Kendall (1969) to calculate the gas boundary-layer properties. BLIMPL is a nonsimilar, variable-property, boundary-layer solver, developed by Gross and Kendall (1970), based on BLIMP. It is modified for liquid layers such as those found in transpiration-cooling systems. The air-over-water calculations were made by first running BLIMP under conditions of a gas-over-water where quasi-steady equilibrium was assumed between the liquid and the gas at the interface. The interfacial shear and mass transfer, along with the equilibrium temperature, were calculated. These results were then used as input to BLIMPL, which in turn calculated the velocity and temperature distributions in the liquid.

Depending on the wall conditions of the liquid and the amount of blowing, an iterative procedure was carried out between the two programs to get the convergent results.

Integral boundary-layer properties (such as boundary-layer thickness, free-stream conditions, and Reynolds numbers) were taken from BLIMPL so that the mean-flow calculations correspond very accurately to the flowfield down to the measuring capacitance gauges.

For the case of laminar boundary layers the results are similar to those of Bordner et al (1975). The comparison between the theory and the experiments is based on the maximum amplified waves. The theory predicts the trends in the experimental data but the quantitative agreement is poor.

Calculations are also made for turbulent boundary layers. Figure 12 shows the comparison between the predicted and observed frequencies. The agreement is poor. The case of pure water is not shown, but the calculations show the corresponding curve to be in the region of 10 kHz. Figure 13 shows the predicted wavenumbers. Due to the thinness of the liquid film (high shear) in this case, it is not possible to obtain wavenumber measurements.

Calculations are also made for subsonic boundary layers. BLIMPL is not used in this case. The mean flow properties correspond to the following experimental test matrix:

TYPE OF FLOW	FREESTREAM PRESSURE (atm)	STAGNATION TEMPERATURE (°K)	MACH NUMBER	$\frac{Re}{m} \times 10^{-6}$
LAMINAR	0.510	464	0.72	3.94
TURBULENT	2.687	497	0.85	20.54

Figures 14 and 15 show the amplification rates for laminar and turbulent flows, respectively. Comparing these curves with the work of Bordner et al (1975) and our calculations for the supersonic case, we see that the range of wavenumbers for which a positive amplification rate exists is much higher in the subsonic case, for the conditions corresponding to those in the experiments. Hence, we conclude that, in spite of the improvements made, the linear model is still inadequate to predict the observed waves. A nonlinear analysis is needed in order to obtain better agreement with the experiments and predict the waveamplitudes, something that the linear theory cannot do.

Bordner (1973) found that the waves are weakly dispersive for low wavenumbers, which include the experimentally observed ones. Hence, the nonlinear theory should include a number of harmonics in the first-order solution. Figure 16 supports this argument. It shows the variation of the phase speed with the wavenumber. The curve shows that at low wavenumbers, harmonic resonances may occur; that is, waves with wavenumbers which are multiple integer of each other have the same or approximately the same phase speed. Experimental evidence comes from Saric et al (1976). At each liquid Reynolds number for the

turbulent flows, two waves having frequencies in the ratio of two to three are observed. Our calculations show that in the case of laminar flows, the fundamental frequency is below 40 Hz, which cannot be measured, due to the finite length of the model.

Figure 17 shows that for low liquid Reynolds numbers resonance conditions do not exist, which is supported by experimental observations. Figure 18 compares the predicted frequencies for a turbulent gas boundary layer with the observed frequencies. The predicted frequencies correspond to conditions of perfect resonance.

With the experimental evidence that the observed waves are due to harmonic interactions, we proceed in the next chapter to describe a nonlinear stability analysis that accounts for second-harmonic resonance.

5. THE NONLINEAR STABILITY ANALYSIS

Nayfeh and Saric (1973) studied the nonlinear stability of dispersive waves on a thin film adjacent to a supersonic gas stream. They assumed an inviscid irrotational gas and obtained a solution valid for $\alpha << 1$ and $R = O(1)$. They found that waves grow according to

$$\frac{da}{dt} = c_1 a + \varepsilon^2 c_3 a^3 \qquad (5.1.1)$$

where c_1 is the linear amplification rate, c_3 is the nonlinear correction to the amplification rate, and εa is the wave amplitude (relative to the film thickness).

The most significant result of Nayfeh and Saric is that c_3 is negative. This means that linearly unstable waves ($c_1 > 0$) will grow to a finite amplitude of $\varepsilon\alpha = \sqrt{-c_1/c_3}$ and remain at this amplitude. This result is in quantitative agreement with observations in supersonic experiments. Also, the stabilizing effect of amplitude may explain the low entrainment rates observed by some experimenters. However, they neglected the gas viscosity and mean profile in calculating the pressure perturbations exerted by the gas on the interface. In spite of the success of this new model in predicting the existence of the experimentally observed periodic waves, it cannot predict quantitatively the observed wavelengths and their corresponding amplitudes. Therefore, this model was improved by Bordner and Nayfeh (1974) by including the effects of gas viscosity and mean profile in calculating the pressure and shear perturbations exerted by the gas on the gas/liquid interface. In the next section, we use this analysis with the improved gas model of Chapter 3 to correlate the data.

5.1 Comparison with the Experiments, for the Model of Bordner and Nayfeh

As we mentioned in the previous section, the observed frequencies do not correspond to the maximum amplified disturbances suggested by the linear theory. The nonlinear theory shows that due to the stabilizing effect of the nonlinearity, these disturbances do not grow indefinitely, but achieve steady-state amplitudes. Moreover, the steady-state amplitude of the maximum amplified wave according to the linear theory does not have the largest steady-state amplitude. In fact, it is very much smaller than the steady-state amplitude of the wave corresponding to $Im(c_3) \approx 0$. Therefore, we follow Bordner and Nayfeh (1974) and correlate the observed frequencies and wavenumbers with those corresponding to $Im(c_3) = 0$.

For the case of laminar boundary layers, the predicted frequencies and wavenumbers agree closely with the new experimental data (figures 19 and 20). An important result is that for small wavenumbers we observe positive nonlinear amplification rates, which means growing waves contrary to the experimental observations. By examining this region of wavenumbers more carefully, we found a second zero of the nonlinear amplification rate. However, it occurs at a frequency and a wavenumber too small to be measured.

For the case of turbulent boundary layers, we made again the "quasi-laminar" assumption (i.e., the disturbances and the turbulent fluctuations are uncorrelated). The nonlinear theory predicts two maximum-amplitude waves; that is, there are two frequencies for which

$Im(c_3) = 0$. This is in agreement with the experiments which show two dominant frequencies for each run. The variation of the predicted frequencies with the liquid Reynolds number is shown in Figure 21 along with the observed frequencies. Moreover, the variation of the predicted wavenumbers with the liquid Reynolds number is shown in Figure 22. We are not able to determine accurately the wavelengths from the data, for the reason explained before.

In spite of the success of the present nonlinear analysis in predicting the observed frequencies, it cannot predict quantitatively the observed amplitudes.

The principle assumptions made in the analysis of Bordner and Nafeh (1974) are:

1. long waves ($\alpha << 1$)
2. small amplitude ($\varepsilon << 1$), and
3. dispersive waves.

The prediction of observed wave properties will be made on the basis of maximum amplitude, rather than maximum amplification.

Some obvious deficiencies of the dispersive model are its inability to predict wave amplitude and its inability to predict wave speeds and frequencies corrected for amplitude effects. Bordner and Nayfeh (1974) noted that wave speeds for the two modes approach each other at low wavenumbers. For the range of wavenumbers where the difference in (real) wave speeds is $O(\varepsilon)$, the waves are weakly dispersive.

The discovery that waves are weakly dispersive at the lower range of wavenumbers, which indluces the observed wavenumbers, is a very significant result. It means that the behavior of observed waves and

the factors affecting their stability are quite different than what we expected. For example, an initial sinusoidal disturbance in this region will grow to a periodic disturbance which deviates appreciably from a sinusoidal shape. Also, wave modes will interact strongly or, in other words, energy will be readily transferred from higher to lower harmonics. The number of modes involved in the process could be two, three, or more depending on the size of the detuning for the high modes.

Bordner and Nayfeh (1974) improved upon their solution by carrying out an expansion with the first-order term containing the fundamental and its second harmonic; they found that the steady-state amplitudes of the fundamental and its second harmonic are finite, but the amplitude of the third harmonic has a singularity. Adding the third harmonic to the first-order solution, they found that the amplitude of the fourth harmonic has a singularity. Thus, the waves are weakly dispersive for small α and it appears that either a large number of harmonics needs to be included in the first-order solution or a new method of analysis, such as the method of strained coordinates (expansion in terms of characteristics), needs to be employed.

Figure 23 shows the anomaly of the dispersive wave solution, in the case of a turbulent boundary layer. Below $\alpha \approx 0.3$ we note that the amplitudes of the fundamental wave and the second harmonic are comparable in magnitude. This violates the assumption made that the amplitude of the fundamental is $O(\epsilon)$ and the amplitude of the second harmonic is $O(\epsilon^2)$. However, we should note also that the amplitude of the second harmonic is very small at high wave numbers, where the waves seem to be dispersive.

Before we attempt to analyze the nonlinear stability of weakly dispersive waves, we digress a little and look over a simpler case, a third-order resonant interaction.

5.2 Third-Order Resonant Wave Interactions

The rippling observed on small progressing gravity waves has been investigated since the beginning of the century. Harrison (1909) and Wilton (1915) found nonlinear resonances to occur at a denumerable set of critical wavenumbers $k = (\rho g/nT)^{1/2}$, where g is the gravity acceleration, ρ and T the density and surface tension of the liquid, and n is any integer greater than unity. The first two correspond to wavelengths of 2.44 and 2.99 cm for the case of deep water. These resonances occur whenever waves having different wavenumbers have the same (or approximately the same) phase speed.

Different investigators proposed quite different mechanisms for the generation of the ripples. Louquet, Higgins (1963) and Crapper (1970) considered the capillary waves as a small disturbance on a main gravity wave. However, McGoldrick (1972) pointed out that this approach has the following limitations: the ratio of the wavelength of the disturbance to that of the gravity wave is small and the resonant waves must have identical phase speeds, which do not always meet experimental verification.

Kim and Hanratty (1971) proposed quadratic interactions as the generating mechanism for the appearance of higher harmonics on progressing capillary-gravity waves. Their model and their experiments refer

also to the shallow water case, where the waves, in addition to being weakly nonlinear, are also weakly dispersive.

McGoldrick (1970) used the method of multiple scales to investigate the second-harmonic resonant case, both analytically and experimentally. He reported large differences in the measured surface tension and viscosity of the water used in his experiment from their nomimal values. The reason is the dirtiness of the water surface. Nayfeh (1973) examined the temproal and spacial modulation of the interacting harmonics for the second-harmonic resonant case. McGoldrick (1972) examined experimentally third and higher-order resonances. He observed that peak interactions occur slightly off the exact resonant frequency. Admitting that the algebra required to analyze these waves is too cumbersome, he used a model equation (Bretherton's equation) to explain qualitatively the results of his experiments. Nayfeh (1971) used the method of multiple scales to analyze the third-harmonic resonant case when the frequencies are exactly in the ratio of three to one.

In this investigation, we extend the results of Nayfeh (1971) to examine the third-harmonic resonant case when the frequencies are not exactly commensurable and compare quantitatively the analytical results with the experimental results of McGoldrick. Hopes of extending this kind of analyses to higher order relies on the use of the computer to handle the necessary algebraic operations, as Schwartz did (1974) for Stokes waves.

5.2.1 Problem Formulation

We introduce a Cartesian coordinate system whose x-axis lies in the undisturbed free surface and its y-axis is directed away from the liquid. The governing equation for the velocity potential ϕ is

$$\nabla^2\phi = 0 \tag{5.2.1}$$

in the region

$$-\infty < x < \infty , \quad -\infty < y \leq \eta(x,t)$$

The surface elevation is given by $\eta(x,t)$. Here, lengths are normalized with $k_c = (\rho g/T)^{1/2}$ and time with $(gk_c)^{-1/2}$, where ρ is the liquid density, T is the surface tension, and g is the body acceleration directed toward the liquid. The boundary conditions at the interface are

$$\eta - \phi_t = \eta_{xx}(1 + \eta_x^2)^{-3/2} - \frac{1}{2}(\phi_x^2 + \phi_y^2) \text{ at } y = \eta \tag{5.2.2}$$

$$\eta_t + \phi_y = \eta_x\phi_x \quad \text{at } y = \eta \tag{5.2.3}$$

For deep water

$$\nabla\phi \to 0 \quad \text{as } y \to -\infty \tag{5.2.4}$$

Equations (5.2.1)-(5.2.4) are solved by use of the method of multiple scales (Nayfeh, 1973). We introduce the "slow" variable $T_2 = \varepsilon^2 t$ and "long" variable $X_2 = \varepsilon^2 x$, where ε is proportional to the steepness ratio of the waves. Moreover, we seek a uniform third-order expansion in the form

$$\eta(x,t) = \sum_{n=1}^{3} \varepsilon^n \eta_n(X_0,X_2,T_0,T_2) + O(\varepsilon^4) \tag{5.2.5}$$

$$\phi(x,y,t) = \sum_{n=1}^{3} \varepsilon^n \phi_n(y,X_0,X_2,T_0,T_2) + O(\varepsilon^4) \tag{5.2.6}$$

Here, T_0 and X_0 are the usual time and length variables t and x.

Substituting equations (5.2.5) and (5.2.6) into equations (5.2.1)-(5.2.4) and equating coefficient of like power of ε, we obtain equations (2.9) - (2.17) of Nayfeh, the only difference being the presence of a k in his equations due to the different nondimensionalization.

The solution of the $O(\varepsilon)$ problem gives the dispersion relation:

$$\omega^2 = k^3 + k \tag{5.2.7}$$

Since we are interested in the third-harmonic resonant case (i.e., $k^2 \approx 1/3$), we let the first-order solution contain both the fundamental and its resonating third harmonic; that is

$$\eta_1 = A_1(X_2,T_2)\exp(i\theta) + A_3(X_2,T_2)\exp(3i\theta + i\Gamma) + cc \tag{5.2.8}$$

$$\phi_1 = i\,\frac{\omega_1}{k_1}\,A_1(X_2,T_2)\exp(i\theta + k_1y) + i\,\frac{\omega_3}{k_3}\,A_3(X_2,T_2)\exp(3i\theta + k_3y + i\Gamma) + cc \tag{5.2.9}$$

where $\theta = k_1X_0 - \omega_1T_0$ is a fast varying phase, the A_n are the amplitudes, and

$$\Gamma = (k_3 - 3k_1)X_0 - (\omega_3 - 3\omega_1)T_0 = \sigma_kX_2 - \sigma_\omega T_2 \tag{5.2.10}$$

Substituting this solution into the $O(\varepsilon^2)$ problem, we obtain

$$\eta_2 = k_1[4(A_1^2+4\bar{A}_1A_3\exp i\Gamma)\exp(2i\theta) - 8A_1A_3\exp(i\Gamma + 4i\theta) - \frac{12}{5}\,A_3^2\exp(2i\Gamma + 6i\theta)] + cc \tag{5.2.11}$$

$$\phi_2 = i\omega[3(A_1^2 + 4\bar{A}_1A_3\exp i\Gamma)\exp[2(i\theta + k_1y)] - 12A_1A_3\exp[i\Gamma + 4(i\theta + k_1y) - \frac{27}{5}\,A_3\exp[2i\Gamma + 6(i\theta + k_1y)] + cc \tag{5.2.12}$$

where cc stands for the complex conjugate of the preceding term.

Substituting the solutions of the $O(\varepsilon)$ and $O(\varepsilon^2)$ problems into the $O(\varepsilon^3)$ problem, we obtain inhomogeneous equations whose particular solutions contain secular terms. Elimination of the secular terms leads to the following solvability conditions:

$$\frac{\partial A_1}{\partial T_2} + \omega_1' \frac{\partial A_1}{\partial X_2} = i \frac{3^{\frac{1}{2}}}{108\omega_1} [-77\bar{A}A_1^2 - 369\bar{A}_1^2 A_3 \exp(i\Gamma) - 138A_1A_2\bar{A}_3] \tag{5.2.13}$$

$$\frac{\partial A_3}{\partial T_2} + \omega_3' \frac{\partial A_3}{\partial X_2} = i \frac{3^{\frac{1}{2}}}{108\omega_1} [-205A_1^3 \exp(-i\Gamma) - 230A_1\bar{A}_1A_3 + 261A_3\bar{A}_3] \tag{5.2.14}$$

where the ω_i' are the group velocities. These two hyperbolic first-order equations govern the modulation of the amplitudes and the phases of the interacting harmonics.

5.2.2 Viscous Effects

Before attempting any comparison with the experiments, we shall incorporate the effects of viscosity which, for relatively short waves such as the ones examined here, play a dominant role after some distance of propagation. If the surface is clean and the Reynolds number of the wave $R = \omega/\nu k^2$ is large, the influence of viscous dissipation is to attenuate infinitesimal waves exponentially with distance from the generating source, the modulous of decay (logarithmic decrement) being given by $\Delta = 2\nu k^2/\omega'$ per unit distance. McGoldrick reports an order of magnitude variation in Δ, depending on the cleanliness of the liquid surface. Taking the above factors into account, letting $A_n = \frac{1}{2} a_n \exp(i\beta_n)$, and separating real and imaginary parts in equations (5.2.13) and (5.2.14), we obtain

$$\frac{da_1}{dX_2} = \frac{41(3)^{\frac{1}{2}}}{48\omega_1\omega_1'} a_1^2 a_3 \sin\gamma - \Delta_1 a_1 \qquad (5.2.15)$$

$$\frac{da_3}{dX_2} = \frac{41(3)^{\frac{1}{2}}}{144\omega_1\omega_3'} a_1^3 \sin\gamma - \Delta_3 a_3 \qquad (5.2.16)$$

$$\frac{d\beta_1}{dX_2} = \frac{(3)^{\frac{1}{2}}}{432\omega_1\omega_1'} (77a_1^2 + 369a_1a_3\cos\gamma + 138a_3^2) \qquad (5.2.17)$$

$$\frac{d\beta_3}{dX_2} = \frac{(3)^{\frac{1}{2}}}{720\omega_1\omega_3'} (205 \frac{a_1^3}{a_3} \cos\gamma + 230a_1^2 - 261a_3^2) \qquad (5.2.18)$$

where

$$\gamma = \beta_3 - 3\beta_1 + \Gamma \qquad (5.2.19)$$

Analytical solutions of the system of Equations (5.2.15) - (5.2.19) are not available in general. However, they can easily be integrated numerically using any of the standard forward-integration methods. We used a Runge-Kutta routine with a variable step size and an error control provided by IBM's scientific subroutine package.

5.2.3 Results and Discussion

Caution has been exercised to reproduce McGoldrick's initial conditions. He varied the frequency of the wavemaker and plotted the response as a function of the period; σ_k is related to the period by

$$\sigma_k = 3\Delta\omega \left(\frac{1}{\omega_3'} - \frac{1}{\omega_1'}\right) \qquad (5.2.21)$$

where $\Delta\omega$ is the difference between the operating frequency and the resonant frequency. Figure 24 shows a comparison between the analytical and experimental results. By neglecting viscous dissipation one overpredicts the maximum amplitude of the third harmonic by about 100%. Including the viscous effects leads to a good prediction of the

maximum amplitude but not the period at which it occurs. Figure 24 shows that maximum interaction occurs at a period slightly less than the exact-resonant value, which is 119.5 msec.

The above calculations were based on the static value for surface tension. However, it is well known that the "dynamic" surface tension is less than the "static" one. Moreover, our numerical results show that the period corresponding to the maximum interaction is very sensitive to the value of the surface tension. In fact, Figure 24 shows that basing the analytical results on a value of the surface tension that is about 2% less than the static value leads to an agreement with the experimentally observed period for maximum interaction.

It should be noted that, although the analytical results can be made to predict the maximum amplitude and the period of interaction by choosing a value for the surface tension, the theory cannot predict the amplitude at periods below the one corresponding to the maximum amplitude.

Figure 25 shows the variation of the amplitudes of the two harmonics with distance. Unfortunately McGoldrick did not repeat his measurements at different axial stations. Figure 25 shows the initial growth of the third harmonic and the subsequent decay of both harmonics as the viscous effects dominate the nonlinear interaction. These results are in qualitative agreement with McGoldrick's earlier experiments. Measurements at different axial stations seem to be very important, because the amplitude of the third harmonic changes considerably over relatively short distances.

Figure 26 shows the variation of the amplitude of the fundamental with period, 120 cm away from the wavemaker. To compare the analytical and experimental results, we need to estimate the value of Δ, because nominal values overpredict the amplitude at the period corresponding to exact resonance by a factor of about 3. In Figure 26 , the values of Δ were choosen to reproduce the experimental results away from resonance. Figure 26 shows that the analysis overpredicts the amplitude of the fundamental in the region near resonance by a factor of about 3, which means that the assumption that viscosity acts independently from the nonlinear interactions is not good when its effects are dominant. An improvement of the solution in the region where viscosity is important could be obtained if its effect was calculated from a series expansion (in terms of the Reynolds number). The first term would be the one used in (5.2.15).

5.3 Second-Harmonic Resonant Interactions

The linear analysis of Chapter 4 and the experimental results of Saric et al (1976) indicate the existence of resonant interactions among the harmonics of the waves.

In this section, we examine the case of second harmonic resonance. The present analysis is based on the gas model of Chapter 3 which does not restrict the extent of the disturbance layer to regions close to the walls in which the mean profiles are linear.

5.3.1 First-order problem

The results of Chapter 4 show that for the wavenumbers of interest

and for any pair in the ratio two to one, the quantities

$$\mathrm{Re}(c_1 - c_2) \quad , \mathrm{Im}(c_i)$$

are $O(\varepsilon)$. Thus, a near second-harmonic resonant condition exists. To determine a uniform expansion, we include both the fundamental and its harmonic in the solution of the first-order problem; that is, we let

$$\eta_1 = \sum_{m=1}^{2} A_m(T_1)e^{i\theta_m} + \text{c.c.} \tag{5.3.1}$$

$$\psi_1 = \sum_{m=1}^{2} A_m(T_1)\phi_m(y)e^{i\theta_m} + \text{c.c.} \tag{5.3.2}$$

where

$$\theta_m = m(x - c_m t) \tag{5.3.3}$$

The phases θ_m are fast varying functions and the amplitudes A_m are slowly varying functions.

Substituting (5.3.1) - (5.3.3) into (2.1.32) - (2.1.36) and separating harmonics, we obtain the following linear problems for the liquid phase as in Chapter 4:

$$\mathcal{L}^{(m)}\phi_m(y) = 0 \tag{5.3.4}$$

$$\phi_m = \phi_m' = 0 \qquad \text{at } y = 0 \tag{5.3.5}$$

$$\phi_m''' - 3(m\alpha)^2\phi_m' - im\alpha R[(m\alpha)^2 W - G - (c_m - 1)\phi_m' - \phi_m] - im\Lambda_1^{(m)} = 0$$

$$\text{at } y = 1 \tag{5.3.6}$$

$$\phi_m'' + (m\alpha)^2\phi_m = \chi_1^{(m)} \quad \text{at } y = 1 \tag{5.3.7}$$

$$c_m = 1 + \phi_m \tag{5.3.8}$$

where

$$\mathcal{L}^{(m)} = \frac{d^4}{dy^4} - (m\alpha)[2(m\alpha) + i\alpha R(y - c_m)] \frac{d^2}{dy^2} + (m\alpha)^2[(m\alpha) + iR(y-c_m)] \tag{5.3.9}$$

in the Orr-Sommerfeld operator for Couette flow.

Equations (5.3.4) - (5.3.8) are solved as in Chapter 4 by letting

$$w_1^{(m)} = \phi_m, \; w_2^{(m)} = \phi_m', \; w^{(m)} = \phi_m'', \; w^{(m)} = \phi_m''' \tag{5.3.10}$$

and hence transforming them to

$$\frac{dw_i^{(m)}}{dy} - \sum_{j=1}^{4} \beta_{ij}^{(m)} w_j^{(m)} = 0 \qquad i = 1,\ldots 4 \tag{5.3.11}$$

$$w_1^{(m)} = w_2^{(m)} = 0 \qquad \text{at } y = 0 \tag{5.3.12}$$

$$w_4^{(m)} + \gamma_{11}^{(m)} w_1^{(m)} + \gamma_{12}^{(m)} w_2^{(m)} = im\Lambda_1^{(m)} + e^{(m)} \qquad \text{at } y = 1 \tag{5.3.13}$$

$$w_3^{(m)} + \gamma_{21}^{(m)} w_1^{(m)} = \chi_1^{(m)} \qquad \text{at } y = 1 \tag{5.3.14}$$

where the $\beta_{ij}^{(m)}$ and $\gamma_{ij}^{(m)}$ are given in Appendix C, the $\Lambda_1^{(m)}$ and $\chi_1^{(m)}$ are determined from the gas analysis and are given in Appendix D, and

$$e^{(m)} = i(m\alpha)R[(m\alpha)^2 W - G] \tag{5.3.15}$$

Similarly, the solution of the first-order gas problem is written in the form

$$\zeta_1(x,y,t) = \sum_{m=1}^{2} A_m(T_1) z^{(m)}(Y) e^{i\theta_m} \tag{5.3.16}$$

where ζ_1 stands for any of the first-order gas properties and the z's are defined in (3.1.4). Substituting (5.3.16) into (2.2.13) - (2.2.17), we obtain

$$\frac{dz_i^{(m)}}{dY} - \sum_{j=1}^{6} \alpha_{ij}^{(m)} z_j^{(m)} = 0 \quad i = 1,\ldots 6 \tag{5.3.17}$$

where the $\alpha_{ij}^{(m)}$ are given in Appendix A. The boundary conditions and the method of solution of (5.3.17) are given in Chapter 3 and in Appendices A and B.

5.3.2 Second-Order Problem

Substituting the solution of the first-order problem into the second-order equations leads to an inhomogeneous set of equations and boundary conditions. The homogeneous part of these equations is the same as the first-order problem. Since the first-order problem has a nontrivial solution, the second-order inhomogeneous problem will have a solution if, and only if, a solvability conditions is satisfied (i.e. secular terms are eliminated). We note that, since the fundamental and its harmonic travel with the same phase speed, all terms proportional to $\exp[i(\theta_2 - 2\theta_1)]$ and $\exp(2i\theta_1)$ as well as those proportional to $\exp(i\theta_1)$ and $\exp(i\theta_2)$ produce secular terms.

To determine the solvability conditions, we seek a particular solution for the second-order problem in the form

$$\eta_2 = \sum_{m=1}^{2} H_m \exp(i\theta_m) + \text{c.c.} \tag{5.3.18}$$

$$\Psi_2 = \sum_{m=1}^{2} \Phi_m(y)\exp(i\theta_m) + \text{c.c.} \tag{5.3.19}$$

Substituting (5.3.18) and (5.3.19) into (2.1.37) - (2.1.41) and equating the coefficients of $\exp(i\theta_m)$ on both sides, we obtain

$$\frac{df_i^{(m)}}{dy} - \sum_{j=1}^{4} \beta_{ij}^{(m)} f_j^{(m)} = IL_i^{(m)} \quad i = 1,\ldots 4 \tag{5.3.20}$$

$$f_1^{(m)} = f_2^{(m)} = 0 \quad \text{at } y = 0 \tag{5.3.21}$$

$$f_4^{(m)} + \gamma_{11}^{(m)} f_1^{(m)} + \gamma_{12}^{(m)} f_2^{(m)} = im\Lambda_2^{(m)} + e^{(m)} H_m + IL_5^{(m)} \quad \text{at } y = 1 \tag{5.3.22}$$

$$f_3^{(m)} + \gamma_{21}^{(m)} f_1^{(m)} = \chi_2^{(m)} + IL_6^{(m)} \tag{5.3.23}$$

$$f_1^{(m)} = (c_m - 1)H_m + IL_7^{(m)} \tag{5.3.24}$$

where

$$f_1^{(m)} = \Phi_m,\ f_2^{(m)} = \Phi_m',\ f_3^{(m)} = \Phi_m'',\ f_4^{(m)} = \Phi_m''' \tag{5.3.25}$$

Equation (5.3.24) follows from the kinematic conditon. The IL_i are inhomogeneities in the liquid phase, are functions of the first-order liquid problem, and are defined in Appendix C.

Similary, we seek a particular solution for the second-order gas problem in the form

$$\zeta_2(x,y,t) = \sum_{m=1}^{2} \omega^{(m)}(Y)\exp(i\theta_m) \tag{5.3.26}$$

where

$$\omega_1^{(m)} = u_2\ , \quad \omega_3^{(m)} = v_2^{(m)}\ , \quad \omega_5^{(m)} = T_2^{(m)}$$
$$\omega_2^{(m)} = \frac{du_2^{(m)}}{dY}\ , \quad \omega_4^{(m)} = p_2^{(m)}\ , \quad \omega_6^{(m)} = \frac{dT_2^{(m)}}{dY} \tag{5.3.27}$$

Substituting (5.3.26) - (5.3.27) into (2.2.18) - (2.2.23) and equating the coefficients of $\exp(i\theta_1)$ and $\exp(i\theta_2)$ on both sides, we obtain

$$\frac{d\omega_i^{(m)}}{dY} - \sum_{j=1}^{6} \alpha_{ij}^{(m)} \omega_i^{(m)} = IG_i^{(m)} \quad i = 1,\ldots 6 \tag{5.3.28}$$

where the IG_i are functions of the solution of the first-order gas problem and are defined in Appendix D.

The boundary conditions at the wall (2.2.26) can be rewritten as

$$\begin{aligned} \omega_1^{(m)} &= - H_m U_0' + IG_7^{(m)} \\ \omega_3^{(m)} &= IG_8^{(m)} \quad \text{at} \quad \text{at } Y = 0 \\ \omega_5^{(m)} &= - H_m T_0' + IG_9^{(m)} \end{aligned} \tag{5.3.29}$$

Moreover, the second-order pressure and shear-perturbation parameters (2.2.29) - (2.2.30) can be rewritten as

$$im\Lambda_2^{(m)} = \delta_1^{(m)}\omega_1^{(m)} + \delta_4^{(m)}\omega_4^{(m)} + IG_{10}^{(m)} \tag{5.3.30}$$

$$\text{at } Y = 0$$

$$\chi_2^{(m)} = r_2^{(m)}\omega_2^{(m)} + r_5^{(m)}\omega_5^{(m)} + IG_{11}^{(m)} \tag{5.3.31}$$

5.3.3 Solvability Condition

To determine the solvability condition of the inhomogeneous second-order problem, we multiply (5.3.20) by $q_i^{(m)}(y)$, (5.3.28) by $g_i^{(m)}(y)$, integrate the result by parts in the corresponding intervals to transfer the derivatives from f_n and ω_n to q_n and g_n and obtain

$$f_i^{(m)}q_i^{(m)}\Big]_0^1 + \int_0^1 \Big[- f_i^{(m)} \frac{dq_i^{(m)}}{dy} - \Big(\sum_{j=1}^{4} \beta_{ij}^{(m)} f_j^{(m)}\Big) q_i^{(m)}\Big] dy$$

$$= \int_0^1 IL_i^{(m)} q_i^{(m)} dy \qquad i = 1,\ldots 4 \tag{5.3.32}$$

$$\omega_i^{(m)}g_i^{(m)}\Big]_0^\infty + \int_0^\infty \Big[-\omega_i^{(m)} \frac{dg_i^{(m)}}{dY} - \Big(\sum_{j=1}^{6} \alpha_{ij}^{(m)}\omega_j^{(m)}\Big) g_i^{(m)}\Big] dY$$

$$= \int_0^\infty IG_i^{(m)} g_i^{(m)} dY \quad i = 1,\ldots 6 \tag{5.3.33}$$

We choose the q_i and g_i to be solutions of the adjoint homogeneous problem. To define the adjoint homogeneous problem, we first set the

inhomogeneities $IL_i^{(m)}$ and $IG_i^{(m)}$ equal to zero in (5.3.32) and (5.2.33). Then, we equate to zero each of the coefficients of f_n and ω_n in the integrands in (5.3.32) and (5.2.33). Using the homogeneous boundary conditions of the second-order problem and manipulating the remaining terms in the sum of (5.3.32) and (5.3.33), we determine the boundary conditions to be satisfied by q_n and g_n. The result is

$$q_3^{(m)} = q_4^{(m)} = 0 \qquad \text{at } y = 0 \tag{5.3.34}$$

$$\frac{dq_i^{(m)}}{dy} + \sum_{j=1}^{4} \beta_{ji}^{(m)} q_j^{(m)} = 0 \quad i = 1,..4 \tag{5.3.35}$$

$$q_2^{(m)} - \gamma_{12}^{(m)} q_4^{(m)} = 0 \qquad \text{at } y = 1 \tag{5.3.36}$$

$$(c_m - 1)q_1^{(m)} + [\gamma_{21}^{(m)}(1 - c_m) - r_5^{(m)} T_0'(0)]q_3^{(m)} + [e^{(m)} - \delta_1^{(m)} U_0'(0) + \gamma_{11}^{(m)}(1 - c_m)]q_4^{(m)} + g_1^{(m)} U_0'(0) + g_5^{(m)} T_0'(0) = 0$$

$$\text{at } y = 1,\ Y = 0 \tag{5.3.37}$$

$$g_2^{(m)} - r_2^{(m)} q_3^{(m)} = 0 \quad \text{at } y = 1,\ Y = 0 \tag{5.3.38}$$

$$g_4^{(m)} - \delta_4^{(m)} q_4^{(m)} = 0 \quad \text{at } y = 1,\ Y = 0 \tag{5.3.39}$$

$$g_6^{(m)} = 0 \qquad \text{at} \qquad Y = 0 \tag{5.3.40}$$

$$\frac{dg_i^{(m)}}{dY} + \sum_{j=1}^{6} \alpha_{ji}^{(m)} g_j^{(m)} = 0 \qquad i = 1,...6 \tag{5.3.41}$$

$g_i^{(m)}$ bounded as $Y \to \infty$

With the q_n and g_n defined, the solvability condition can be determined by adding (5.3.32) and (5.3.33), taking into consideration (5.3.34) - (5.3.40), and obtaining

$$\sum_{i=1}^{4}\int_0^1 IL_i^{(m)}q_i^{(m)}dy + \sum_{i=1}^{6}\int_0^\infty IG_i^{(m)}g_i^{(m)}dY + [(\delta_1^{(m)}q_4^{(m)} - q_1^{(m)})IG_7^{(m)}$$

$$- IG_8^{(m)}g_3^{(m)} + (r_5^{(m)}q_3^{(m)} - g_5^{(m)})IG_9^{(m)} + (q_1^{(m)} - \gamma_{21}^{(m)}q_3^{(m)}$$

$$- \gamma_{11}^{(m)}q_4^{(m)})IL_7^{(m)} + q_4^{(m)}(IL_5^{(m)} + IG_{10}^{(m)})$$

$$+ (IL_6^{(m)} + IG_{11}^{(m)})q_3^{(m)}]_{\substack{y=1\\Y=0}} = 0 \qquad (5.3.42)$$

Rearranging (5.3.42) for m = 1 and 2 yields the following coupled equations:

$$\frac{dA_1}{dT_1} + E_1\bar{A}_1A_2\exp[iRe(\theta_2 - 2\theta_1) + 2Im(c_2)t] = 0 \qquad (5.3.43)$$

$$\frac{dA_2}{dT_1} + E_2A_1^2\exp[-iRe(\theta_2 - 2\theta_1) + 2Im(c_1 - c_2)t] = 0 \qquad (5.3.44)$$

where E_1, E_2 are given in Appendix F. Letting

$$A_m^* = A_m(T_1)\exp[m\,Im(c_m)t] \qquad (5.3.45)$$

we rewrite (5.3.43) and (5.3.44) in the form

$$\frac{dA_1^*}{dT_1} - Im(c_1)A_1^* + E_1\bar{A}_1^*A_2^*\exp(i\Gamma T_1) = 0 \qquad (5.3.46)$$

$$\frac{dA_2^*}{dT_1} - 2Im(c_2)A_2^* + E_2A_1^{*2}\exp(-i\Gamma T_1) = 0 \qquad (5.3.47)$$

where

$$\Gamma = 2Re(\frac{c_1 - c_2}{\varepsilon}) \qquad (5.3.48)$$

is the detuning parameter. Putting

$$E_m = 2\tau_m\exp(i\phi_m)\ ,\quad A_m^* = \frac{1}{2}\,a_m\exp(i\beta_m)\ , \qquad (5.3.49)$$

and separating real and imaginary parts in (5.3.46) - (5.3.47), we obtain

$$\frac{da_1}{d\bar{T}_1} - Im(c_1)a_1 + \tau_1 a_1 a_2 \cos(\beta_2 - 2\beta_1 + \phi_1 + \Gamma T_1) = 0 \qquad (5.3.50)$$

$$\frac{d\beta_1}{d\bar{T}_1} + \tau_1 a_2 \sin(\beta_2 - 2\beta_1 + \phi_1 + \Gamma T_1) = 0 \qquad (5.3.51)$$

$$\frac{da_2}{d\bar{T}_1} - 2Im(c_2)\alpha_2 + \tau_2 a_1^2 \cos(-\beta_2 + 2\beta_1 + \phi_2 - \Gamma T_1) = 0 \qquad (5.3.52)$$

$$a_2 \frac{d\beta_2}{d\bar{T}_1} + \tau_2 a_1^2 \sin(-\beta_2 + 2\beta_1 + \phi_2 - \Gamma T_1) = 0 \qquad (5.3.53)$$

These equations govern the time modulation of the amplitudes and the phases of the interacting harmonics.

5.3.4 Solution of the Adjoint Problem

Equations (5.3.34) - (5.3.40) constitute the adjoint homogeneous problem. It can be observed that because of the form of the interface conditions (5.3.37), (5.3.38) and (5.3.39) the gas problem and the liquid problem cannot be solved in succession, as it was done for the original problem. The solution of the adjoint problem is obtained as follows.

For Y greater than the boundary-layer thickness, (5.3.41) consists of a system of equations having constant coefficients, having solutions in the form

$$g_i^{(m)} = \sum_{j=1}^{6} c_{ij}^{(m)} \exp(\lambda_j Y) \quad i = 1,\ldots 6 \qquad (5.3.55)$$

We note that the λ's are the same as the ones for the original problem, (3.1.10). Discarding the solutions that grow exponentially leaves three linearly independent solutions that decay exponentially with Y. Hence, as $Y \to \infty$, the boundary conditions are taken in the form

$$D^*g = 0 \quad \text{at } Y = Y_0 \qquad (5.3.56)$$

where Y_0 is any value larger than the boundary-layer thickness and D* is a 6 x 3 constant coefficient matrix that is defined in Appendix E.

Using the boundary conditions (5.3.56), we numerically integrate the homogeneous system of equations (5.3.41) to generate two linear independent solutions $g_i^{(1)}$ and $g_i^{(2)}$ satisfying, respectively, the following two wall conditions:

$$\begin{Bmatrix} g_2^{(1)} \\ g_4^{(1)} \\ g_6^{(1)} \end{Bmatrix} = \begin{Bmatrix} 1 \\ 0 \\ 0 \end{Bmatrix}, \quad \begin{Bmatrix} g_2^{(2)} \\ g_4^{(2)} \\ g_6^{(2)} \end{Bmatrix} = \begin{Bmatrix} 0 \\ 1 \\ 0 \end{Bmatrix}. \tag{5.3.57}$$

Then, the general solution of the gas problem can be written as

$$g_i = C_1 g_i^{(1)} + C_2 g_i^{(2)} \qquad i = 1, \ldots 6 \tag{5.3.58}$$

We also generate two linear independent solutions $q_i^{(1)}$ and $q_i^{(2)}$ for the liquid problem.

These solutions satisfy the system (5.3.35), the wall boundary conditions (5.3.34) and

$$\begin{Bmatrix} q_3^{(1)} \\ q_4^{(1)} \end{Bmatrix} = \begin{Bmatrix} \frac{1}{r_2^{(m)}} \\ 0 \end{Bmatrix}, \quad \begin{Bmatrix} q_3^{(2)} \\ q_4^{(2)} \end{Bmatrix} = \begin{Bmatrix} 0 \\ \frac{1}{\delta_4^{(m)}} \end{Bmatrix} \tag{5.3.59}$$

at the interface, respectively. Then, the general solution of the liquid problem can be written as

$$q_i = C_1 q_i^{(1)} + C_2 q_i^{(2)} \tag{5.3.60}$$

The interface conditions (5.3.36) - (5.3.37) are used to determine the

coefficients C_1 and C_2. Since they are homogeneous, the determinant of the system

$$q_2^{(1)} C_1 + (q_2^{(2)} - \frac{\gamma_{12}^{(m)}}{\delta_4^{(m)}}) C_2 = 0 \tag{5.3.61}$$

$$\left\{(c_m - 1) q_1^{(m)} + [\gamma_{21}^{(m)}(1-c_m) - r_5^{(m)} T_0'(0)]/r_2^{(m)} + g_1^{(1)} U_0'(0) + g_5^{(1)} T_0'(0)\right\} C_1 + \left\{(c_m - 1) q_2^{(2)} + [e^{(m)} - \delta_1^{(m)} U_0'(0) + \gamma_{11}^{(m)}(1 - c_m)]/\delta_4^{(m)} + g_1^{(2)} U_0'(0) + g_5^{(2)} T_0'(0)\right\} C_2 = 0 \tag{5.3.62}$$

must vanish, which provides a check for the eigenvalue determined from the solution of the original problem. The solution of the adjoint problem is then determined by letting

$$C_1 = \frac{\gamma_{12}^{(m)}}{\delta_4^{(m)}} - q_2^{(2)} \tag{5.3.63}$$

$$C_2 = q_2^{(1)} \tag{5.3.64}$$

5.3.5 Results and Discussion

The solutions of the linear problem and its adjoint provide the coefficients τ_1, τ_2, ϕ_1 and ϕ_2 of the system (5.3.50) - (5.3.53). This system and the initial values for the wave amplitudes at $t = t_0$ constitute an initial-value problem for a_1 and a_2. Since these initial conditions are unknown, we cannot repeat the procedure of Section 5.2. Moreover, since we are examining self-sustained oscillations and since the experiments indicate stable finite-amplitude waves, it is of interest to look at steady-state solutions of the system (5.3.50) - (5.3.53).

For the case of phase-modulated waves, the steady-state amplitudes are given by the solution of the system

$$\begin{aligned}
&\mathrm{Im}(c_1) - \tau_1 a_1 \cos(\beta_2 - 2\beta_1 + \Gamma T_1 + \phi_1) && = 0 \\
&2\mathrm{Im}(c_2) a_2 - \tau_2 a_1^2 \cos(-\beta_2 + 2\beta_1 - \Gamma T_1 + \phi_2) && = 0 \\
&\Gamma - \tau_2 a_1^2 \sin(-\beta_2 + 2\beta_1 - \Gamma T_1 + \phi_2) \\
&\qquad + 2\tau_1 a_2 \sin(\beta_2 - 2\beta_1 + \Gamma T_1 + \phi_1) && = 0 \\
&\beta_2 - 2\beta_1 + \Gamma T_1 && = \text{constant}
\end{aligned} \tag{5.3.65}$$

This system has been solved by using a standard Newton-Raphson iteration scheme. To cover the range of wavenumbers from 0 to 0.5 in steps of 0.05, one needs computing times the order of 60 minutes on an IBM 370/158 computer. For the case of a turbulent gas boundary layer, the estimated computation time is the order of 10 hours. In this case, the disturbance field is assumed to be uncorrelated with the turbulent fluctuations to $O(\varepsilon^2)$.

Figures 27, 28 and 29 show the variation of the steady-state amplitudes with wavenumber, at different liquid Reynolds numbers. The pre-

dicted wave amplitudes are the order of the observed ones. This constitutes an improvement over the previous nonlinear results which overpredict the maximum amplitudes by an order of magnitude. Moreover, the results show that the wave amplitude decreases as the liquid Reynolds number increases. This implies that the effect of the second-harmonic resonance is less important at the higher liquid Reynolds numbers. For the case of high wavenumbers, the second harmonic is highly attenuated and the iteration scheme fails to converge to a solution.

Figure 30 compares the predicted and observed r.m.s. wave amplitudes. The predicted amplitude is calculated from the steady-state amplitudes a_1 and a_2. The agreement is good for the 40/60 water/glycerin mixture. The present model is an improvement over the dispersive model and the previous weakly dispersive model. However, the solution is still useful only in the intermediate range of Reynolds numbers as was the previous weakly dispersive model. This limitation is due to the fact that the wavespeeds approach unity as the liquid Reynolds number becomes large and therefore the waves are less dispersive. At large Reynolds numbers, the calculated amplitudes are unrealistic because they are bigger than the mean liquid depth. Consequently, the present model is inadequate for large liquid Reynolds numbers.

For the case of low Reynolds numbers, the results overpredict the amplitudes by a factor of about 3. It should be mentioned that the experiments do not show a second frequency for this range of Reynolds numbers.

The experiments show that, although there is a dominant frequency at each Reynolds number, and, in some cases, a dominant fundamental and

second harmonic, the spectrum contains also the higher harmonics. Moreover, the results of the linear problem indicate the possibility of the interaction of the fundamental frequency with its second and third harmonics, as we can see in Figures 16 and 17. Therefore, the range of validity of the present model could be extended by adding more harmonics to the solution. However, the algebraic labor would increase considerably because of the gas problem.

Figures 31 and 32 compare the predicted with the observed frequencies and wavenumbers. These results show that the present model constitutes an improvement over the previous models (Saric, et al 1976).

Additional solutions of the system (5.3.50) - (5.3.53) were not found despite a numerical search with different initial guesses. Our numerical results show that the steady-state amplitudes are weakly dependent on the transverse location outside the mean boundary layer at which the freestream conditions are applied.

6. CONCLUSIONS AND RECOMMENDATIONS

The stability of a film adjacent to a compressible boundary layer was analyzed by using a model that accounts for the viscosity and the mean velocity profiles of the liquid and the gas, body forces, surface tension, compressibility and thermal conductivity of the gas, and nonlinear effects. The main acheivement of the present study is an improved method for analyzing wave stability and obtaining quantitative predictions of the wave characteristics. Some specific results of the present study are enumerated below:

1) All assumptions used in the previous studies regarding the wavelength and the liquid Reynolds number were removed. The explicit appearance of the Reynolds number in the equations for the gas phase necessitated the use of orthonormalization procedures for solving these equations. A general purpose code (SUPORT) utilizing these procedures was used. Finite differences and Kaplan's filtering method could not be used for the case of turbulent boundary layers due to the presence of extreme growth rates.

2) The results of Chapter 3 show that Lighthill's model is inadequate to describe steady disturbances in a compressible turbulent boundary layer because the disturbance sublayer does not lie within the linear portion of the mean profiles of the main boundary layer. Hence, future studies of shock-wave boundary-layer interactions should include viscous effects on the disturbance throughout the flow field.

3) The results of the linear stability model (Chapter 4) show that it can be used for order of magnitude estimates but it cannot be used to predict the observed wave characteristics for turbulent flows, in agreement with previous work. Moreover, the phase speed calculations show that the waves are subject to resonance conditions at low wavenumbers, which include the experimentally observed ones.

4) The dispersive wave model of Bordner and Nayfeh (1974) was used to calculate the wave characteristics for the case of turbulent gas flows. The results show that two conditions exist at which the amplitude is maximum for the same liquid Reynolds number, in agreement with the experimental results. But the dispersive model is inadequate to predict wave amplitudes. Moreover, the appearance of the second harmonic in the experiments suggests the presence of a nonlinear resonant interaction.

5) Based on the estimates of the linear theory and the experimental information, a model was developed (Chapter 5) that analyzes second-harmonic resonant interactions. The steady-state amplitudes calculated using this model suggest that, for the intermediate range of liquid-Reynolds numbers, the observed waves are a result of this type of interaction. For the higher liquid-Reynolds numbers more harmonics are probably needed to predict the amplitudes.

The present nonlinear analysis is capable of predicting part of the experimental observations. Including the third harmonic in the weakly dispersive model may extend the validity of the analysis to higher liquid-

Reynolds numbers. However, the algebraic labor and the computational times involved would increase considerably. Also, three-dimensional effects need to be considered. A simple analysis with a linear model would determine if conditions for strong nonlinear wave-wave interactions are present. Furthermore, the effects of mass transfer at the interface need to be ascertained. Although the mass transfer slightly affects the eigenvalues (Saric, Touryan and Scott, 1976) for the problem of slag deposition in an MHD generator, it may have a non-negligible effect on the nonlinear problem through changes in the eigenfunctions. Finally, hypersonic effects need to be included in the analysis to properly model the reentry environment.

REFERENCES

Anderson, L. W. and Kendall, R. M. 1969 Boundary Layer Integral Matrix Procedure. Vols. I and II, AFWL-TR-69-114, Kirtland Air Force Base, New Mexico.

Benjamin, T. B. 1959 Shearing Flow Over a Wavy Boundary. J. Fluid Mech., Vol. 6, pp. 161.

Bordner, G. L. 1973 Nonlinear Stability of Liquid Films Adjacent to Compressible Streams. Ph.D. Dissertation, Virginia Polytechnic Institute and State University, Blacksburg, Virginia

Bordner, G. L. and Nayfeh, A. H. 1974 Nonlinear Stability of a Liquid Film Adjacent to a Viscous Supersonic Stream. Tech. Report, VPI-E-74-11, Virginia Polytechnic Institute and State University, Blacksburg, Virginia.

Bordner, G. L., Nayfeh, A. H., and Saric, W. S. 1975 Stability of Liquid Films Adjacent to Compressible Streams. Z. A. M. P., Vol. 26, pp. 771.

Brown, W. B. 1967 Stability of Compressible Boundary Layers. AIAA Journal, Vol. 5, pp. 1753.

Chang, L. D. and Russell, P. E. 1965 Stability of a Liquid Layer Adjacent to a High Speed Gas Stream. Phys. Fluids, Vol. 8, pp. 1018.

Cohen, L. S. and Hanratty, T. J. 1965 Generation of Waves in the Concurrent Flow of Air and a Liquid. AICHE J., Vol. 31, pp. 437.

Craik, A. D. D. 1966 Wind-Generated Waves in Thin Liquid Films. J. Fluid Mech., Vol. 26, pp. 369.

Craik, A. D. D. 1971 Nonlinear Resonant Instability in Boundary Layers. J. Fluid Mech., Vol. 50, pp. 393.

Crapper, G. D. 1970 Nonlinear Capillary Waves Generated by Steep Gravity Waves. J. Fluid Mech., Vol. 40, pp. 149.

Cresci, T. J. and Starkenburg, J. 1971 Liquid Film Cooling on Hypersonic Slender Bodies. XXII International Astronautical Congress, Brussels.

Fannelöp and I. Flügge-Lotz 1963 Ingenieur-Archiv, Vol. 33, pp. 94.

Gater, R. L. and L'Ecuyer, M. R. 1971 A Fundamental Investigation of the Phenomena that Characterize Liquid Film Cooling. Int'l. J. Heat Mass Trans., Vol. 13, pp. 1925.

Godunov, S. 1961 On the Numerical Solution of Boundary Value Problems for Systems of Linear Ordinary Differential Equations. Uspekhi Mat. Nauk., Vol. 16, pp. 171.

Gold, H. 1973 Surface Fluid and Boundary Layer Interaction Aspects of Transpiration Cooled Nosetip Concepts. Tech. Report, AFM-TR-73-8, Wright-Patterson Air Force Base, Ohio.

Gold, H., Otis, J. H., Jr., and Schlier, R. E. 1971 Surface Liquid Film Characteristics: An Experimental Study. AIAA Paper No. 71-623.

Grabow, R. M. and White, C. O. 1972 A Surface Flow Approach for Predicting Cross-Hatch Patterns. AIAA Paper No. 72-718.

Grose, R. G. and Kendall, R. M. 1970 The Homogeneous BLIMP with Liquid Layer. Report 70-3, Aerotherm Corp., Mountain View, Calif.

Harrison, W. J. 1909 The Influence of Viscosity and Capillarity on Waves of Finite Amplitude. Pro. Lond. Math. Soc., Vol. A7, pp. 197.

Inger, G. R. 1971 Compressible Boundary Layer Flow Past a Swept Wavy Wall with Heat Transfer and Ablation. Astronautical Acta, Vol. 16, pp. 325.

Kendall, R. M. and Bartlett, E. P. 1972 Nonsimilar Solution of the Multi-Component Laminar Boundary Layer by an Integral-Matrix Method. AIAA J., Vol. 6, pp. 1089.

Kim, Y. Y. and Hanratty, T. 1971 Weak Quadratic Interactions of Two Dimensional Waves. J. Fluid Mech., Vol. 50, pp. 107.

Lekoudis, S. G., Nayfeh, A. H., and Saric, W. S. 1976 Compressible Boundary Layers Over Wavy Walls. Physics Fluids, Vol. 19, pp. 4.

Lees, L. and Reshotko, E. 1962 Stability of the Compressible Laminar Boundary Layer. J. Fluid Mech., Vol. 12, pp. 555.

Lighthill, M. J. 1953 On Boundary Layers and Upstream Influence II. Supersonic Flows Without Separation. Pro. Roy. Soc., Vol. A217, pp. 478.

Loquet-Higgins, M. S. 1963 The Generation of Capillary Waves by Steep Gravity Waves. J. Fluid Mech., Vol. 16, pp. 138.

Mack, L. M. 1974 On the Application of Linear Stability Theory to the Problem of Supersonic Boundary-Layer Transmission. AIAA Paper No. 74-134.

Marshall, B. W. and Tiederman, W. G. 1972 A Capacitance Depth Gauge for Thin Liquid Films. Rev. Sci. Instr., Vol. 43, pp. 544.

Mason, Inger Analytic Investigation of Transonic Normal Shock Boundary Layer Interaction. V.P.I.-Aero-027 (1974).

McGoldrick, L. F. 1970 An Experiment on Second-Order Capillary Gravity Resonant Wave Interactions. J. Fluid Mech., Vol. 40, pp. 251.

McGoldrick, L. F. 1972 On the Rippling of Small Waves: A Harmonic Nonlinear Nearly Resonant Interaction. J. Fluid Mech., Vol. 52, pp. 725.

Miles, J. W. 1957 On the Generation of Surface Waves by Shear Flows. J. Fluid Mech., Vol. 3, pp. 185.

Miles, J. W. 1960 The Hydrodynamic Stability of a Thin Film of Liquid in Uniform Shearing Motion. J. Fluid Mech., Vol. 8, pp. 38.

Miles, J. W. 1962 On the Generation of Surface Waves by Shear Flows, Part 4. J. Fluid Mech., Vol. 13, pp. 433.

Nachtsheim, P. R. 1970 Stability of Crosshatched Wave Patterns in Thin Liquid Films Adjacent to Supersonic Stream. Phys. Fluids, Vol. 13, pp. 2432.

Nayfeh, A. H. 1973 PERTURBATION METHODS. Wiley-Interscience.

Nayfeh, A. H. 1973 Second Harmonic Resonance in the Interaction of an Air Stream with Capillary-Gravity Waves. J. Fluid Mech., Vol. 59, pp. 803.

Nayfeh, A. H. 1971 Third Harmonic Resonance in the Interaction of Capillary and Gravity Waves. J. Fluid Mech., Vol. 48, pp. 385.

Nayfeh, A. H. and Saric, W. S. 1971a Nonlinear Kelvin-Helmholz Instability. J. Fluid Mech., Vol. 46, pp. 209.

Nayfeh, A. H. and Saric, W. S. 1971b Stability of a Liquid Film. AIAA J., Vol. 9, pp. 750.

Nayfeh, A. H. and Saric, W. S. 1973 Nonlinear Stability of a Liquid Film Adjacent to a Supersonic Stream. J. Fluid Mech., Vol. 58, pp. 39.

Nayfeh, A. H. and Saric, W. S. 1973 Nonlinear Stability of a Liquid Adjacent to a Supersonic Stream. Physics Fluids, Vol. 12, pp. 2089.

Norris, H. L. and Reynolds, W. C. 1975 Turbulent Channel Flow with a Moving Wavy Boundary. T-pt. TF-17, Stanford University.

Polak, A., Werbe, M. J., Vatsa, V. N. and Bertke, S. D. 1975 Supersonic Laminar Boundary Layer Flow Past a Wavy Wall with Multiple Separation Regions. Report No. AFL-74-12-15, Univ. of Cincinnati.

Saric, W. S., Nayfeh, A. G. and Lekoudis, S. G. 1976 Experiments on the Stability of Liquid Films Adjacent to Supersonic Boundary Layers. J. Fluid Mech., in Press.

Saric, W. S. and Marshall, B. W. 1971 An Experimental Investigation of the Stability of a Thin Liquid Layer Adjacent to a Supersonic Stream. AIAA J., Vol. 9, pp. 1546.

Saric, W. S., Touryan, K. J., and Scott, M. R. 1976 Stability of Slag in Turbulent MHD Boundary Layers. AIAA Paper No. 76-314.

Schwartz, L. W. 1974 Computer Extension and Analytic Continuation of Stokes' Expansion for Gravity Waves. J. Fluid Mech., Vol. 62, pp. 553.

Scott, M. R. and Watts, H. A. 1976 Computational Solution of Linear Two-Point Boundary-Value Problems Via Orthonormalization. S.I.A.M. J. Numer. Anal., to appear.

Stewartson, K. 1964 THE THEORY OF LAMINAR BOUNDARY LAYERS IN COMPRESSIBLE FLUIDS. Oxford U.P., Oxford, pp. 61.

Stewartson, K. and Williams, P. G. 1969 Self-Induced Separation. Proc. Roy. Soc., London, A312, pp. 181-206.

Williams, E. P. and Inger, G. R. 1970 Investigation of Ablation Surface Cross-Hatching. SAMSO TR 70-246, McDonnell Douglas.

Wilton, J. R. 1915 On Ripples. Phil. Mag., Vol. 29, pp. 688.

Whitham, J. B. 1974 LINEAR AND NONLINEAR WAVES. Wiley-Interscience.

APPENDIX A

$$a_{11}^{(m)} = a_{13}^{(m)} = a_{14}^{(m)} = a_{15}^{(m)} = a_{16}^{(m)} = 0 \ , \ a_{12}^{(m)} = 1 \tag{A.1}$$

$$a_{21}^{(m)} = m^2 + im\frac{R_G U_0}{T_0} \ , \ a_{22}^{(m)} = -\frac{\mu_0'}{\mu_0} \ , \ a_{23}^{(m)} = \frac{R_G U_0'}{\mu_0 T_0} - im\left(\frac{\mu_0'}{\mu_0} + \frac{T_0'}{3T_0}\right)$$

$$a_{24}^{(m)} = im\frac{R_G}{\mu_0} - \frac{m^2}{3}\gamma U_0 M_\infty^2, \ a_{25}^{(m)} = -\frac{b_1 U_0''}{\mu_0} + \frac{m^2 U_0}{3T_0} \ ,$$

$$a_{26}^{(m)} = -\frac{b_1 U_0'}{\mu_0} \tag{A.2}$$

$$a_{31}^{(m)} = -im, \ a_{33}^{(m)} = \frac{T_0'}{T_0} \ , \ a_{34}^{(m)} = -im\gamma U_0 M_\infty^2, \ a_{35}^{(m)} = im\frac{U_0}{T_0} \ ,$$

$$a_{32}^{(m)} = a_{36}^{(m)} = 0 \tag{A.3}$$

$$a_{41}^{(m)} = -\frac{im}{P}\left(2\mu_0' + \frac{4\mu_0 T_0'}{3T_0}\right), \ a_{42}^{(m)} = -\frac{im\mu_0}{P} \ , \ a_{43}^{(m)} = \left[-m^2\mu_0 - im\frac{R_G U_0}{T_0}\right.$$

$$\left. + \frac{4}{3}\left(\frac{\mu_0 T_0''}{T_0} + \frac{\mu_0' T_0'}{T_0}\right)\right]/P, \ a_{44}^{(m)} = -\frac{4}{3}\frac{i\gamma m M_\infty^2}{P}\left[\mu_0 U_0' + U_0\left(\mu_0' + \frac{\mu_0 T_0'}{T_0}\right)\right],$$

$$a_{45}^{(m)} = \frac{i}{P}\left[b_1 m U_0' + \frac{4m}{3T_0}\left(\mu_0 U_0' + U_0\mu_0'\right)\right], \ a_{46}^{(m)} = \frac{4im\mu_0 U_0}{3T_0} \tag{A.4}$$

$$a_{51}^{(m)} = a_{52}^{(m)} = a_{53}^{(m)} = a_{54}^{(m)} = a_{55}^{(m)} = 0 \ , \ a_{56}^{(m)} = 1 \tag{A.5}$$

$$a_{61}^{(m)} = 0, \ a_{62}^{(m)} = -2(\gamma-1)M_\infty^2 U_0' P_r, \ a_{63}^{(m)} = \frac{R_G P r T_0'}{\mu_0} - 2imU_0' Pr(\gamma-1)M_\infty^2 \ ,$$

$$a_{64}^{(m)} = -im\frac{R_G P r U_0}{\mu_0} \ , \ a_{65}^{(m)} = \frac{imU_0 R_G Pr}{\mu_0} + m^2 - \frac{b_1 T_0''}{T_0}$$

$$- \frac{b_1 Pr U_0'^2}{\mu_0}(\gamma-1)M_\infty^2 \ , \ a_{66}^{(m)} = -\frac{\mu_0' + b_1 T_0'}{\mu_0} \tag{A.6}$$

$$P = R_G + im\frac{4}{3}\gamma\mu_0 U_0 M_\infty^2 \tag{A.7}$$

APPENDIX B

$$a_{11}^{(m)} = a_{13}^{(m)} = a_{14}^{(m)} = a_{15}^{(m)} = a_{16}^{(m)} = 0,\ a_{12}^{(m)} = 1 \tag{B.1}$$

$$a_{21}^{(m)} = m^2 + imR_G,\ a_{22}^{(m)} = a_{23}^{(m)} = 0,\ a_{24}^{(m)} = -\frac{m^2}{3}\gamma M_\infty^2 + imR_G,$$

$$a_{25}^{(m)} = \frac{m^2}{3},\ a_{26}^{(m)} = 0 \tag{B.2}$$

$$a_{31}^{(m)} = -im,\ a_{32}^{(m)} = a_{33}^{(m)} = 0,\ a_{34}^{(m)} = -im\gamma M_\infty^2,\ a_{35}^{(m)} = im,\ a_{36}^{(m)} = 0 \tag{B.3}$$

$$a_{41}^{(m)} = 0,\ a_{42}^{(m)} = -im/(R_G + \frac{4i}{3}m\gamma M_\infty^2),\ a_{43} = (-m^2 - imR_G)/(R_G + \frac{4i}{3}m\gamma M_\infty^2),$$

$$a_{44}^{(m)} = a_{45}^{(m)} = 0,\ a_{46}^{(m)} = \frac{4}{3}im/(R_G + \frac{4}{3}im\gamma M_\infty^2) \tag{B.4}$$

$$a_{51}^{(m)} = a_{52}^{(m)} = a_{53}^{(m)} = a_{54}^{(m)} = a_{55}^{(m)} = 0,\ a_{56}^{(m)} = 1 \tag{B.5}$$

$$a_{61}^{(m)} = a_{62}^{(m)} = a_{63}^{(m)} = 0,\ a_{64}^{(m)} = -imRPr(\gamma-1)M_\infty^2,\ a_{65}^{(m)} = imR_GPr + m^2,$$

$$a_{66}^{(m)} = 0 \tag{B.6}$$

$$\Xi_1^{(m)} = a_{24}^{(m)}a_{42}^{(m)} + a_{34}^{(m)}a_{43}^{(m)} + a_{64}^{(m)}a_{46}^{(m)} \tag{B.7}$$

$$\Xi_2^{(m)} = a_{25}^{(m)}a_{42}^{(m)} + a_{35}^{(m)}a_{43}^{(m)} + a_{65}^{(m)}a_{46}^{(m)} \tag{B.8}$$

$$\lambda_{1,2}^{(m)} = \pm\{m^2 + imR_G\}^{\frac{1}{2}} \tag{B.9}$$

$$\lambda_{3,5}^{(m)} = \pm\{\frac{1}{2}(\Xi_1^{(m)} + a_{65}^{(m)}) + [\frac{1}{4}(\Xi_1^{(m)} - a_{65}^{(m)}) + \Xi_2^{(m)}a_{65}^{(m)}]^{\frac{1}{2}}\}^{\frac{1}{2}} \tag{B.10}$$

$$\lambda_{5,6}^{(m)} = \pm\{\frac{1}{2}(\Xi_1^{(m)} + a_{65}^{(m)}) - [\frac{1}{4}(\Xi_1^{(m)} - a_{65}^{(m)})^2 + \Xi_2^{(m)}a_{64}^{(m)}]^{\frac{1}{2}}\}^{\frac{1}{2}} \tag{B.11}$$

The boundary conditions as $Y \to \infty$ read

$$D^{(m)} z^{(m)} = 0 \tag{B.12}$$

where $D^{(m)}$ is a 6 x 3 matrix consisting of the first three rows of the matrix $[B^{(m)}]^{-1}$. The matrix $B^{(m)}$ has the elements:

$$B^{(m)}(1,i) = F_1^{(m)} \tag{B.13}$$

$$B^{(m)}(2,i) = \lambda_i^{(m)} F_1^{(m)} \tag{B.14}$$

$$B^{(m)}(3,i) = (a_{31}^{(m)} F_1^{(m)} + a_{34}^{(m)} F_2^{(m)} + a_{35}^{(m)} F_3^{(m)})/\lambda_i^{(m)} \tag{B.15}$$

$$B^{(m)}(4,i) = F_2^{(m)} \tag{B.16}$$

$$B^{(m)}(5,i) = F_3^{(m)} \tag{B.17}$$

$$B^{(m)}(6,i) = \lambda_i^{(m)} F_3^{(m)} \tag{B.18}$$

where for $\lambda_i^{(m)} = \lambda_{1,2}^{(m)}$

$$F_1^{(m)} = 1, \; F_2^{(m)} = F_3^{(m)} = 0 \tag{B.19}$$

and for $\lambda_i^{(m)} = \lambda_{3,4,5,6}^{(m)}$

$$F_1^{(m)} = \frac{a_{24}^{(m)}(a_{65}^{(m)} - \lambda_i^2) - a_{65}^{(m)} a_{64}^{(m)}}{\lambda_i^2 - a_{21}^{(m)}} \tag{B.20}$$

$$F_2^{(m)} = a_{65}^{(m)} - \lambda_i^2 \tag{B.21}$$

$$F_2^{(m)} = - a_{65}^{(m)} \tag{B.22}$$

APPENDIX C

$$\beta_{11}^{(m)} = \beta_{13}^{(m)} = \beta_{14}^{(m)} = 0,\ \beta_{12}^{(m)} = 1 \tag{C.1}$$

$$\beta_{21}^{(m)} = \beta_{22}^{(m)} = \beta_{24}^{(m)} = 0,\ \beta_{23}^{(m)} = 1 \tag{C.2}$$

$$\beta_{31}^{(m)} = \beta_{32}^{(m)} = \beta_{33}^{(m)} = 0,\ \beta_{34}^{(m)} = 1 \tag{C.3}$$

$$\beta_{41}^{(m)} = -(m\alpha)^3[(m\alpha) + iR(y - c_m)],\ \beta_{42}^{(m)} = 0 \tag{C.4}$$

$$\beta_{43}^{(m)} = (m\alpha)[2(m\alpha) + iR(y - c_m)]\ ,\ \beta_{44}^{(m)} = 0 \tag{C.5}$$

$$\gamma_{11}^{(m)} = im\alpha R\ ,\ \gamma_{12}^{(m)} = -3(m\alpha)^2 + i(m\alpha)R(c_m - 1) \tag{C.6}$$

$$\gamma_{21}^{(m)} = (m\alpha)^2 \tag{C.7}$$

$$IL_1^{(m)} = IL_2^{(m)} = IL_3^{(m)} = 0 \tag{C.8}$$

$$IL_4^{(m)} = \alpha R(\psi_{1y}\psi_{1xyy} - \psi_{1x}\psi_{1yyy}) + \alpha^3 R(\psi_{1y}\psi_{1xxx} - \psi_{1x}\psi_{1xxy}) \tag{C.9}$$

$$IL_5^{(m)} = \frac{\partial}{\partial x}[-2\alpha^2(\psi_{1yy} - \alpha^2\psi_{1xx})\eta_{1x} - (p_{1y} + 2\alpha^2\psi_{1xyy})\eta_1] \text{ at } y = 1 \tag{C.10}$$

$$IL_6^{(m)} = 4\alpha^2\psi_{1xy}\eta_{1x} - \eta_1(\psi_{1yyy} - \alpha^2\psi_{1xxy}) \text{ at } y = 1 \tag{C.11}$$

$$IL_7^{(m)} = -(\eta_1 + \psi_{1y})\eta_1 - \eta_1\psi_{1xy} \quad \text{at } y = 1 \tag{C.12}$$

APPENDIX D

$$im\Lambda_1^{(m)} = \delta_1^{(m)} z_1^{(m)} + \delta_4^{(m)} z_4^{(m)} \tag{D.1}$$

$$\chi_1^{(m)} = r_2^{(m)} z_2^{(m)} + r_5^{(m)} z_5^{(m)} \tag{D.2}$$

where

$$\delta_1^{(m)} = -\frac{2(m\alpha)^2 \mu_0(0)}{R_G} \quad , \quad \delta_4^{(m)} = \frac{im\alpha^2}{c_f} \tag{D.3}$$

$$r_2^{(m)} = \frac{\alpha \mu_0(0)}{c_f R_G} \quad , \quad r_5^{(m)} = \frac{\alpha b_1 U_0'(0) \mu_0(0)}{c_f R_G} \tag{D.4}$$

$$IG_1^{(m)} = 0 \tag{D.5}$$

$$IG_2^{(m)} = -\frac{b_2' U_0'}{\mu_0} T_1^2 - \frac{2 b_2 U_0'}{\mu_0} T_1 T_1' - \frac{im}{3} IG_3^{(m)} + \frac{\alpha R_G}{\mu_0}$$
$$\left\{ (\rho_1 U_0 + \rho_0 u_1) u_{1x} + (\rho_1 U_0' + \rho_0 u_{1Y}) v_1 - \frac{1}{\mu_0} [\mu_1 (u_{1YY} \right.$$
$$\left. + \frac{4}{3} \mu_{1xx} + \frac{1}{3} v_{1xY}) + \mu_{1x} (\frac{4}{3} u_{1x} - \frac{2}{3} v_{1Y}) + \mu_{1Y} (u_{1Y} + v_{1x})] \right\} \tag{D.6}$$

$$IG_3^{(m)} = -\alpha [\rho_{1x} u_1 + \rho_1 u_{1x} + \rho_{1Y} v_1 + v_{1Y} \rho_1 + \frac{U_0}{T_0} (\rho_1 T_1)_x] \tag{D.7}$$

$$IG_4^{(m)} = \left\{ \frac{4\mu_0}{3} (\frac{T_0'}{T_0} IG_3^{(m)} + \frac{dIG_3^{(m)}}{dY}) + \frac{4\mu_0'}{3} IG_3^{(m)} + 2 b_1 U_0' T_1 T_{1x} \right.$$
$$- \alpha R [(\rho_0 U_1 + \rho_1 U_0) v_{1x} + \rho_0 v_1 v_{1Y}) + \alpha [\mu_1 (v_{1xx} + \frac{4}{3} v_{1YY}$$
$$\left. + \frac{1}{3} u_{1xY}) + \mu_{1x} (\mu_{1Y} + v_{1x}) + \mu_{1Y} (\frac{4}{3} v_{1YY} - \frac{2}{3} u_{1x})] \right\}$$
$$x (R_G + \frac{4}{3} im\mu_0 \gamma M_\infty U_0)^{-1} \tag{D.8}$$

$$IG_5^{(m)} = 0 \tag{D.9}$$

$$IG_6^{(m)} = -\frac{(\gamma-1)M_\infty^2 b_1 Pr}{\mu_0} T_1^2 - \frac{2b_1 T_0'}{\mu_0} T_1 T_{1Y} - \frac{T_0' b_2'}{\mu_0} T_1^2 - \frac{b_1 T_0''}{\mu_0} T_1^2$$

$$+ \frac{R_G Pr\alpha}{\mu_0} (\rho_0 u_1 + \rho_1 u_0) T_{1X} + \Big\{(\rho_0 T_{1Y} + \rho_1 T_0')v_1 - (\gamma-1)M_\infty^2$$

$$\Big\{u_1 p_{1X} + v_1 p_{1Y} + \frac{1}{R_G}[2\mu_1 U_0'(\mu_{1Y} + v_{1X}) + \frac{4}{3}(u_{1X}^2 + v_{1y}^2)$$

$$- \frac{4}{3}(u_{1X} + v_{1y}^2) - \frac{4}{3} u_{1X} v_{1y} + (u_{1Y} + v_{1X})^2]\Big\}$$

$$+ \frac{1}{R_G Pr}(\mu_{1X} T_{1X} + \mu_1 T_{1XX} + \mu_{1Y} T_{1Y} + \mu_1 T_{1YY})\Big\} \qquad (D.10)$$

$$IG_7^{(m)} = -\alpha(u_{1Y}\eta_1 + \frac{U_0''}{2}\eta_1^2) \quad \text{at } Y = 0 \qquad (D.11)$$

$$IG_8^{(m)} = -\alpha v_{1Y}\eta_1 \quad \text{at } Y = 0 \qquad (D.12)$$

$$IG_9^{(m)} = -\alpha(T_{1Y}\eta_1 + \frac{T_0''}{2}\eta_1^2) \quad \text{at } Y = 0 \qquad (D.13)$$

$$IG_{10}^{(m)} = -\frac{4\mu_0}{3R_G} IG_3^{(m)} + \alpha[p_{1Y} + \frac{2\mu_0}{R_G}(u_{1XY} - 2v_{1YY})] + \alpha\frac{2\mu_1}{3R_G}(\mu_{1X} + v_{1Y})$$

$$- \frac{2\mu_1}{R_G} v_{1Y} + \frac{2\mu_0\eta_{1X}}{R_G}(\mu_{1Y} + v_{1X}) + \frac{2}{R_G}\mu_1 U_0'\eta_{1X} \quad \text{at } Y = 0 \qquad (D.14)$$

$$IG_{11}^{(m)} = \frac{im\mu_0\alpha}{R_G} v_{1Y} + \eta_1 \frac{b_1 U_0'}{R_G} T_1^2 + \frac{\alpha\eta_1}{R_G}[\mu_0 u_{1YY} + \mu_0'(v_{1XY} + u_{1Y})$$

$$+ \mu_1 U_0'' + \mu_{1Y} U_0'] + \frac{\alpha}{R_G}[\mu_1 u_{1Y} + 2\mu_0\eta_{1X}(v_{1Y} - u_{1X})] \text{ at } Y = 0$$

$$(D.15)$$

APPENDIX E

The boundary conditions for the adjoint gas problem as $Y \to \infty$ read

$$D^{*(m)} g^{(m)} = 0 \tag{E.1}$$

where $D^{*(m)}$ is a 6 x 3 matrix consisting of the first three rows of the matrix $[B^{*(m)}]^{-1}$. The matrix $B^{*(m)}$ has the elements:

$$B^{*(m)}(1,i) = F_1^{*(m)} \tag{E.2}$$

$$B^{*(m)}(2,i) = (- F_i^{*(m)} - a_{42}^{(m)} F_2^{*(m)})/\lambda_i^{(m)} \tag{E.3}$$

$$B^{*(m)}(3,i) = - a_{43}^{(m)} F_2^{*(m)}/\lambda_i^{(m)} \tag{E.4}$$

$$B^{*(m)}(4,i) = F_2^{*(m)} \tag{E.5}$$

$$B^{*(m)}(5,i) = F_3^{*(m)} \tag{E.6}$$

$$B^{*(m)}(6,i) = (- a_{46}^{(m)} F_2^{*(m)} - F_3^{*(m)})/\lambda_i^{(m)} \tag{E.7}$$

where for $\lambda_i^{(m)} = \lambda_{1,2}^{(m)}$

$$F_1^{*(m)} = 1 \tag{E.8}$$

$$F_2^{*(m)} = \frac{(\lambda_i^{(m)2} - a_{65}^{(m)}) a_{24}^{(m)} + a_{25}^{(m)} a_{64}^{(m)}}{(\Xi_1^{(m)} - \lambda_i^{(m)2})(a_{65}^{(m)} - \lambda_i^{(m)2}) - a_{64}^{(m)} \Xi_2^{(m)}} \tag{E.9}$$

$$F_3^{*(m)} = \frac{(\lambda_i^{(m)2} - \Xi_1^{(m)}) a_{25}^{(m)} + a_{24}^{(m)} \Xi_2^{(m)}}{(\Xi_1^{(m)} - \lambda_i^{(m)2})(a_{65}^{(m)} - \lambda_i^{(m)2}) - a_{64}^{(m)} \Xi_2^{(m)}} \tag{E.10}$$

and for $\lambda_i^{(m)} = \lambda_{3,4,5,6}^{(m)}$

$$F_1^{*(m)} = 0 \tag{E.11}$$

$$F_2^{*(m)} = - a_{64}^{(m)} \tag{E.12}$$

$$F_3^{*(m)} = \Xi_1^{(m)} - \lambda_i^{(m)} \tag{E.13}$$

where $a_{ij}^{(m)}$ and $\lambda_i^{(m)}$ are defined in Appendix B.

APPENDIX F

$$E_{(m)} = \left\{ - \sum_{i=1}^{6} \int_0^{\infty} IG_i^{(m)} x g_i^{(m)} dY - \sum_{i=1}^{4} \int_0^{1} IL_i^{(m)} x q_i^{(m)} dy \right.$$

$$+ \left[\left(\delta_1^{(m)} q_4^{(m)} - g_1^{(m)} \right) IG_7^{(m)} - IG_8^{(m)} g_3^{(m)} + \left(r_5^{(m)} q_3^{(m)} - g_5^{(m)} \right) IG_9^{(m)} \right.$$

$$+ \left(q_1^{(m)} - \gamma_{21}^{(m)} q_3^{(m)} - \gamma_{11}^{(m)} q_4^{(m)} \right) IL_7^{(m)} + \left(IL_5^{(m)} + IG_{10}^{(m)} \right) q_4^{(m)}$$

$$\left. + \left(IL_6^{(m)} + IG_{11}^{(m)} \right) q_3^{(m)} \right]_{\substack{Y=0 \\ y=1}} \left. \right\} \left\{ \alpha R \int_0^{1} [\phi_m'' - (m\alpha)^2 \phi_m] q_4^{(m)} dy \right.$$

$$\left. + \left[q_1^{(m)} - \gamma_{21}^{(m)} q_3^{(m)} - \gamma_{11}^{(m)} q_4^{(m)} \right]_{\substack{Y=0 \\ y=1}} \right\}^{-1} \qquad (F.1)$$

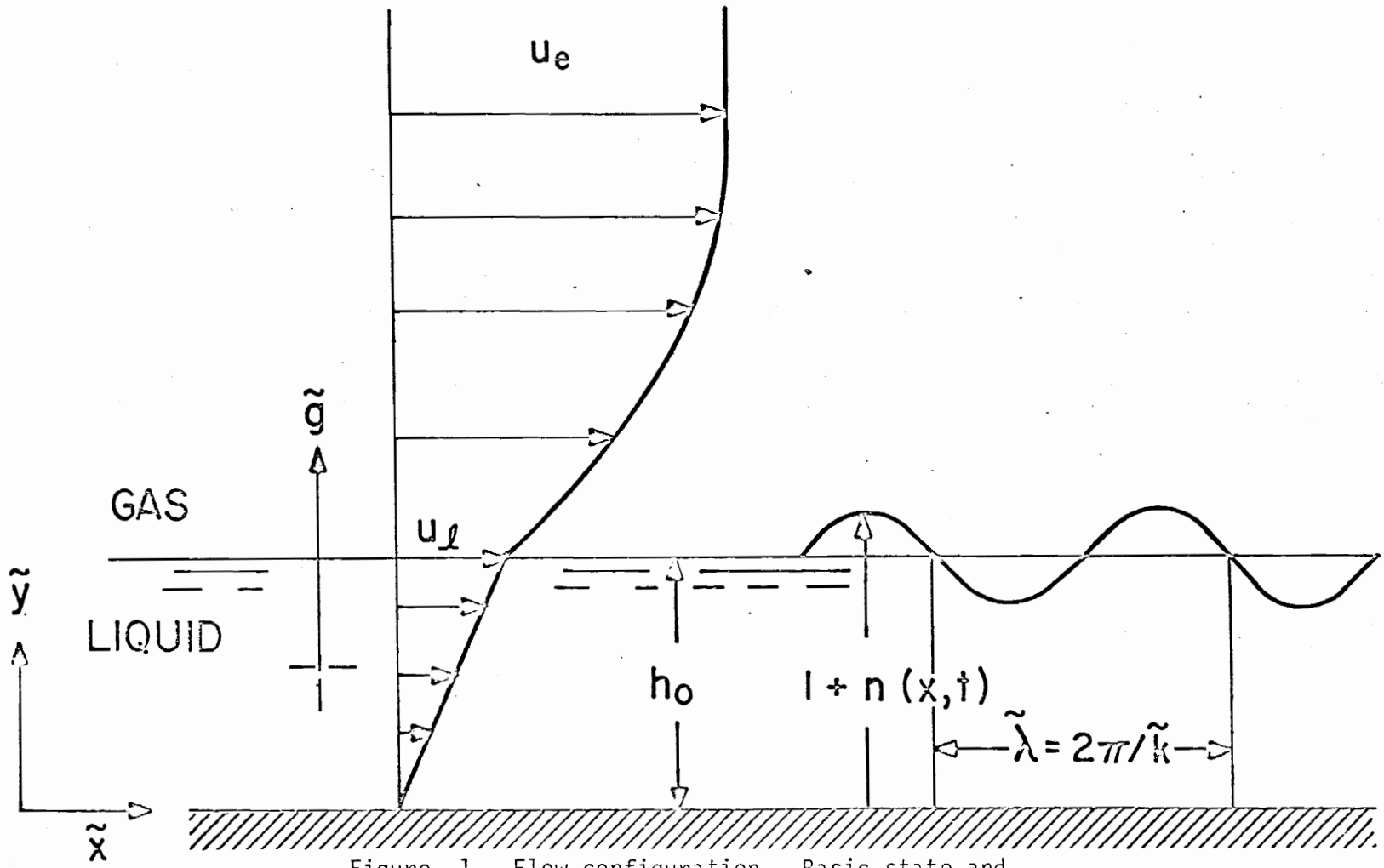

Figure 1. Flow configuration. Basic state and disturbance.

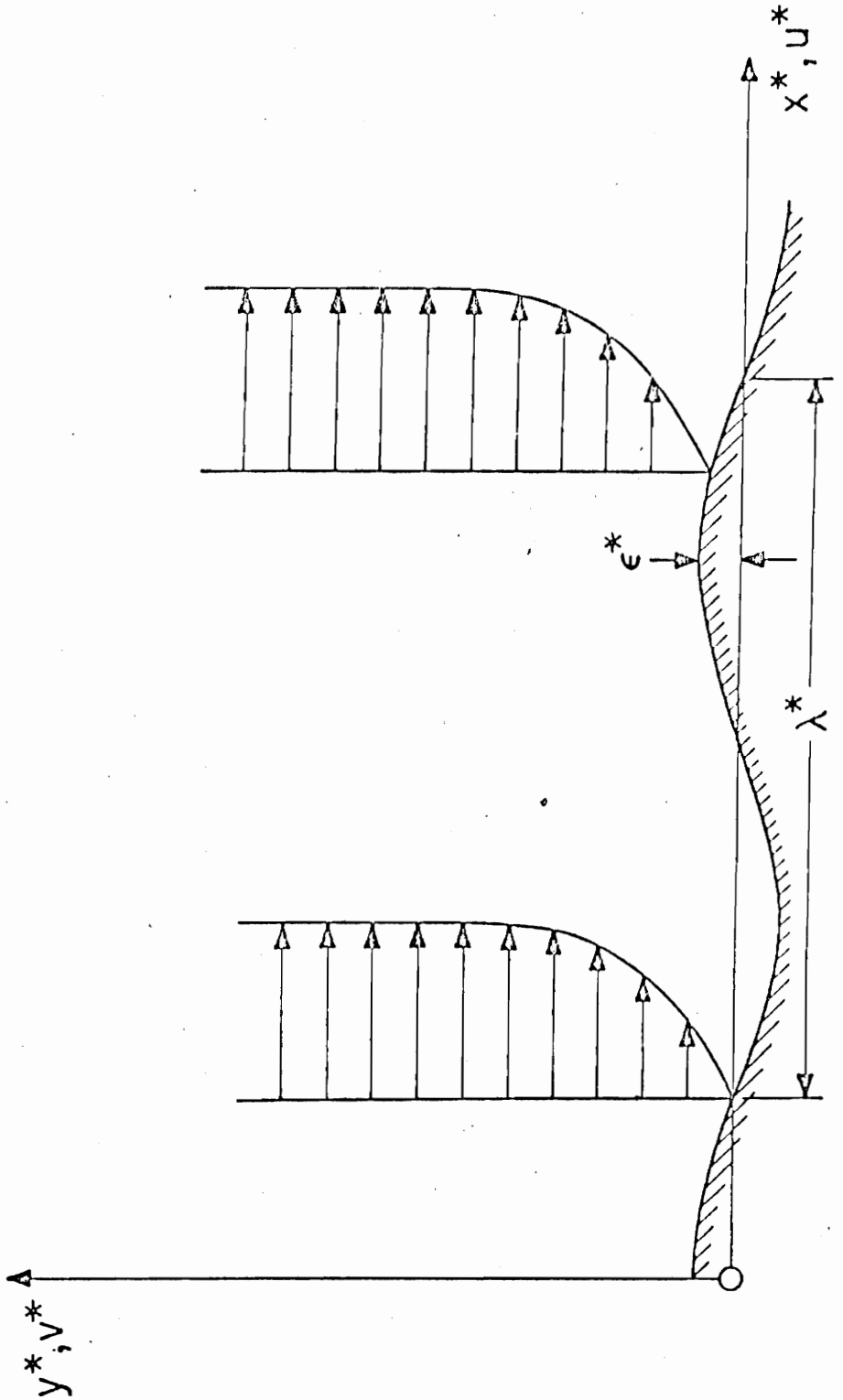

Figure 2. Flow configuration for the wavy wall problem.

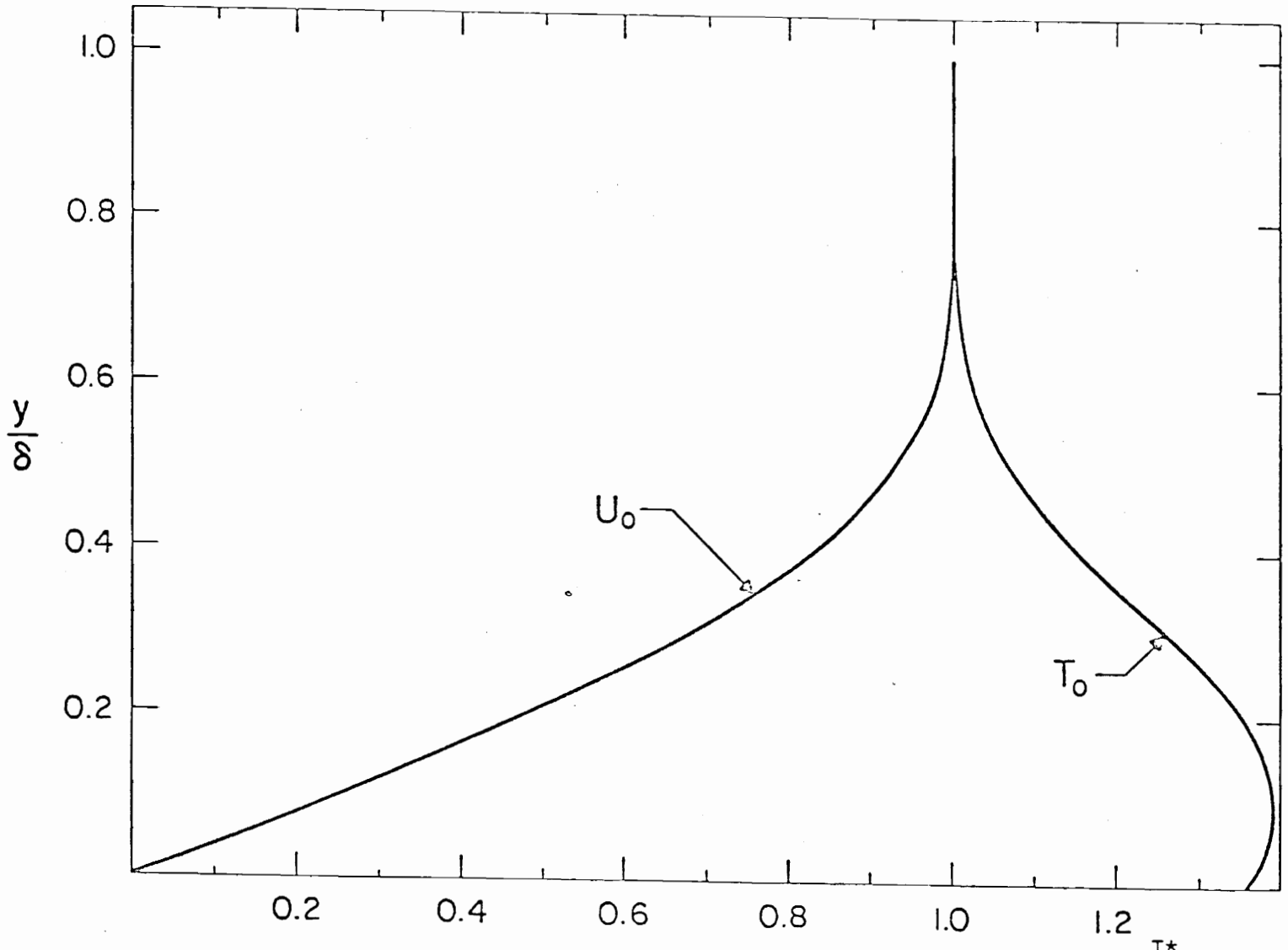

Figure 3. A representative laminar boundary-layer profile (M = 2.0, δ^* = 2cm, $\frac{T^*_w}{T^*_{ad}}$ = 0.8).

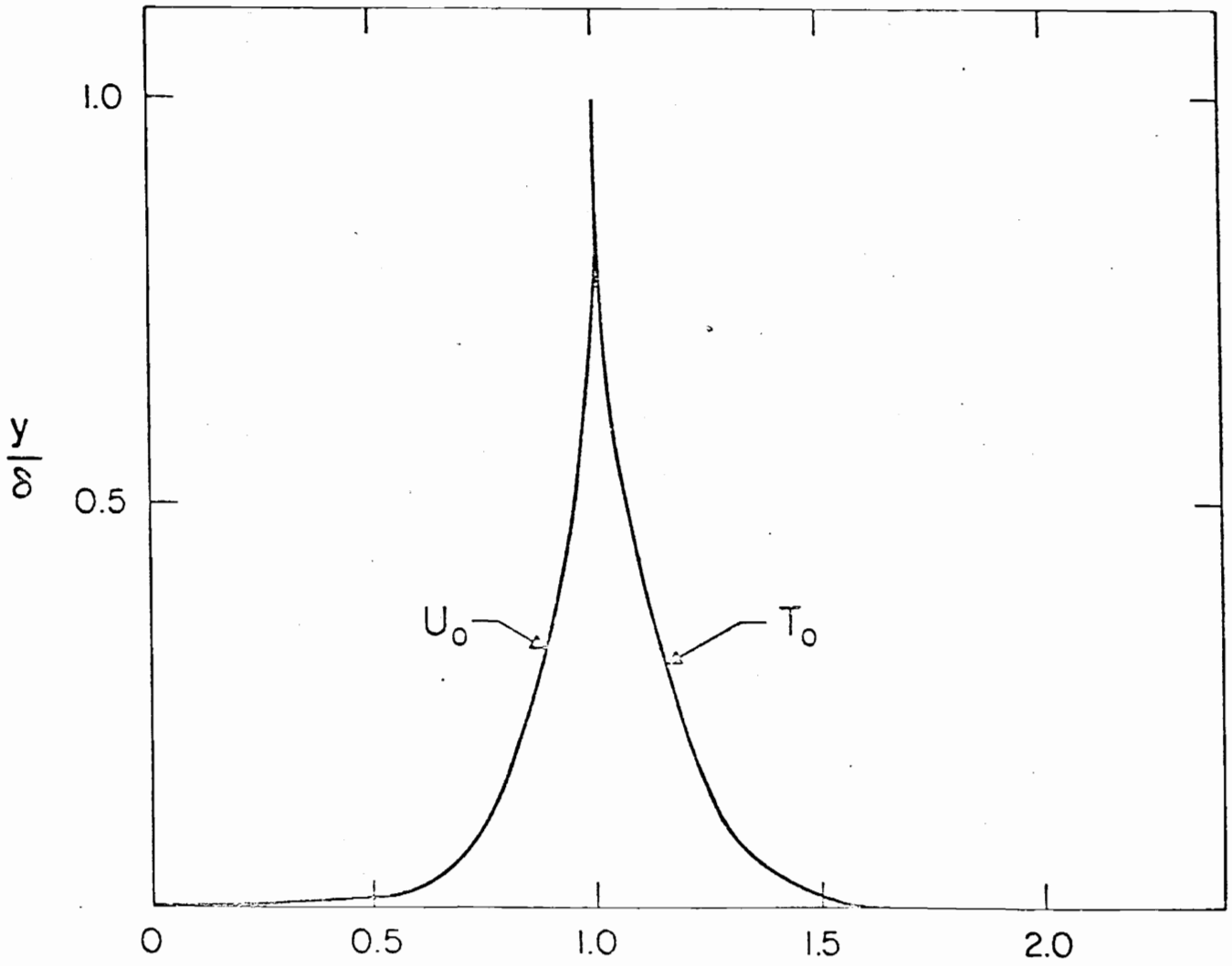

Figure 4. A representative turbulent boundary-layer profile ($M = 2.0$, $\delta^* = 1.27$ cm, $T_w^* \approx T_{ad}^*$).

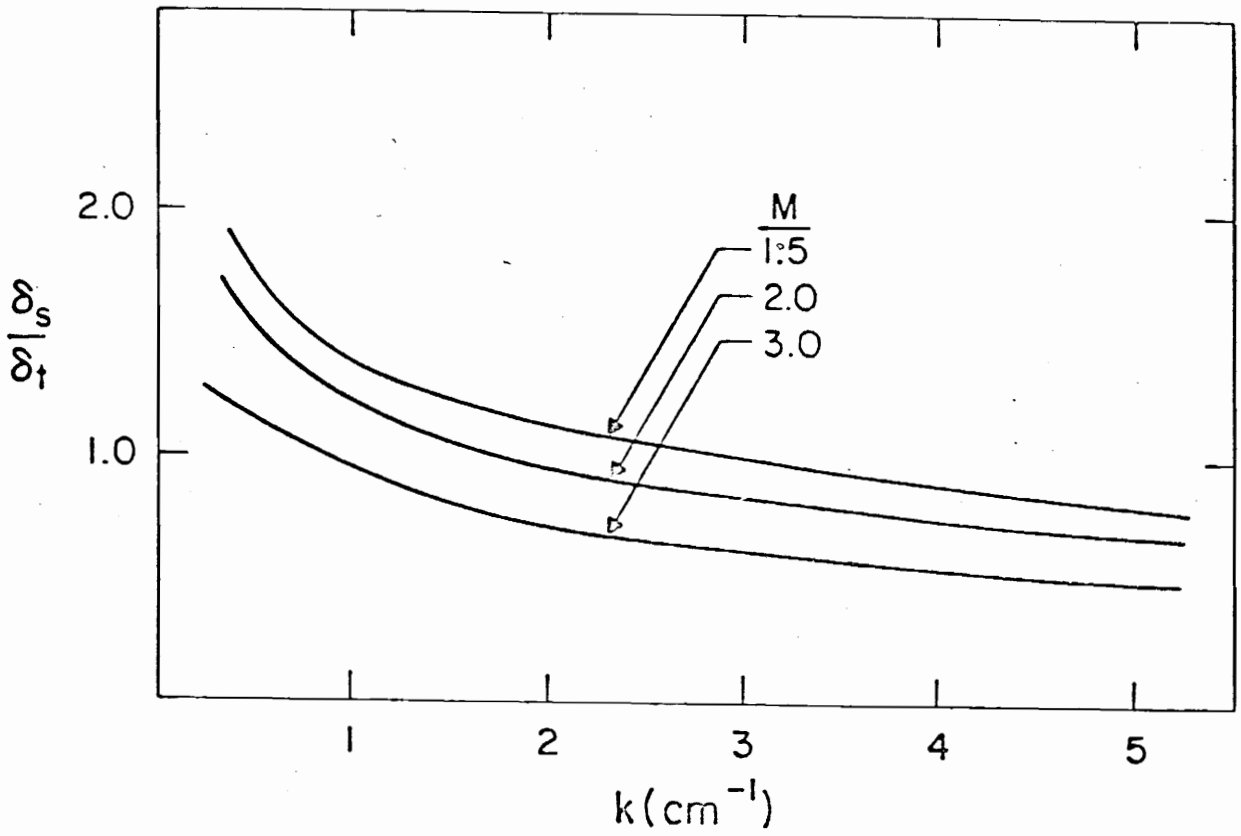

Figure 5. Variation of the ratio of the thicknesses of the disturbance and mean sublayers with the wavenumber (δ = 1.27 cm, $T_w \simeq T_{ad}$).

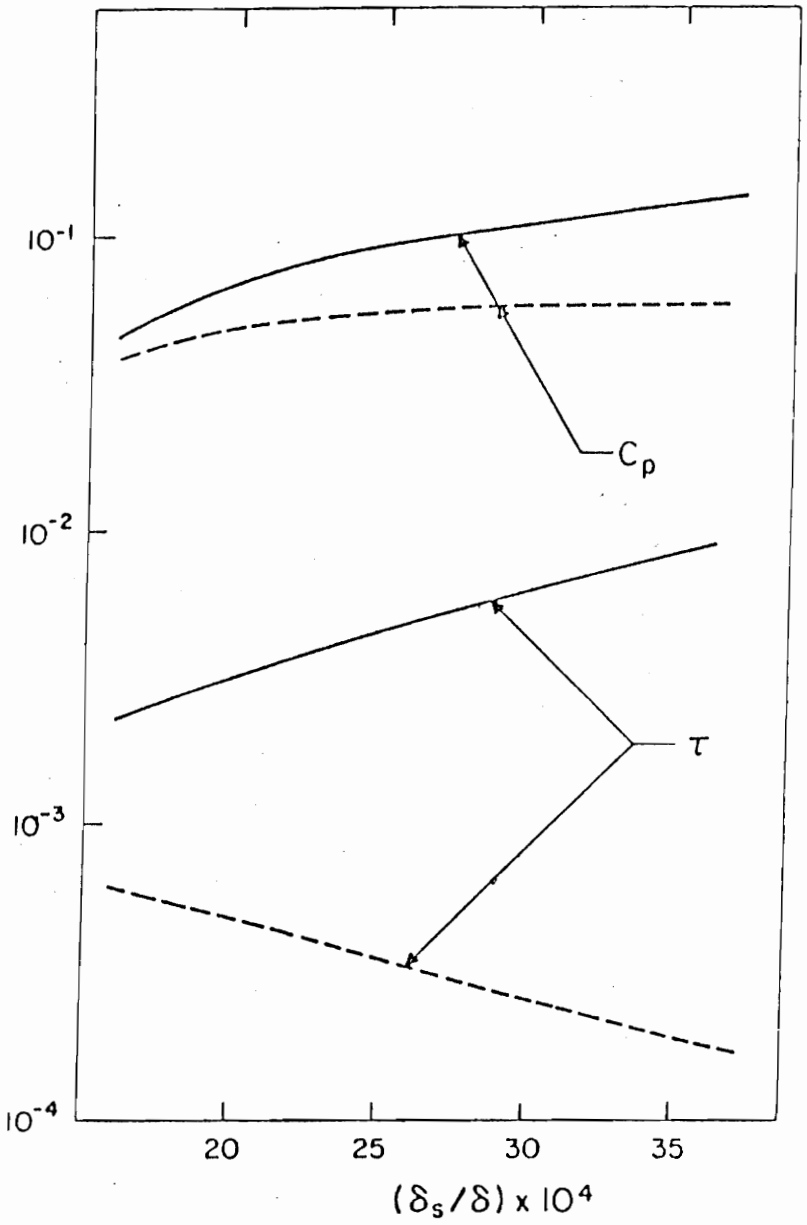

Figure 6. Variation of the amplitude of the pressure and the shear perturbations with the sublayer thickness (δ = 1.27 cm, $T_w \approx T_{ad}$, M = 1.5, ----Lighthill, —— present).

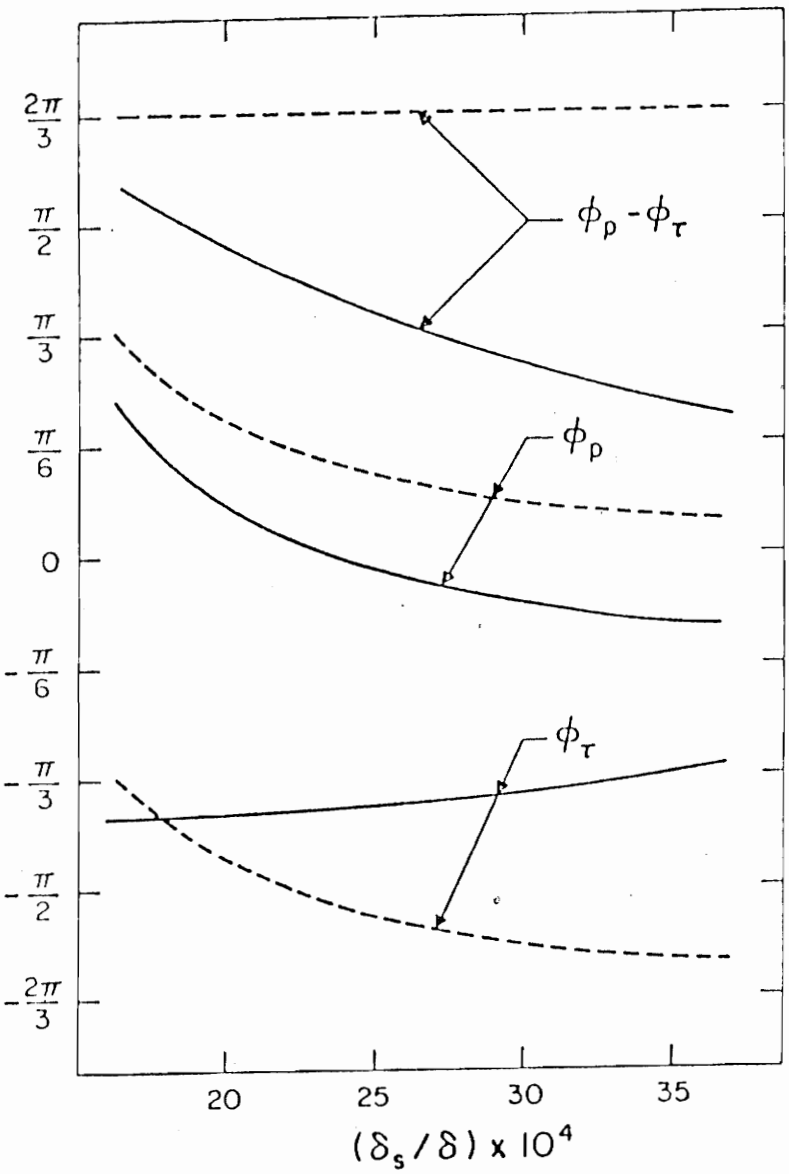

Figure 7. Variation of the positions of the maximum pressure and shear perturbations with the sulayer thickness (δ = 1.27 cm, $T_w \approx T_{ad}$, M = 1.5, ---- Lighthill, —— present).

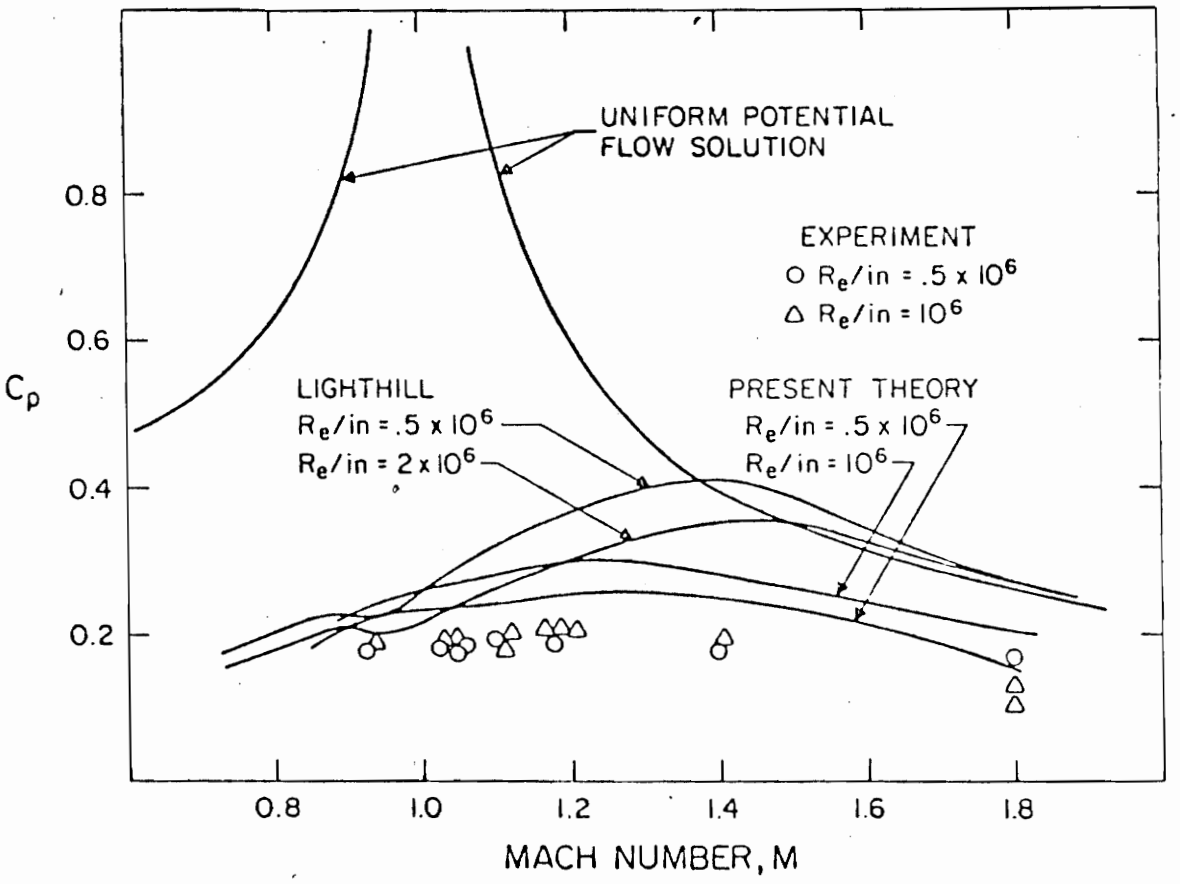

Figure 8. Variation of the pressure coefficient with the Mach number.

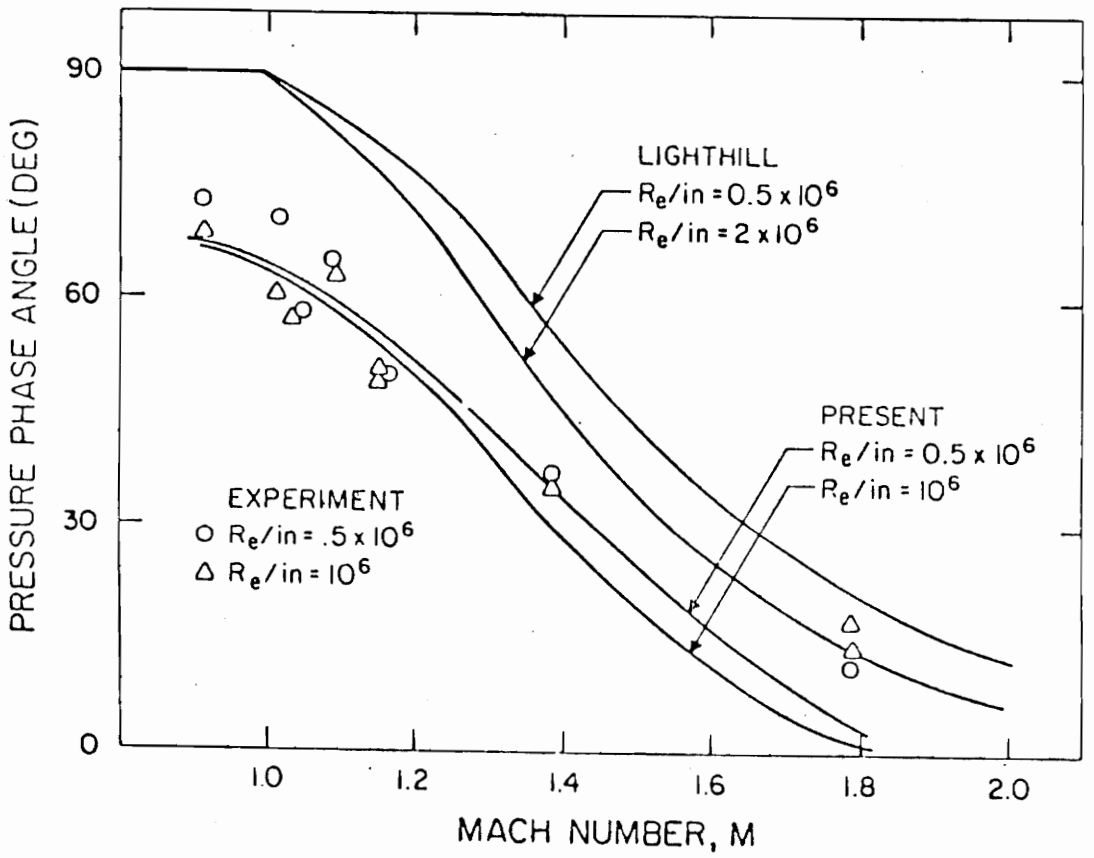

Figure 9. Variation of the position of the maximum pressure with the Mach number.

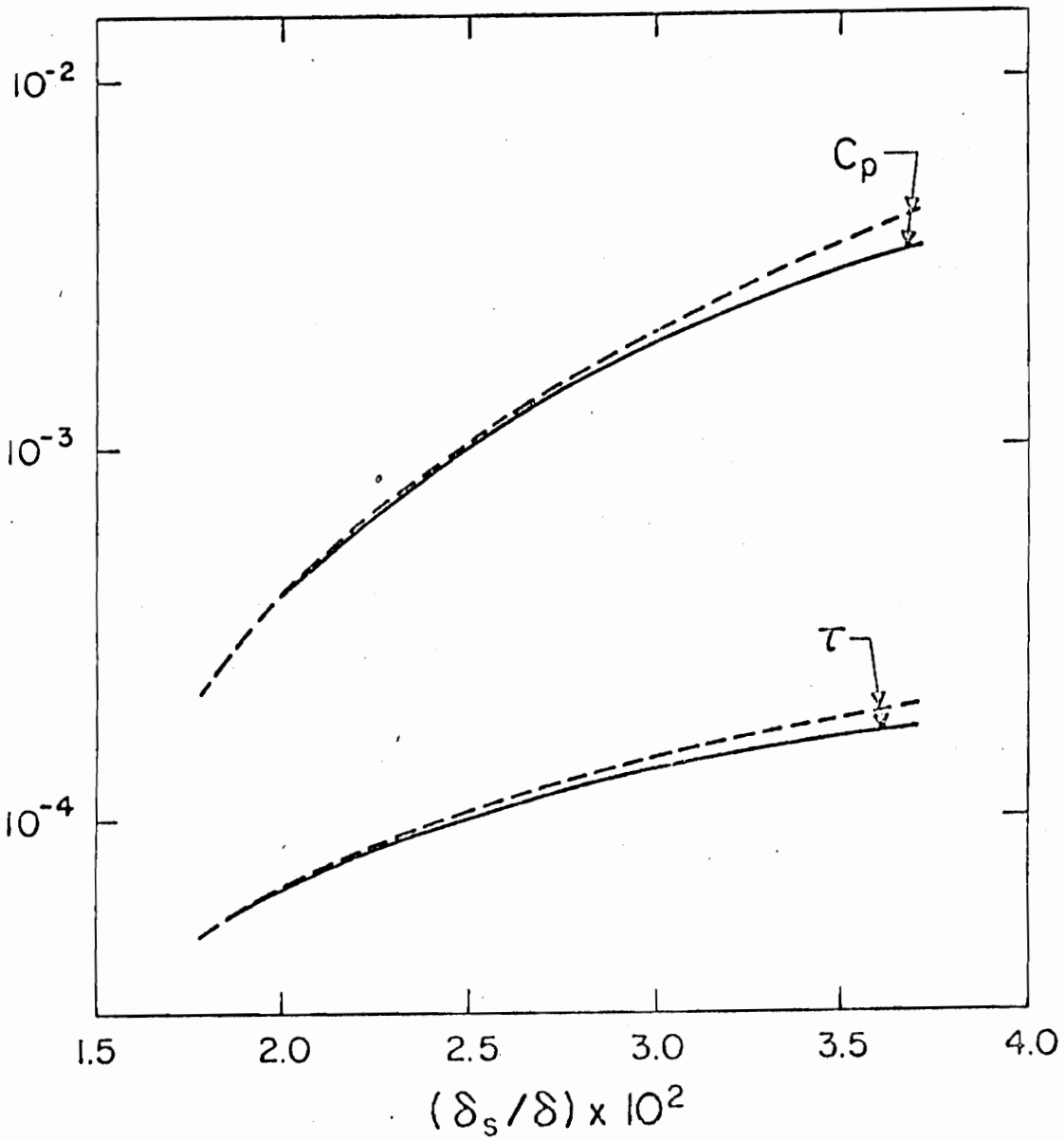

Figure 10. Variation of the amplitude of the pressure and the shear perturbation with the sublayer thickness (δ = 2cm, $\frac{T_w}{T_{ad}}$ = 0.8, M = 5.0, ---- Lighthill, —— present).

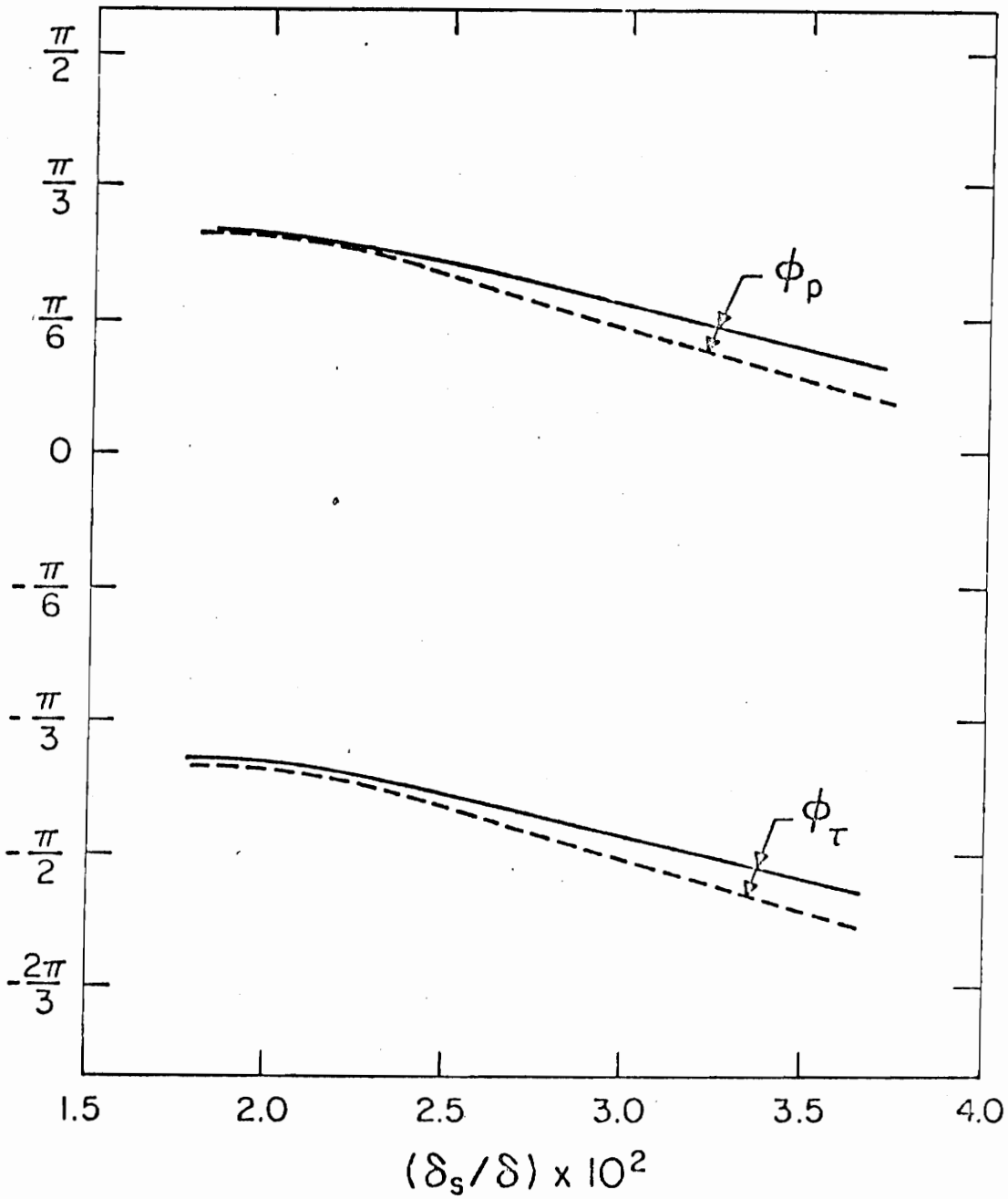

Figure 11. Variation of the positions of the maximum pressure and shear perturbations with the sublayer thickness (δ = 2cm, $\frac{T_w}{T_{ad}}$ = 0.8, M = 5.0, ---- Lighthill, —— present).

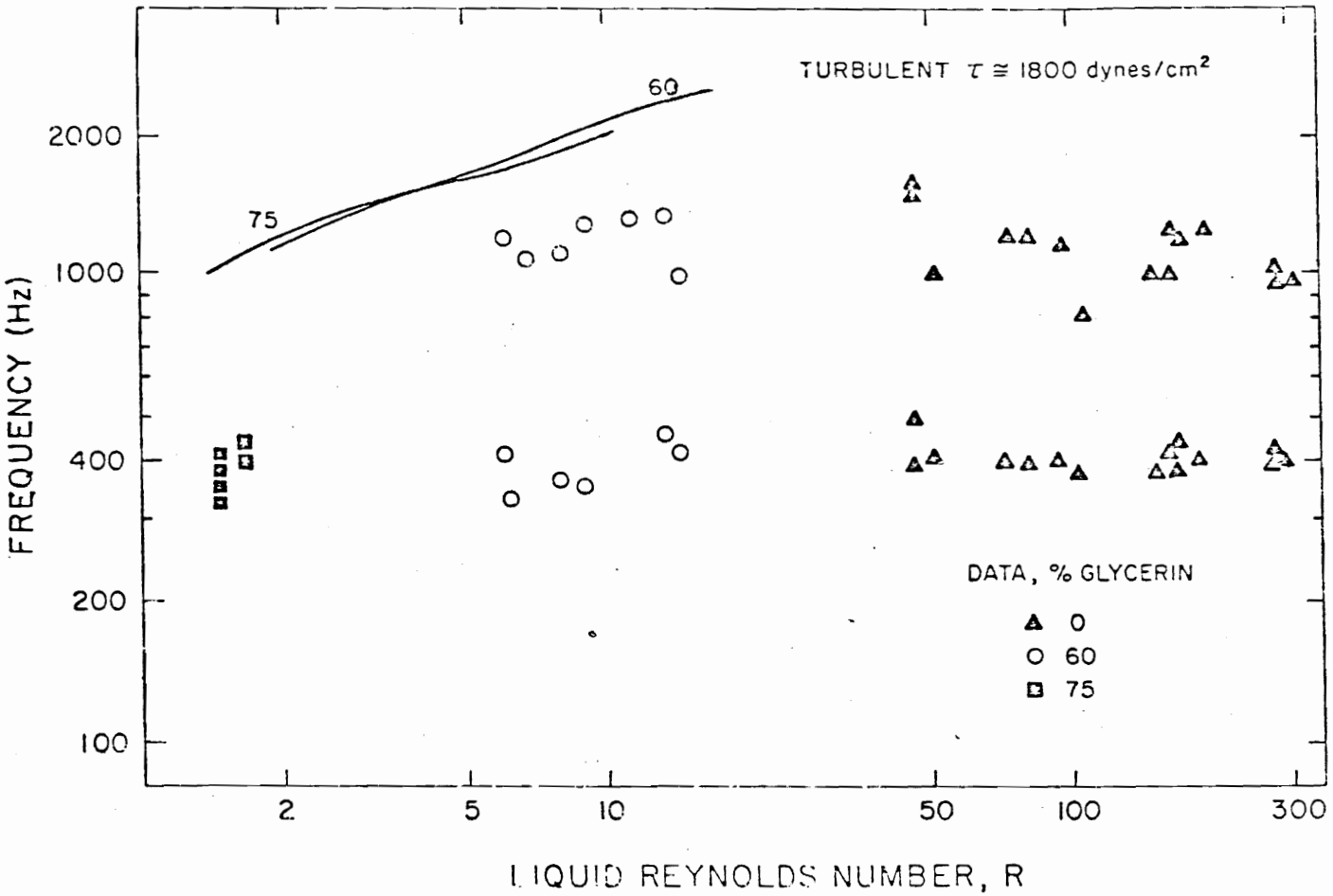

Figure 12. Comparison of predicted with observed frequencies for the linear theory using a turbulent boundary layer.

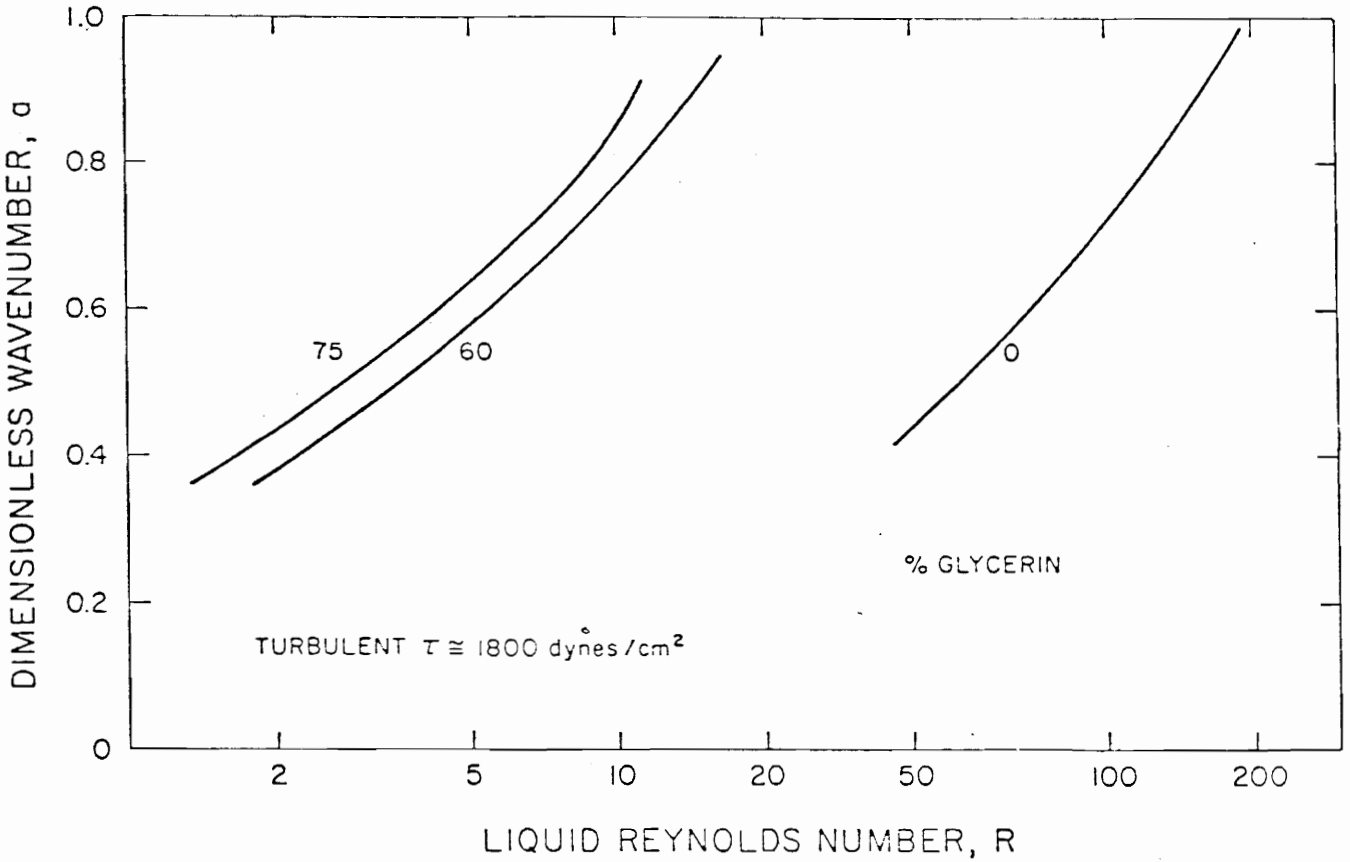

Figure 13. Wavenumbers predicted by the linear theory for the case of a turbulent boundary layer.

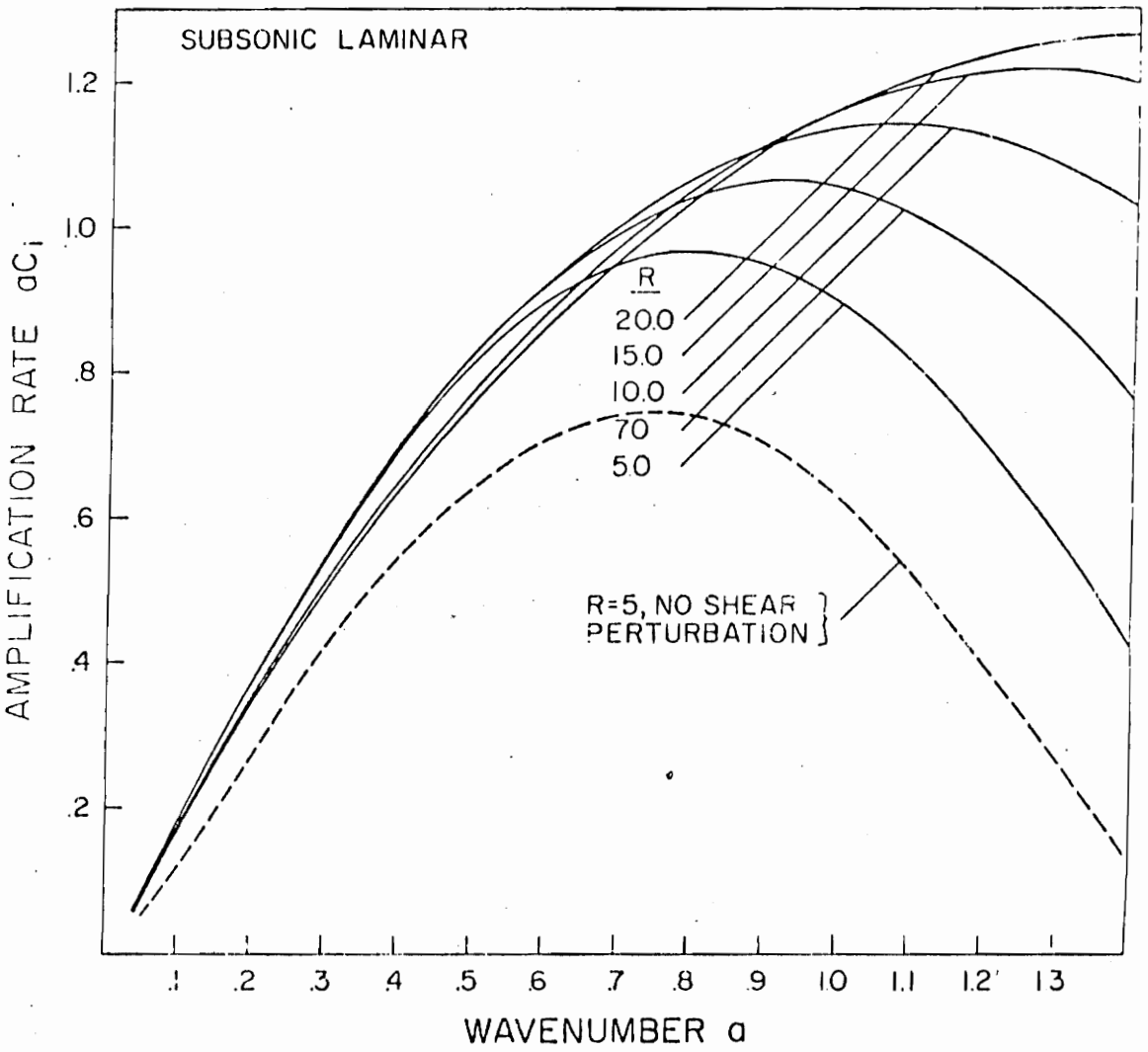

Figure 14. Amplification rates for the case of a subsonic laminar boundary layer.

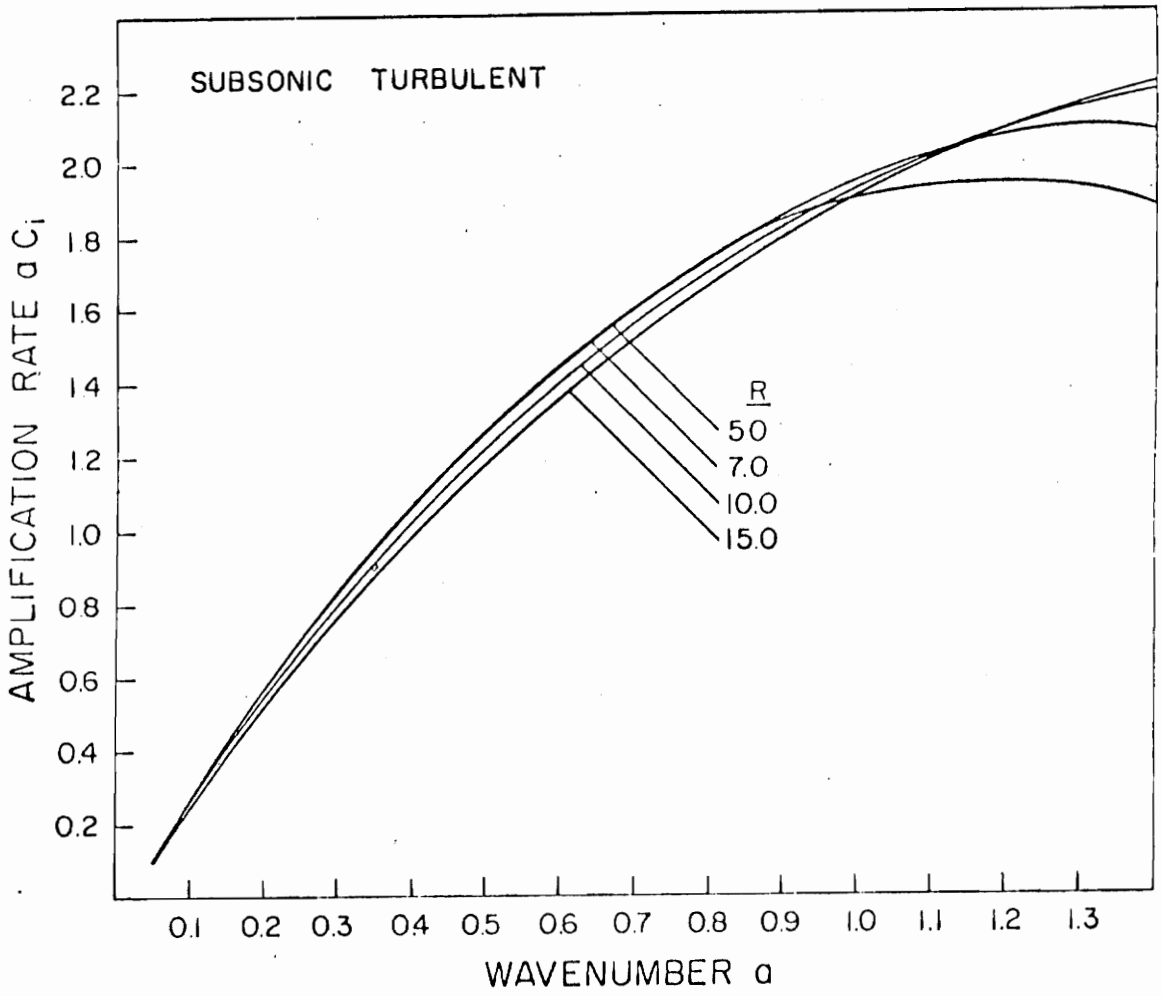

Figure 15. Amplification rates for the case of a subsonic turbulent boundary layer.

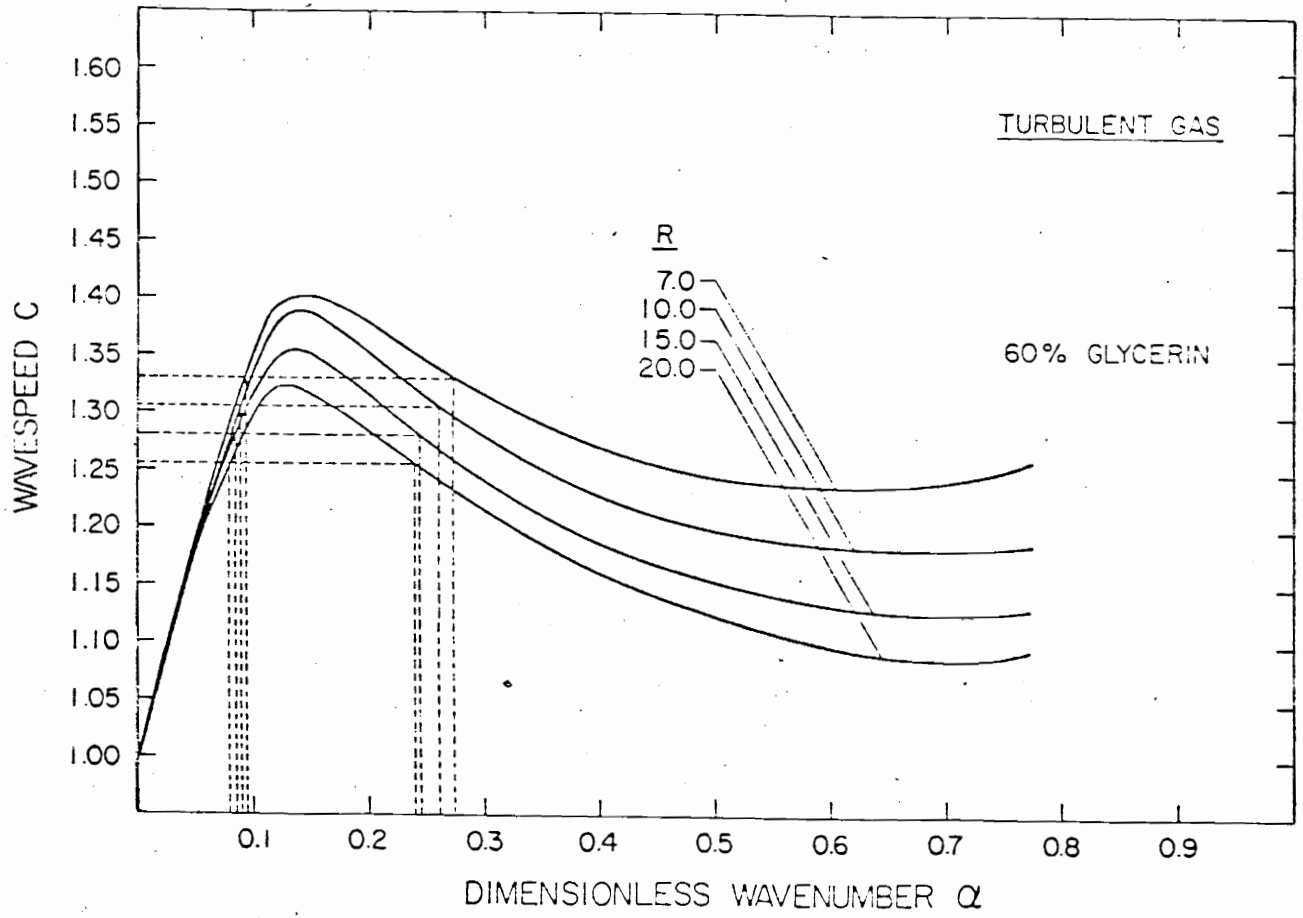

Figure 16. Wavespeed vs wavenumber, indicating resonance conditions.

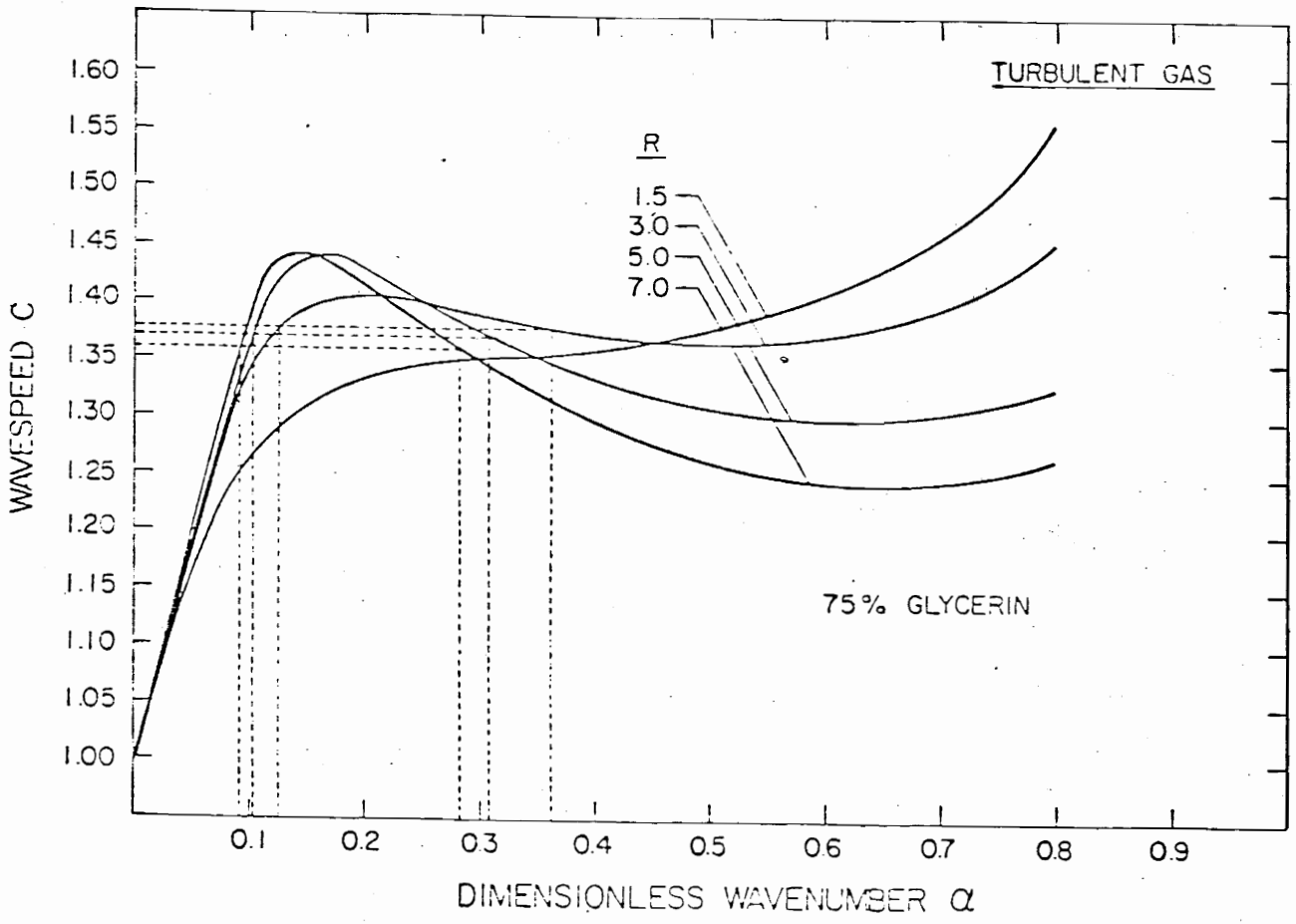

Figure 17. Wavespeed vs wavenumber, indicating resonance conditions.

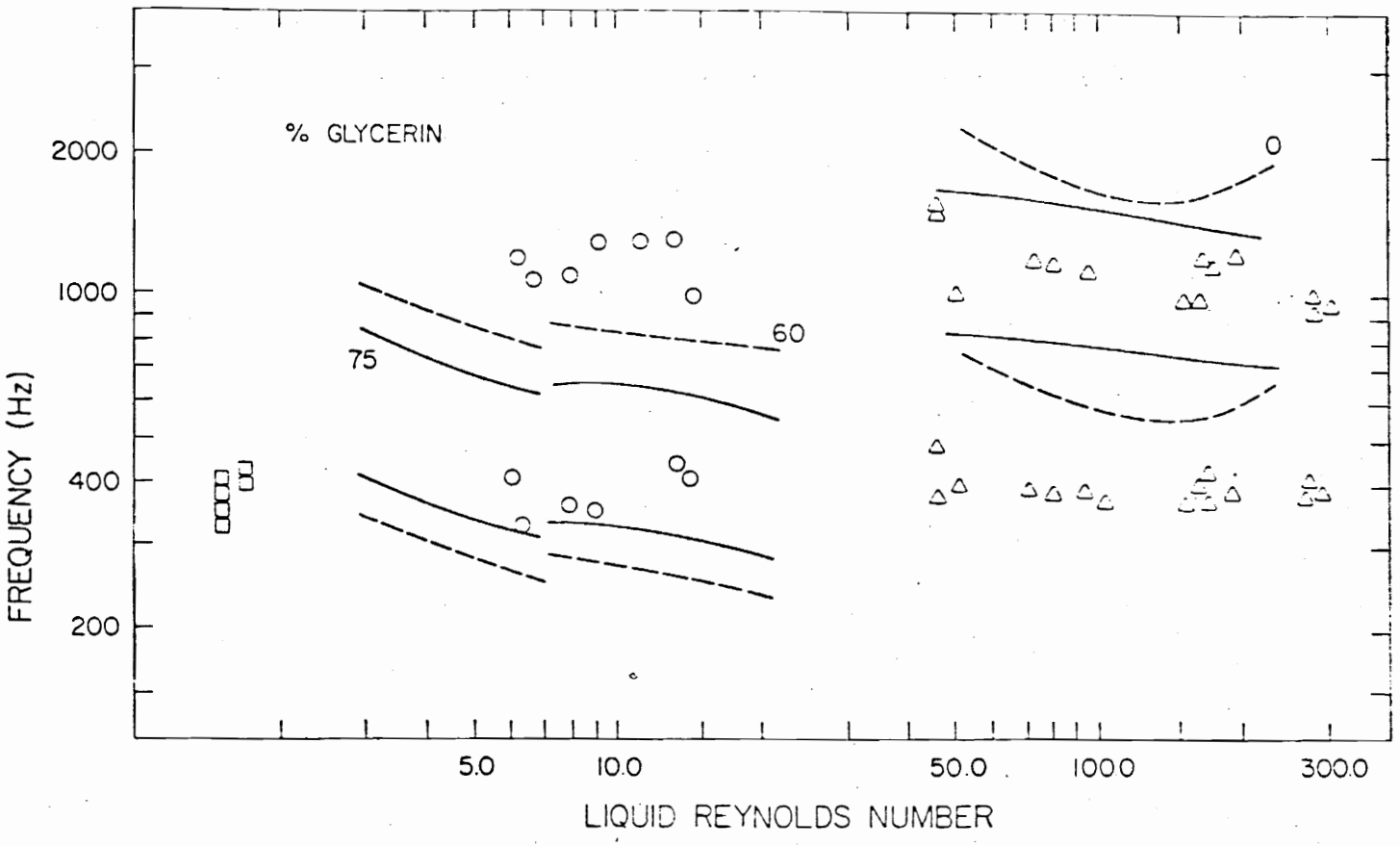

Figure 18. Predicted and observed frequencies for the case of a turbulent boundary layer. Prediction based on perfect resonance conditions: two to one resonance (——), three to one resonance (-----).

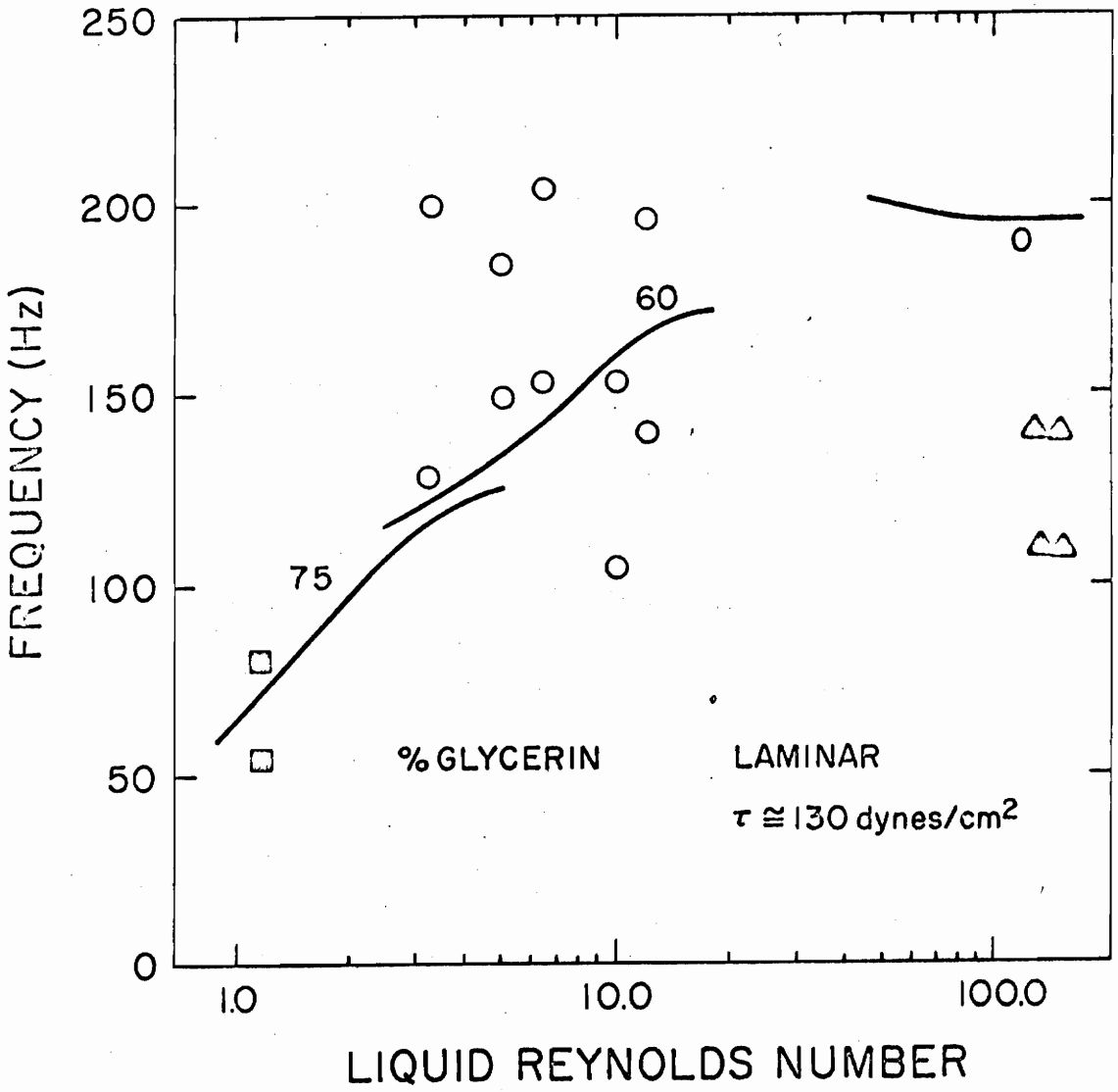

Figure 19. Comparison of predicted with observed frequencies for the viscous nonlinear theory using a laminar boundary layer. Solid line indicates theory and , 0, & correspond to 75%, 60%, and 0% glycerin mixtures.

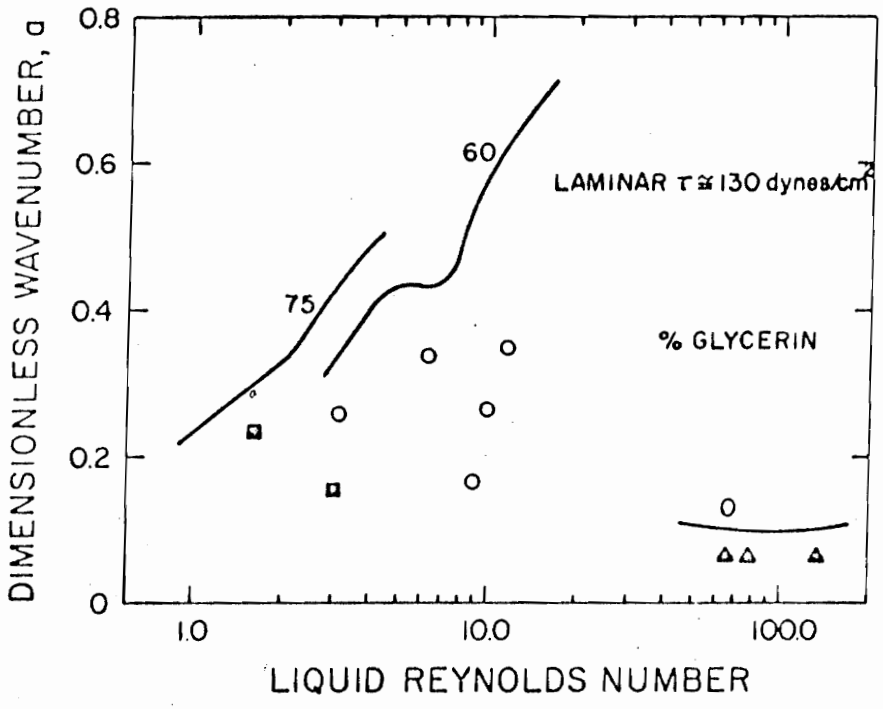

Figure 20. Comparison of predicted with observed wavenumbers for the viscous nonlinear theory using a laminar boundary layer. Solid line indicates theory and , 0, & correspond to 75%, 60%, and 0% glycerin mixtures.

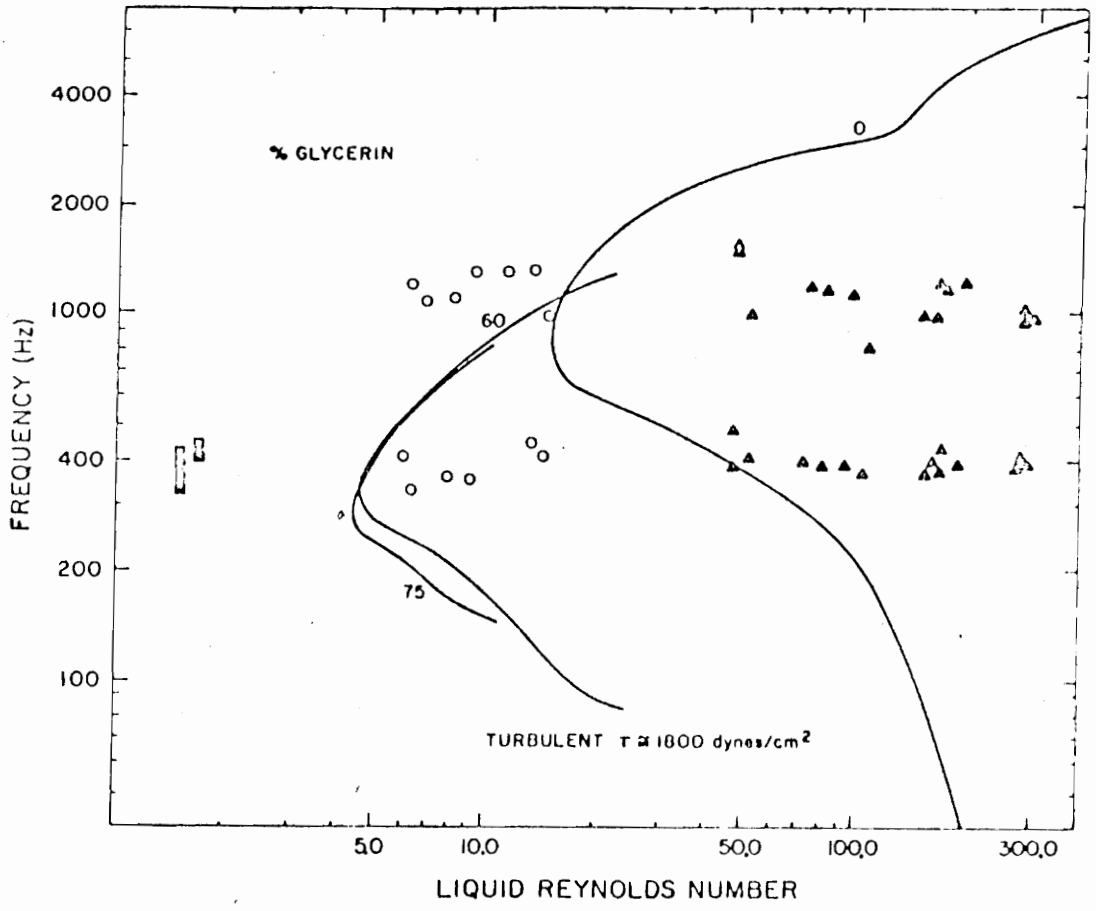

Figure 21. Comparison of predicted with observed frequencies for the viscous nonlinear theory using a turbulent boundary layer. Solid line indicates theory and , 0, & correspond to 75%, 60%, and 0% glycering mixtures.

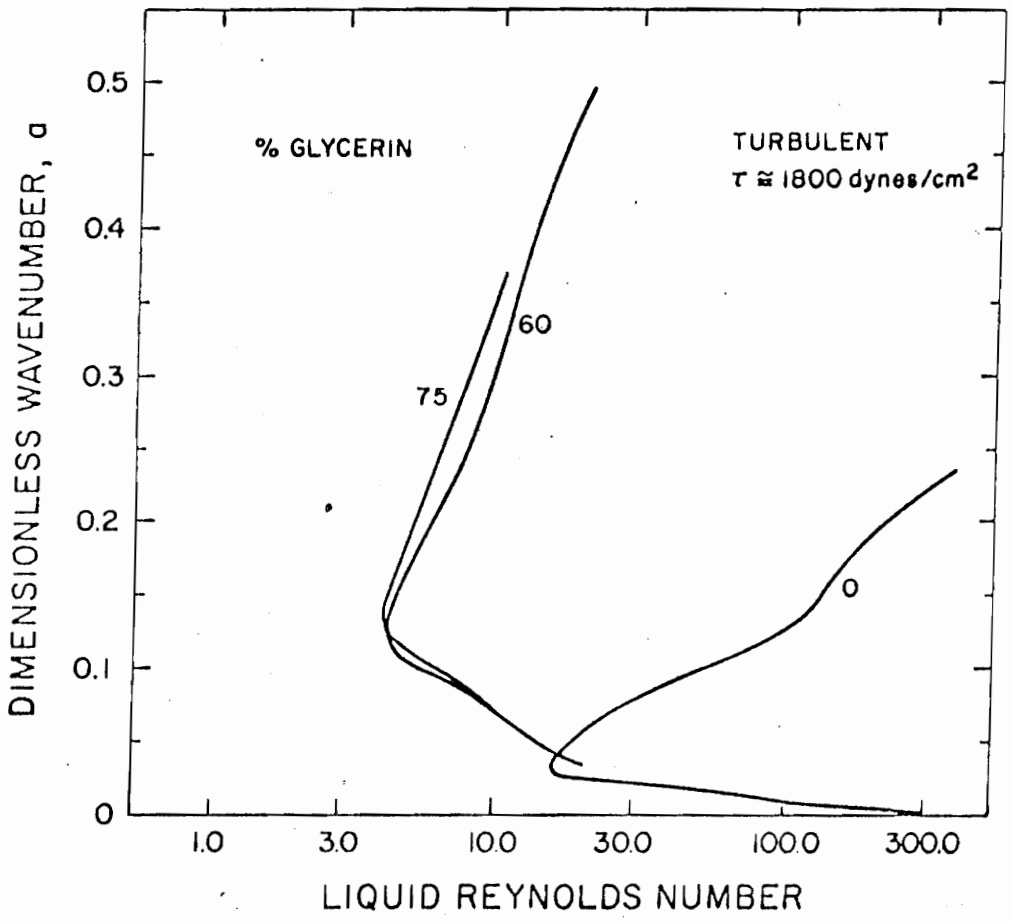

Figure 22. Predicted wavenumbers for the case of a turbulent boundary layer.

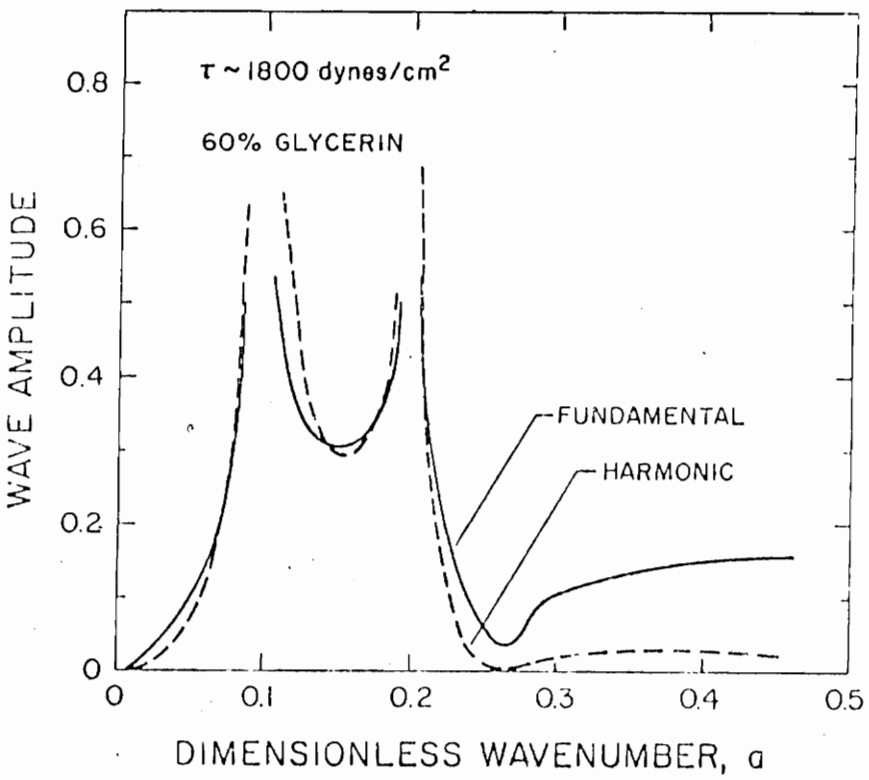

Figure 23. Variation of the amplitude of the fundamental and its second harmonic for the case of a turbulent boundary layer, for the viscous nonlinear theory.

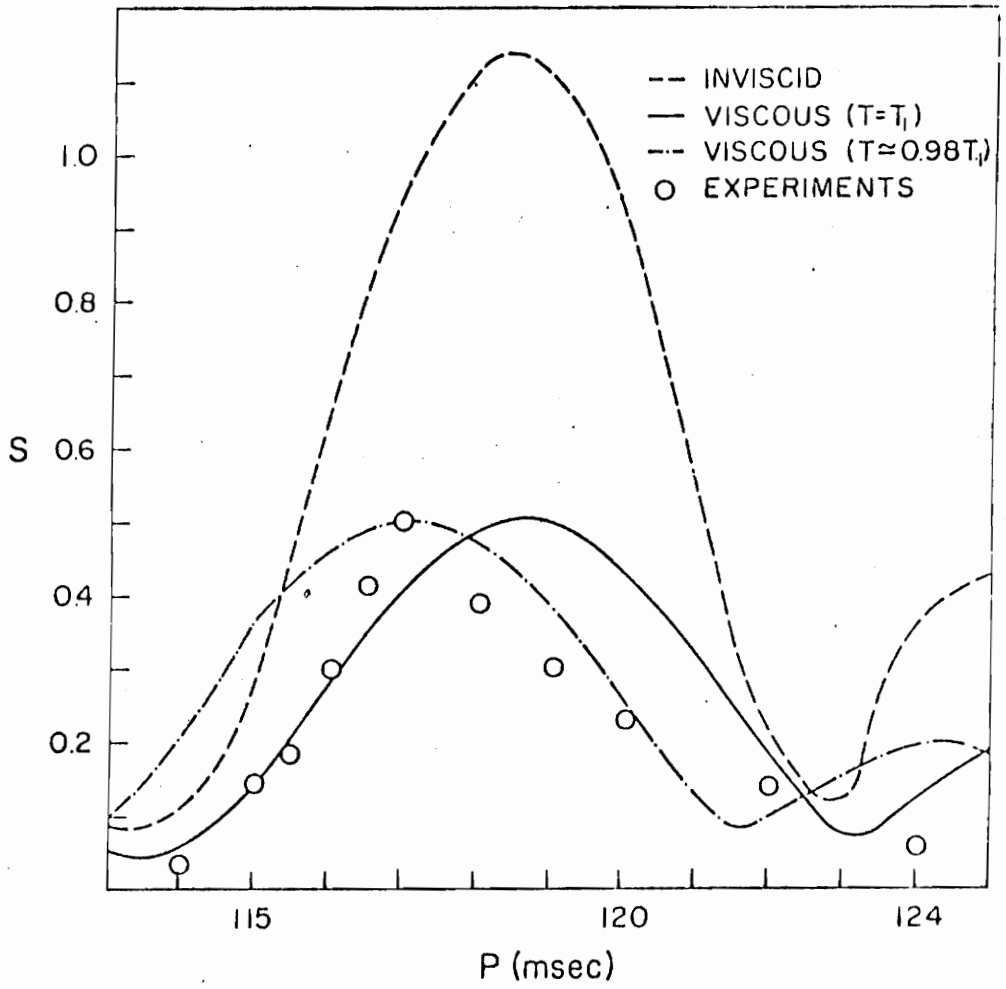

Figure 24. The ratio S of the steepness of the third harmonic 40 cm from the wavemaker to the steepness of the fundamental near the wavemaker.

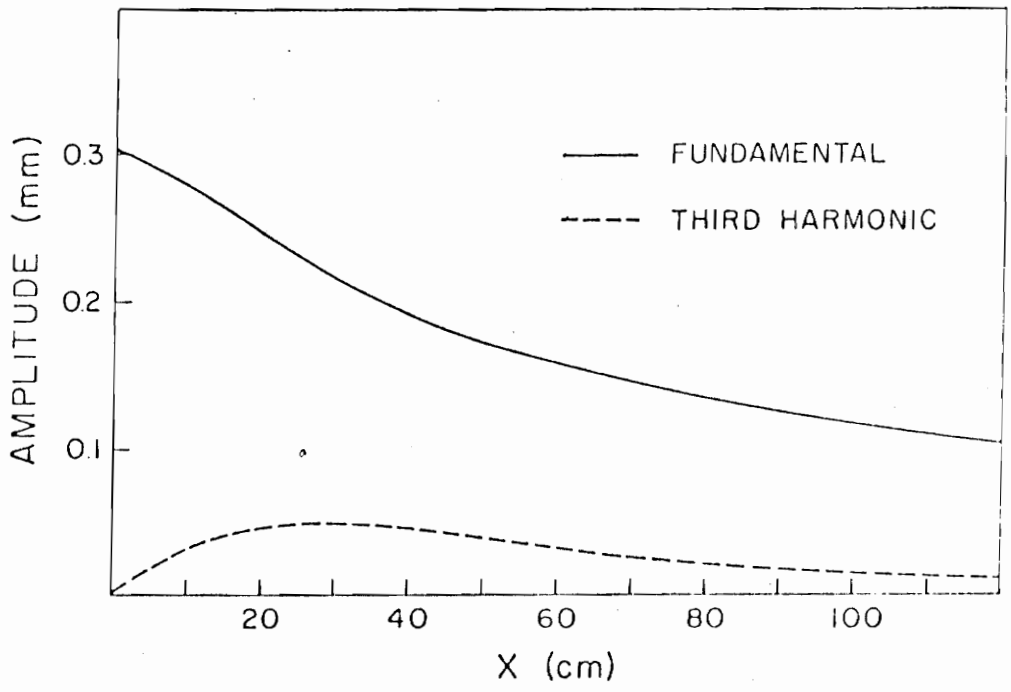

Figure 25. The amplitude of the fundamental and its third harmonic verses the length of propagation at period 119.25 m/sec.

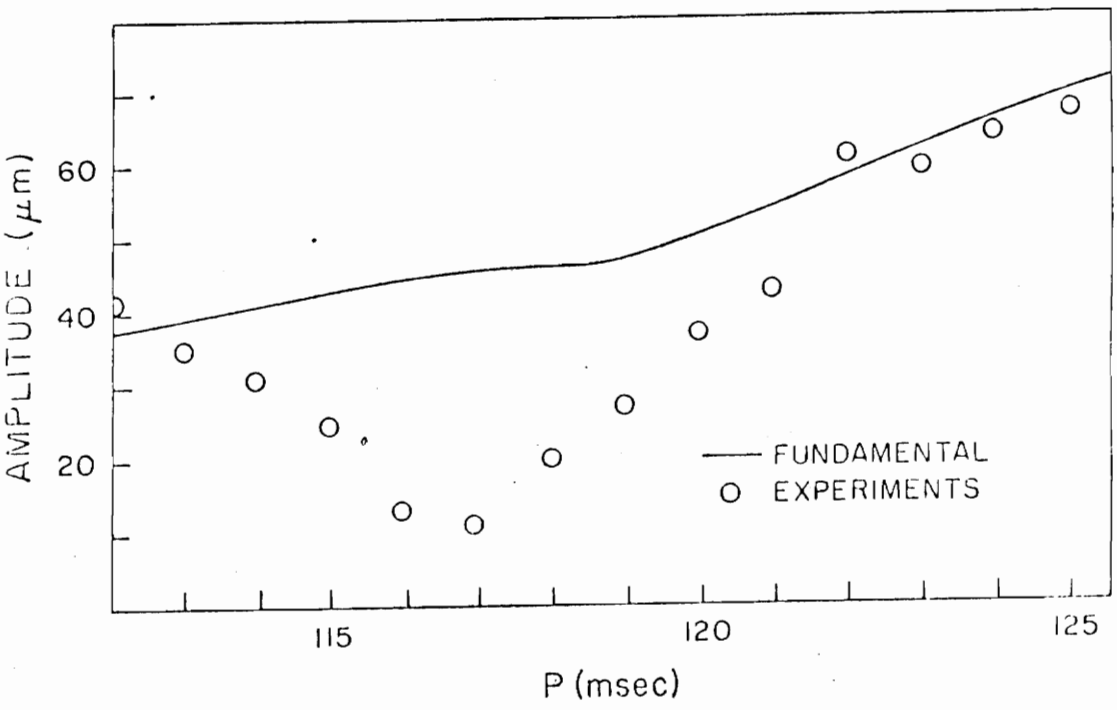

Figure 26. The amplitude of the fundamental at 120 cm from the wavemaker.

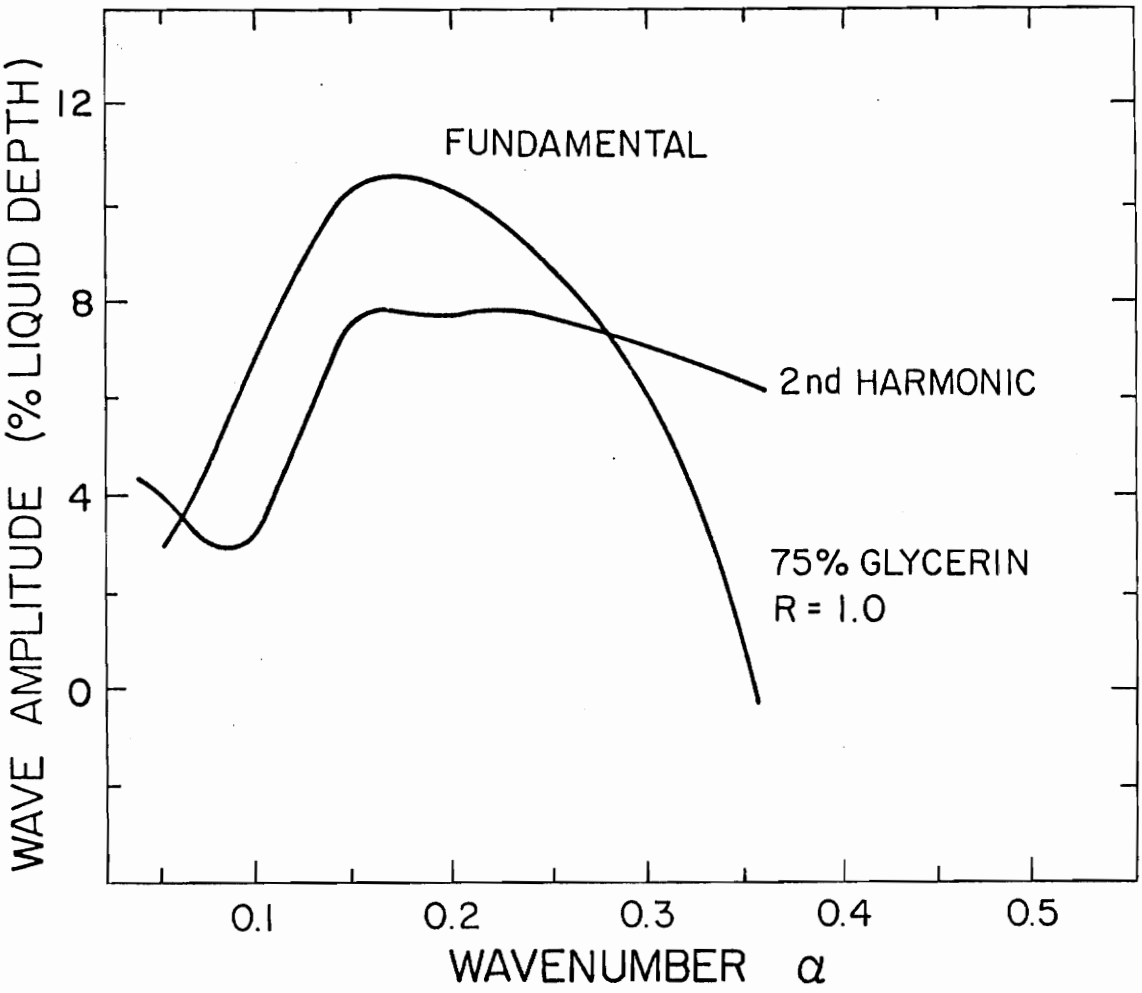

Figure 27. The harmonic amplitudes versus wavenumber as predicted by the two-harmonic solution.

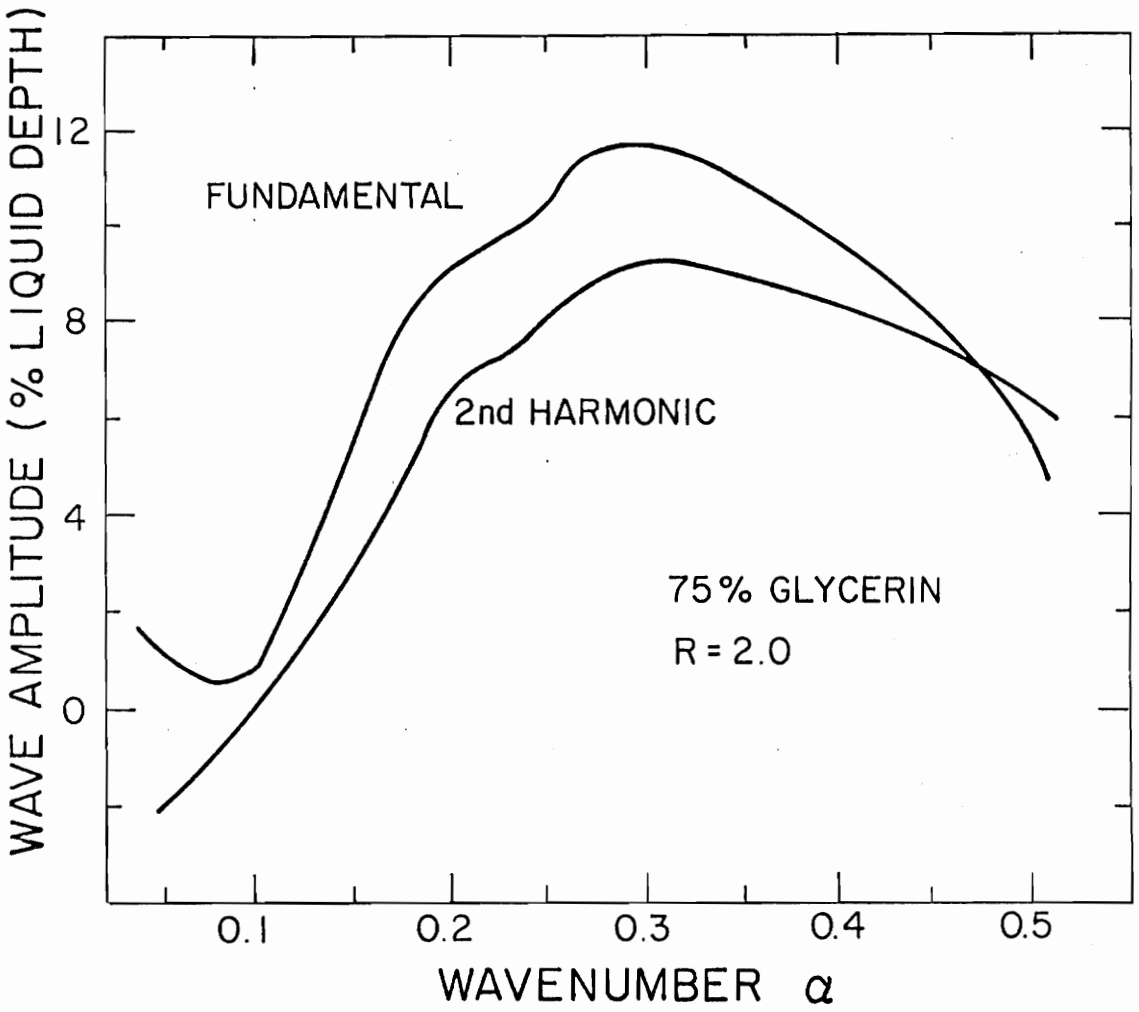

Figure 28. The harmonic amplitudes versus wavenumber as predicted by the two harmonic solutions.

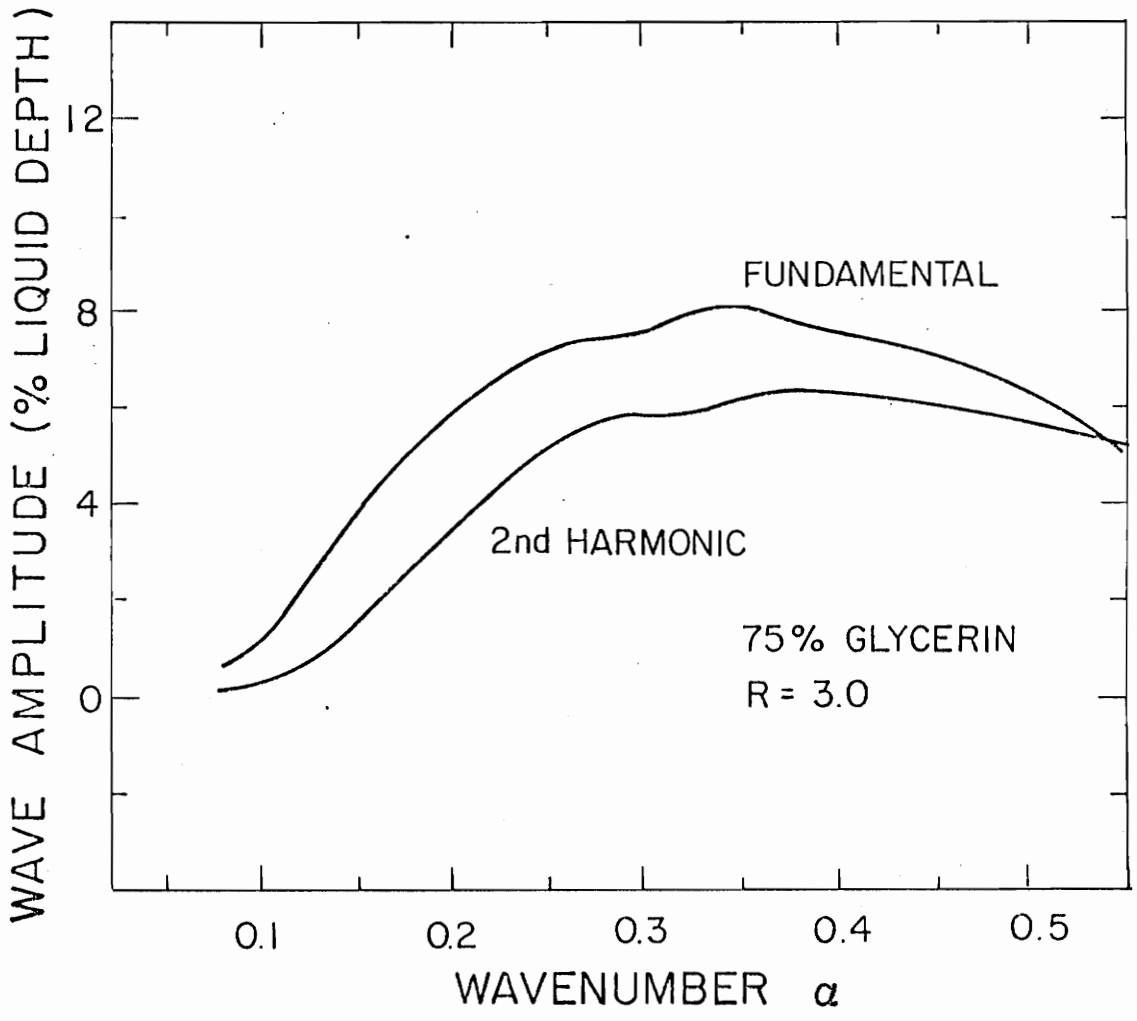

Figure 29. The harmonic amplitudes versus wavenumber as predicted by the two-harmonic solutions.

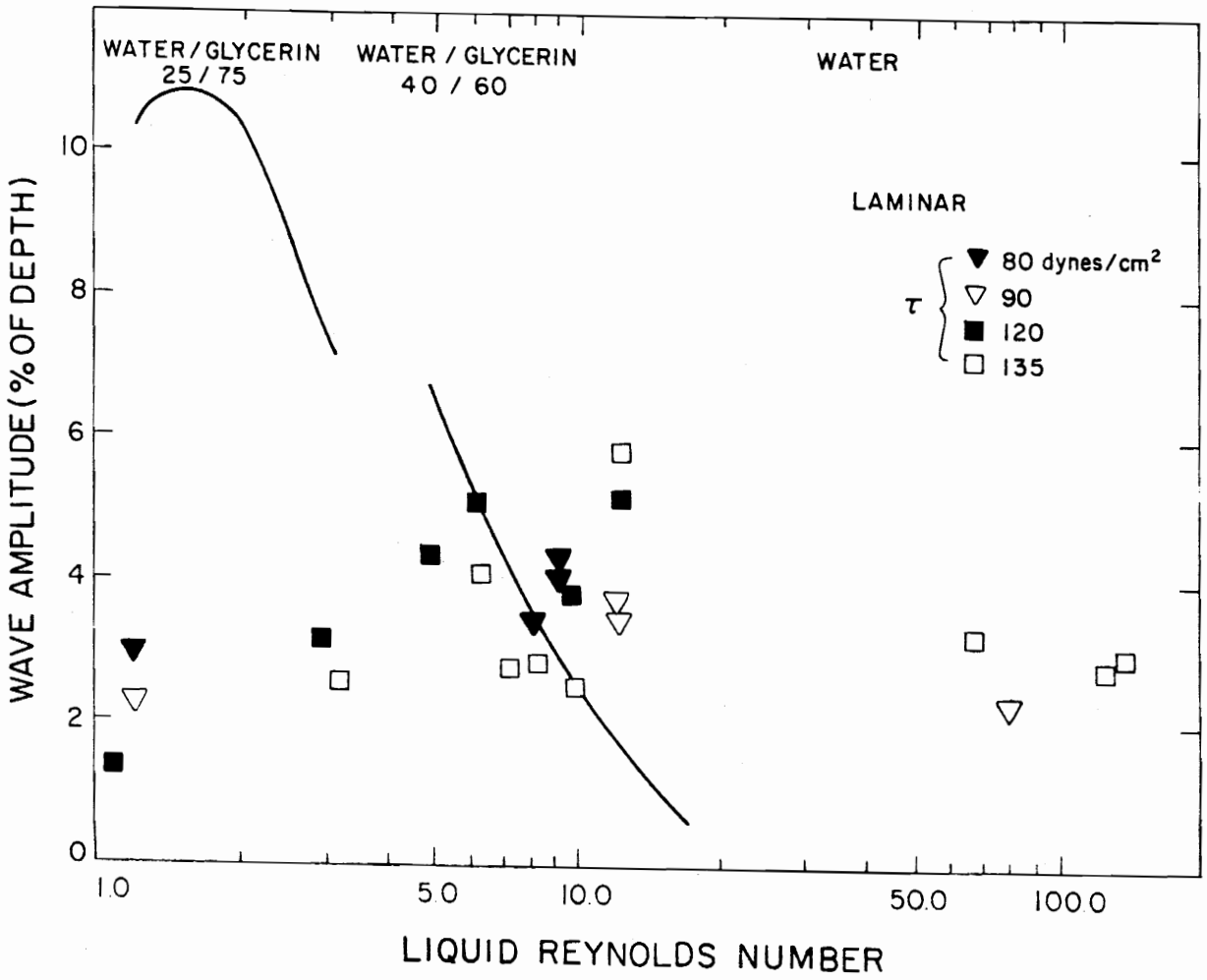

Figure 30. Comparison of predicted and observed r.m.s. waveamplitudes, using the two harmonic solutions.

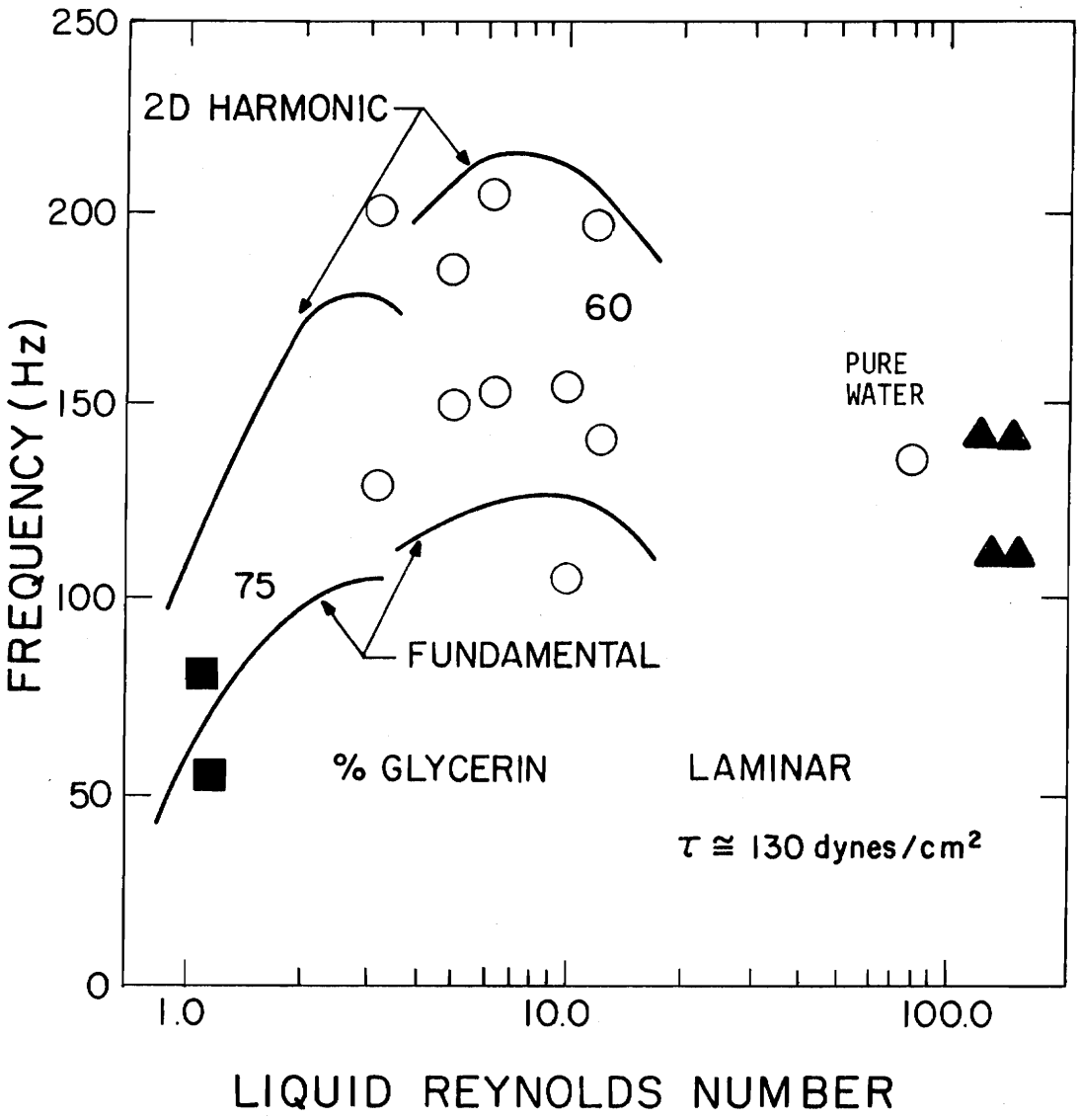

Figure 31. Comparison of predicted and observed frequencies using the two-harmonic solutions.

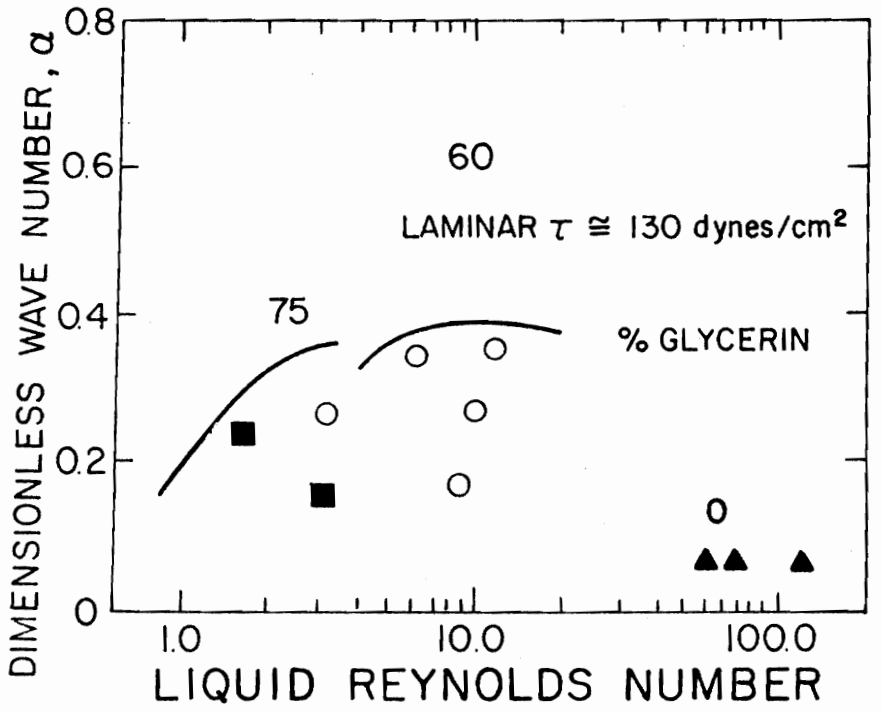

Figure 32. Comparison of predicted and observed wavenumbers using the two harmonic solutions.

VITA

The author was born in Komotini Rodopis, Greece on July 13, 1949. He attended public schools in Komotini and subsequently enrolled at the National Technical University of Athens in September 1967. As an undergraduate, he received government fellowships for being at the top 10% of his class. He received a B.Sc, with distinction, in Mechanical Engineering in July 1972. He won a Fulbright international scholarship and subsequently enrolled in the Department of Engineering Science and Mechanics of the Virginia Polytechnic Institue and State University, where he received a M.Sc. in November, 1973. He then continued his studies toward the PH.D. degree. He is currently employed as a consultant at the Lockheed Georgia Company.

NONLINEAR WAVE INTERACTIONS IN SUPERSONIC WIND GENERATED WAVES

by

S. G. Lekoudis

ABSTRACT

The nonlinear stability of thin liquid films adjacent to a compressible gas flow was analyzed by a combination of perturbation and numerical methods. The solution is valid for two-dimensional disturbances and small amplitudes. The model for the liquid layer includes the effects of the mean motion of the film, viscosity, surface tension, gravity, stress perturbations on the interface due to the gas stream and wave amplitude. The gas model considers the mean velocity profile, gas viscosity and compressibility and wave amplitude. The assumption that the viscosity only effects the disturbance in the gas near the wall was found to be inadequate for the case of turbulent boundary layers. It was found that resonant conditions exist and that the waves are nondispersive at the lower range of wave numbers. A model that accounts for second harmonic resonance was developed. This model improves the agreement between the predicted and the observed wave amplitudes.